U S

University of
Stavanger

FACULTY OF SCIENCE AND TECHNOLOGY

MASTER'S THESIS

Study programme/sspecialization: Petroleum Geosciences Engineering	Spring semester, 2018 Open
Author: Siri Gloppen Gjersdal	………………………………………… (signature of author)
Programme coordinator: Supervisor: Dr. Udo Zimmermann	
Title of master's thesis: TEM, SEM and optical microscopy analyses of Berea sandstone cores flooded with sodium silicate polymers for IOR purposes	
Credits: 30	
Keywords: Sodium silicate Berea Sandstone Polymer Optical light microscopy (OLM) Geochemistry (GC) X-ray diffraction (XRD) Scanning electron microscopy (SEM) Energy x-ray dispersive spectrometry (EDS) Transmission electron microscopy (TEM)	Number of pages: 61 + supplemental material/other: 55 Stavanger, 13.07.18 date/year

TEM, SEM and optical microscopy analyses of Berea sandstone cores flooded with sodium silicate polymers for IOR purposes

MSc thesis

by

Siri Gloppen Gjersdal

Petroleum Geosciences Engineering

Faculty of Science and Technology

University of Stavanger

Norway

University of Stavanger

June 2018

Acknowledgements

Table of Contents

List of figures

List of tables

Commonly used abbreviations

IOR – Improved Oil Recovery

SS – Sodium silicate

UiS – Universitetet i Stavanger (University of Stavanger)

OLM – Optical light microscopy

GC - Geochemistry

XRD – X-ray diffraction

SEM – Scanning electron microscopy

EDS – Energy-dispersive X-ray spectroscopy

TEM – Transmission electron microscopy

FIB – Focused ion beam

HCl – Hydrochloric acid

NaCl – Sodium chloride

wt% - weight percent

NIOR – the National IOR Centre of Norway

mD – millidarcy

IRIS – International Research Institute of Stavanger

DW – Deionized water

SSW – Synthetic seawater

Ppm – Parts per million

BSE – Backscattered electrons

SE – Secondary electrons

NTNU – the Norwegian University of Science and Technology (Norges Teknisk-
naturvitenskaplige Universitet)

Abstract

Improved Oil Recovery (IOR) is a "hot topic" in the Oil and Gas industry. Sodium silicate (SS) is a polymer which can be injected into a reservoir as a fluid and due to polymerization it precipitates into a semi rigid gel under given circumstances. However, the knowledge about this polymer on a micron- and nano-scale is restricted.

Berea sandstone cores with permeabilities of 500 mD and 200 mD were flooded with SS and studied by various methods- optical light microscopy (OLM), geochemistry (GC), x-ray diffraction (XRD), scanning electron microscopy (SEM), energy dispersive x-ray spectroscopy (EDS), and transmission electron microscopy (TEM). At low magnifications (OLM) a white substance was first observed in the pore space in both flooded and unflooded cores– the "before" and "after" flooding had very similar features. Utilizing XRD analysis, the bulk-investigation showed little impact of SS – however, it stated the presence of quartz, kaolinite, orthoclase, albite, and rutile. GC analysis revealed a significant increase in iron (from less than 1% to almost 16%) and in the entire range of trace elements after adding HCl to the SS solution. Furthermore, GC data indicated an increase of SS in the flooded contra the unflooded core material. SEM-EDS provided 3D insight into the appearance of dried SS solution before and after mixing with HCl, showing acicular tube-like crystallization as well as NaCl precipitation after adding HCl. EDS-measurements of the flooded core revealed a dramatic decrease in Na-content compared to the solution before injection – in many cases the content was nearly absent. High resolution scan of a FIB/SEM-sample in a TEM showed the variation of Na-content within a single agglomerated gel-particle grown on a quartz-grain, on a nano-scale. EDS point-scans of the same sample area presented spectacular results with approximately identical Si and O content for quartz and the core of the SS-particle, with no Na present, whilst the rim of the SS-particle contained Na. This phenomenon of extraordinary fractionated gelling with a center and a rim was indicated by TEM-EDS. For further studies, there is a need for systematic testing with a series of experiments conducted on the same sample, as well as a thorough analysis of the effluent. However, the application of routinely used methods for mineralogical changes related to EOR research was highly successful in imaging a fractionation of polymer composition. This will have enormous significance for wettability and surface charge interactions.

1 Introduction

1.1 Improved oil recovery

The need to develop methods for Improved Oil Recovery (IOR) is demonstrated by the declining production numbers for the mature oil reservoirs on the Norwegian Continental Shelf (Skrettingland et al., 2016). After almost 50 year of oil production in Norway, more than 50% of the oil remains in the reservoirs. Increasing the oil recovery factor for these fields using environmentally friendly and sustainable methods represents a great value, both for the oil and gas companies and for the society. The OSPAR Commission (Oslo/Paris convention) categorizes sodium silicate (SS) as a green chemical, and it is considered to Pose Little or No Risk to the environment (PLONOR).

Experimental laboratory work and successful testing in the Snorre field in the North Sea in 2011 and 2013 showed that SS can be used as a chemical system for in-depth water diversion to increase sweep efficiency (Fig. 1) (Skrettingland et al., 2016). When the solution polymerizes and forms a gel in the high-permeable zones in the reservoir, the injected water is forced through the low- or non-swept zones of the reservoir, increasing the oil flow towards the producer, resulting in more oil produced. SS has previously been applied for well conformance control and treatment, and in the recent years it has also been used for in-depth conformance control ((Omekeh et al., 2017). To simplify, I will use the abbreviation SS for sodium silicate throughout thesis, along with the terms gel and polymer.
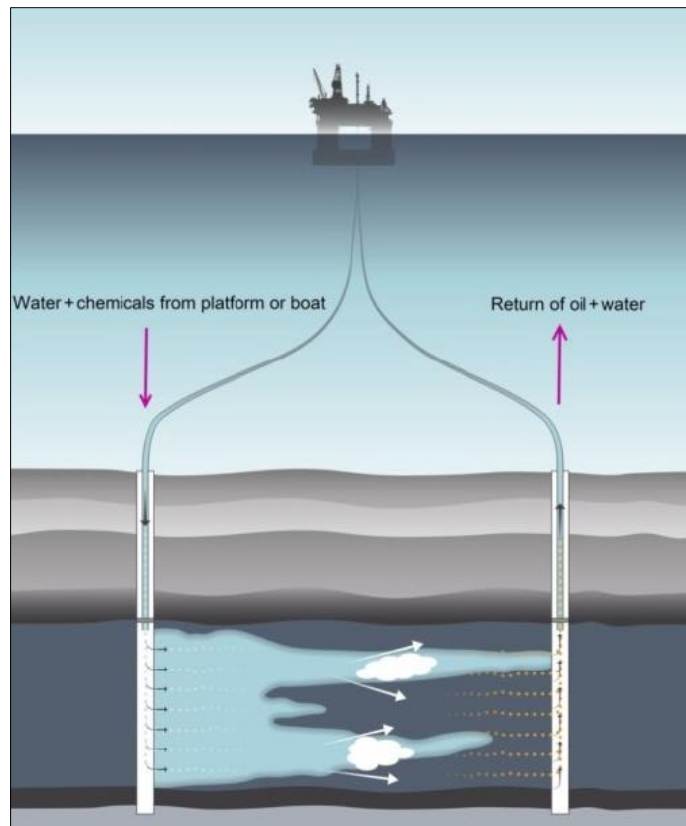
Figure 1. SS used for in-depth water divergent, forcing injected water through un-swept zones, implied by the white arrows (Skrettingland et al., 2014)

1.2 Objectives

The SS observed on a micron- and nano-scale is useful and essential in understanding and improving field-scale operations, as the Centre director of the National IOR centre of Norway (NIOR), Merete Vadla Madland, has emphasized in the annual report for 2016 (Madland et al., 2016). The objective for this study is to investigate the polymer properties and its distribution on a micron- and nano-scale, including its chemistry and the mineralogical and chemical alterations in the host rock after injection. In this project, the polymer composition will be mapped, and particularly the contact with the host rock will be examined in detail. The overall objective is to try to understand and gain more knowledge about the habit of SS in flooded core material, and to decipher which methods are useful to perform in such a study. This includes on a second level if the polymers alter the chemistry and the properties of the

host-rock and to characterize the chemical homogeneity and –composition of the gelled substance.

1.3 Rationale for methodological approach

The challenge and the opportunity within this project is that there are so little previous studies on SS gel on a micron- and nano-scale. Therefore, most of the analyses are novel and simultaneously the best-suited methods for describing the process and determining the gel distribution.

Preliminary information of the gel in polished thin sections in the flooded core sample was given by optical light microscopy (OLM). Bulk investigation of chemical alterations from unflooded to flooded cores was applied by geochemical (GC) analysis and x-ray diffraction (XRD). Examination of the gels appearance and chemical composition on a micron- and nano-scale was preformed using a scanning electron microscope (SEM) coupled with energy-dispersive x-ray spectroscopy (EDS). This method also offered an advantage compared to bulk-analysis: high-resolution chemical composition of a spot size down to 1 µm. To further increase magnification, transmission electron microscope (TEM) was applied to image and to determine the chemistry of the gel and its relation to the host rock on a nano-scale, using a focused ion beam (FIB)/SEM section. The aim of utilizing TEM was to investigate the precipitation of SS on quartz on a nano-scale, to study the shape and size of the gel-particles, as well as the chemical transition from quartz to SS.

2 Theory

2.1 SS to improve the oil recovery

According to Wright and Durphy (2012), polymerization of pure silica gel may be summarized in these main stages (Fig. 2):

- Formation of dimers and oligomers
- Particles are formed due to condensation
- The particles grow…
- …and are finally linked together in chains, forming a 3D-network.

The process in which small particles condense on the surface of larger particles which in turn grow even larger, is called Ostwald ripening. The electric repulsion between particles are reduced when adding an acid to the solution, e.g. hydrochloric acid (HCl), and as pH decrease below 11, gelation initiates and viscosity of the solution increase rapidly (Wright and Dupuy, 2012). This is due to the silicate species forming high order oligomers by aggregating, before the polymer chains turns into a 3D-network and the initially transparent solution turns cloudy (Hamouda and Amiri, 2014).
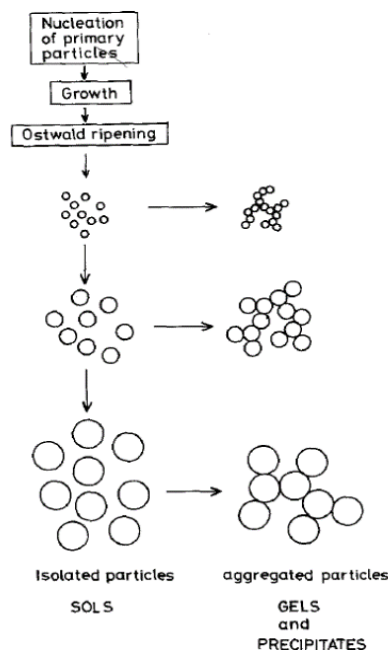
Figure 2. Polymerization process, according to Wright & Durphy (2012).

Silicate polymerization (Fig. 3) is an aid in understanding the SS gelation process. When SS (Na_4SiO_4) is used, polymerization initiates as two units react with each other and grow into a larger particle ($Na_6Si_2O_7$). The polymerization continues when the dimer reacts with another unit of Na_4SiO_4, and in each reaction Na^+ is released and escapes with the fluid. Steps a - c in Figure 3 illustrates the reduction of these ions for each step of polymerization. This process is acid catalysed, and for this study, hydrochloric acid was used as catalyst (activator).
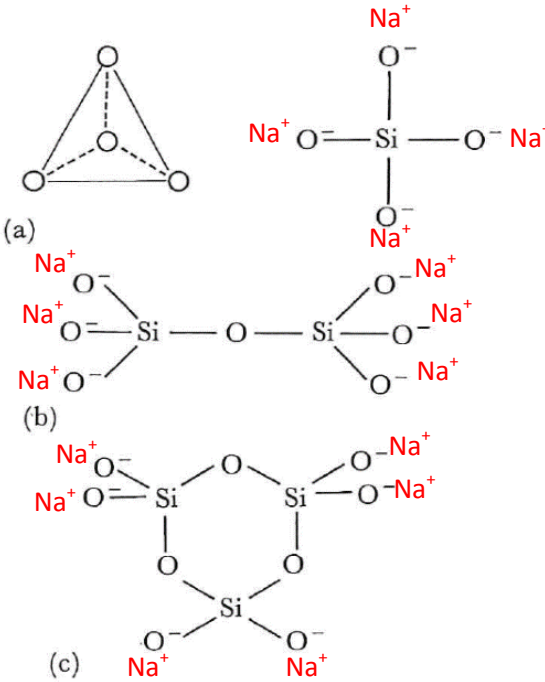
Figure 3. Silicate polymerization, here with Na^+ attached to each O^- to illustrate SS polymerization, based on the same principle as silicate polymerization. Each step (a to c) shows a reduction of Na^+ ions. Modified after (Robinson, 2009).

Gelation kinetics can be affected and accelerated by several parameters, and if the desired conditions for controlled gelation are not met, it can cause polymerization and unwanted plugging e.g. when too close to an injection well (Stenerud et al., 2017). The presence of divalent ions such as Ca^{2+} and Mg^{2+} can shorten the gelation time, as well as increase the gel strength and gel shrinkage (Hamouda and Amiri, 2014). Studies conducted by Hamouda and Amiri (2014) showed that for a solution with silicate-concentration of 4,5 weight percent

(wt%), pH=10,3 and temperature of 20°C, the presence of divalent ions led to maximum gel strength being reached eight times faster than solutions without divalent ions. Gel shrinkage is initiated by fluid expelling from the gel, in worst case causing an increase in the permeability in the blocked zone, which represents a major challenge. In the case of divalent ions in the reservoir, a low saline preflush can be used to dilute the ion concentrations, preventing unwanted plugging (Hamouda and Amiri, 2014). Another controlling factor of the SS reaction rate is the formation temperature (Stavland et al., 2011), as SS is a so-called thermo-gel which reacts to increasing temperature by forming a gel (Stenerud et al., 2017), resulting in a flow restriction as shown in Figure 1.

Commercially, SS is an inorganic system composed of silicon dioxide and sodium oxide $((SiO_2)_n : Na_2O, n<4)$, where the molar ratio between the two chemical compounds (n) reveals the behaviour of the SS. For this study, the molar ratio is 3,26. pH usually ranges between 11-13. Before it starts to polymerize, the viscosity of the solution is like water, however, after a few years in storage, viscosity gradually increases. The polymer is relatively low cost, compared to other gel systems, and it is thermally stable.

To be able to improve the field-scale operations using SS, one need to understand the gelation processes on a pore-scale in the host-rock. The pore-scale results cannot automatically be up-scaled to field-scale, as temperature, salinity of formation water, mineralogy of reservoir rock and pH varies throughout the reservoir (Hamouda and Amiri, 2014). According to the NIOR Annual Report for 2016 (Madland et al., 2016), there is a need for micron- and nano-scale studies of SS to better understand how, when and where possible alterations take place.

2.2 Berea sandstone

During the Lower Mississippian period, sediments were shed into the Appalachian basin by several sources, in delta fans from the north and through river channels from the east. The provenance may be determined primarily by the roundness of heavy minerals such as tourmaline and zircon (Pepper et al., 1954). The Berea Sandstone was primarily deposited in a deltaic environment, which over time became roofed by finer sediments as the ocean transgressed. The Berea sandstone overlies the Bedford shale, together forming a wedge between the Ohio shale below and the Sunbury shale above.

The Berea Sandstone is mined in the Ohio-Pennsylvania area, and for over 25 years it has been used as a standard for core flooding experiments by the oil and gas industry. The well-studied material is (more or less) predictable in terms of homogeneity and mature composition, making it predictable to compare flooding experiments across nations, decades and purposes.

The commercial Berea Sandstone cores mined in Cleveland Quarries, Ohio, range from 19 to 2500 millidarcy (mD), has porosities from 13% to 23% and are both homogeneous and inhomogeneous (Fig. 4). According to the technical data provided by Cleveland Quarries (ClevelandQuarries, 2018) the Berea Sandstones contain 93,1% silica, 3,9% alumina, below a percent of ferric and ferrous oxides, as well as traces of magnesium- and calcium oxide.

Figure 4. Berea Sandstone cores in a variety of diameters, permeabilities and porosities (ClevelandQuarries, 2018).

2.3 Previous studies

SS has been used mainly for near wellbore treatments (Hamouda and Amiri, 2014; Stavland et al., 2011) i.e. conformance control, using gel for water shutoff typically near the production well. However, it was applied as an in-depth blocking agent in the Snorre field, North Sea, where the gel plugged a targeted high permeable zone at a strategic distance into the reservoir (Hamouda and Amiri, 2014). Equinor (former Statoil), in cooperation with the International Research Institute of Stavanger (IRIS), applied SS in the Snorre field for a small-scale test on a single well in 2011 and a large-scale test in 2013, aiming to improve the sweep efficiency (Madland et al., 2016). According to Stenerud et al. (2017), it resulted in reduced water cut, a proven flow restriction, and a marginal increase of oil production (Skrettingland et al., 2016; Stenerud et al., 2017).

Laboratory work performed by Stavland et al., (2011) gives insight into the controlling factors of in-depth placement of the gel. They found that these factors are formation temperature and the SS-concentration. To prevent unwanted plugging, a pre-flush of the reservoir as well as dilution of the SS using desalinated water is recommended.

A silicate gelation model was presented by Omekeh et al. (2017), taking into consideration that the silicate nano-particles need to be transported through the host rock until they reach the targeted area, before polymerizing and increasing viscosity. This work also concludes that gelation time cannot be drawn as a simple exponential function based on silicate concentrations at a given HCl concentration; it underlines the complexity of silicate polymerization.

3 Methodology

3.1 Sample overview and flooding procedure

3.1.1   Sample overview

IRIS provided all the Berea Sandstone core-material (Fig. 5) as well as chemical solutions. In total, four individual flooding experiments were conducted; #1 of a 500 mD core and #2, #3 and #4 of 200 mD cores. Floodings #2 and #3 were unsuccessful due to unwanted plugging too close to inlet; therefore, core material from floodings #1 and #4 was utilized for analyses.

Flooded (#1) ↓   Unflooded ↓

a) 500 mD

Flooded (#2) ↓   Flooded (#3) ↓   Unflooded ↓

b) 200 mD

Flooded (#4) ↓   Unflooded ↓

c) 200 mD
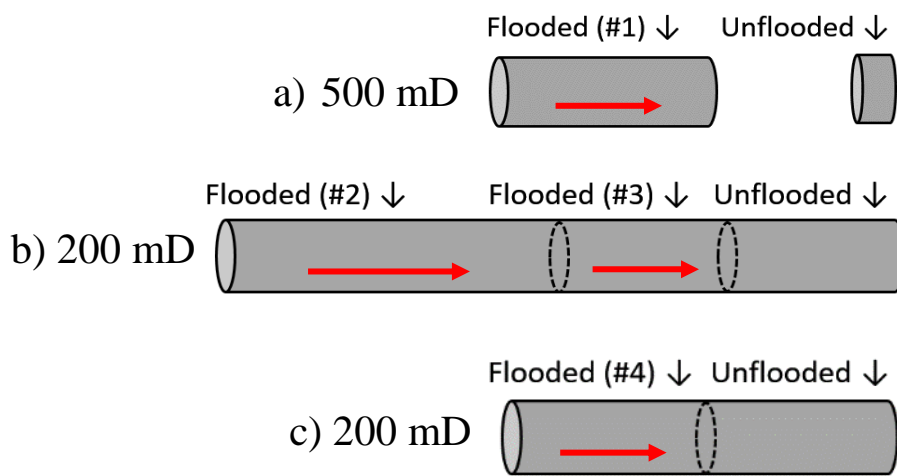
Figure 5. A schematic description of Berea Sandstone core material used for the four different flooding experiments. a) Flooding #1 was conducted on a 500 mD core, where the whole core was flooded. A cm-thick unflooded equivalent from another core was retrieved for comparison of flooded and unflooded material. b) For flooding #2, a 200 mD core was cut in two parts, one was flooded, and one was left unflooded for comparison. Flooding #2 was unsuccessful, therefore the unflooded part was cut in half, where one half was flooded (#3). Flooding #3 was again unsuccessful. c) A 200 mD core was cut in two parts, one for flooding (#4) and one left unflooded for comparison. For figures a) to c), flooding direction is marked with red arrows.
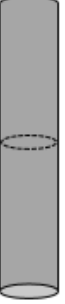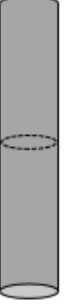
After flooding, the cores were cut into slices of various sizes at UiS, using Struers Accutom 50. Due to the unconsolidated nature of the cores, no water was needed for cooling of the saw blade. Each analysis requiered a certain amount of material; e.g. approximately 4 x 2,5 cm is needed for thin sections, and XRD or GCl analysis requires a certain amount of grams of prepared sample. Therefore, the slices differed in sizes. Table 1 summarizes the core material used and the analysis performed on each sample.

A liquid sample of the SS-solution was collected from flooding #1 directly after 5µm-filtering, whereas the mixed solution of SS + HCl + deionized water (DW) was sampled directly from the piston cell prior to injection. For flooding #4, a sample of SS + HCl + DW was retrieved, as well from the piston cell. According to internal labodatory procedures, no effluent could be sampled. All liquid samples were stored in individual glass beakers (Fig. 6) and dried at 55°C in a heating cabinet to evaporate the water, until the samples were gelled and hard as glass.

Figure 6. Liquid solutions in glass beakers, ready for drying.

Table 1. Sample overview of core material and which samples were utilized for each analysis.

Information	Flooding #1 Flooded	Flooding #1 Unflooded	Flooding #2 Flooded	Flooding #2 Unflooded	Flooding #3 Flooded	Flooding #3 Unflooded	Flooding #4 Flooded	Flooding #4 Unflooded
Material used	Two different core samples. Flooded (#1) ↓ Unflooded ↓		Flooding #2 and #3 was performed on the same core with a common unflooded reference. Flooded (#2) ↓ Flooded (#3) ↓ Unflooded ↓				Flooded and unflooded is of the same core. Flooded (#4) ↓ Unflooded ↓	
Permeability	500 mD		200 mD				200 mD	
Analysis	Sample names and location for analysis							
Optical light microscope (thin section)	SS1, SS2, SS3 (Bureau Veritas, Canada)	UF500 (UiS)	-	-	-	-	FL4in_200 and FL4out_200 (UiS)	UF4_200 (UiS)
SEM and EDS (thin section, core fragment)	FL_500 fragment (UiS), thin sections (B. Veritas, Canada and UiS)	-	-	-	-	-	FL4in_200 (UiS)	-
TEM (FIB-SEM)	FIB-SEM of thin section SS1 (NTNU, Trondheim, Norway)	-	-	-	-	-	-	-
GC	FLin-500 and FLout-500 (Bureau Veritas, Canada)	UF-500 (Bureau Veritas, Canada)	FL2-200 (Bureau Veritas, Canada)	-	-	UF2-200 (Bureau Veritas, Canada)	FL4in-200 and FL4out-200 (Bureau Veritas, Canada)	UF4-200 (Bureau Veritas, Canada)
XRD (milled powder)	FLin-500 (UiS)	UF-500 (UiS)	FL2in-200 (UiS)		FL3in-200 inlet (UiS)	UF2-200 (UiS)	FL4out-200 (UiS)	UF4-200 (UiS)

3.1.2 Flooding procedure

The cores were cut across using a Struers Laboton- 5 saw (Fig. 7a) to achieve the correct size for the core holder. Next, it was covered with Teflon-tape and mounted in a rubber sleeve and into a core holder. Between the sleeve and core holder, high viscous oil was added to help maintain pressure during flooding stage. To prevent the SS to plug the inlet of the core during initial stage of flooding, the solution was filtered through a 5 µm-filter prior to injection, based on experiments conducted on a 500 mD sandstone core by Skrettingland et. al. (Skrettingland et al., 2014). This was time-consuming, as the solution plugged the filter paper several times. Under vacuum, the core was saturated with connate water before a mixture of SS, activator HCl, and DW was injected at room temperature (Fig. 7b). Next, the core-holder was placed in a heating cabinet at 60°C for two days, which is the calculated gelation time for SS with the given parameters. After removing the core from the holder, the Teflon-tape was removed, and flooding direction was marked before wrapping it in plastic foil for storage.
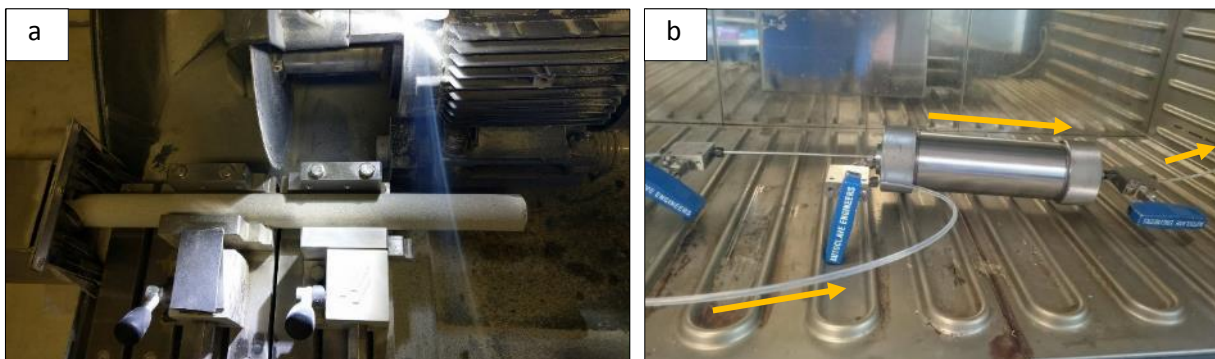
Figure 7. The core-flooding procedure. a) Cutting the core to the appropriate size: one part for flooding, and one unflooded for comparison. b) The mixed solution was injected into the core through the hose on the left side, and effluent went out through the hose to the right - see yellow arrows for direction.

The **main differences** between the individual flooding experiments were as following: A permeability decrease from 500 mD (flooding #1) to 200 mD (flooding #2, #3 and #4). In the first three experiments, the connate water consisted of 50/50 synthetic sea water (SSW)/DW; however, flooding #2 and #3 was unsuccessful due to SS plugging the core. In an attempt to improve the results for flooding #4, the connate water was changed to 2500 parts per million (ppm) NaCl. Flooding #1, #3 and #4 was performed at room temperature, and then placed in a heating cabinet with 60°C, while flooding # 2 was performed at 60°C.

The similar factors were the age of the mother solution- august 2013; prefiltering through 5 µm paper filters; the Na-concentration of 5%, and 14% 1M HCl solution. The total mix was identical; 92 gr SS + 70 gr HC + 337 gr DW.

For a compilation of flooding experiment parameters, see Appendix A.

3.2 Optical light microscopy (OLM)

3.2.1   Sample preparation

In addition to 3 thin sections made at a Bureau Veritas' laboratory in Canada, another 4 thin sections were prepared at UiS; the unflooded 500 mD core, inlet and outlet of the flooded 200 mD core and the unflooded 200 mD core.

Initially, a Lapro Buehler SlabSaw cooled with tap water cut across the cores, before the more precise Struers Accutom 50 cut them lengthwise. To prevent the SS from being mechanically removed from the pore space by a sawblade, the samples were mounted in epoxy consisting of Struers EpoFix Hardener and EpoFix Resin (25:3). The samples were placed in moulds inside the chamber of a Struers Citovac (Fig. 8a). Exposed to vacuum, the epoxy was poured through a hose onto the samples, and shock treatment removed air bubbles. Plastic cups were placed over the samples overnight, before the solid mounts were removed from the moulds (Fig. 8b) and marked properly with sample name and flooding direction. To fully saturate all the pores with epoxy, the samples were cut again (Fig. 8c) and the procedure repeated.
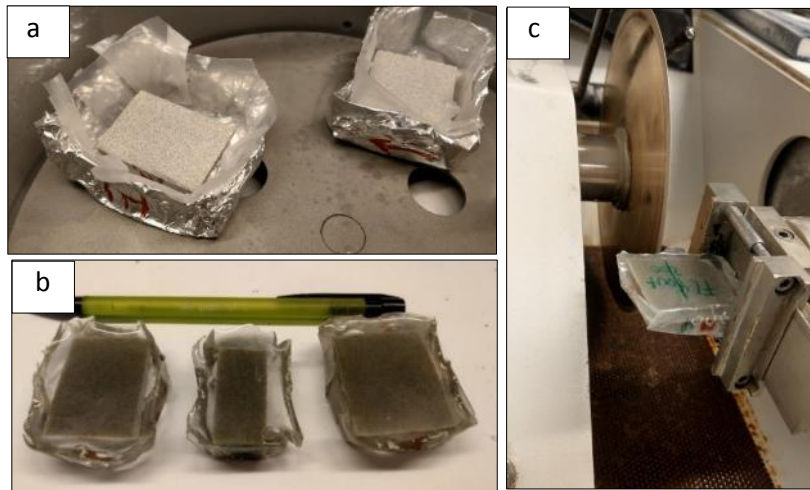
Figure 8. Epoxy saturation of mounts. a) Cut samples were placed in moulds. b) Epoxy has saturated the sample and dried overnight. c) Sample was cut again to assure epoxy being present in all pores.

After overnight drying, the samples were cut and polished with 500 grit sandpaper. The EpoFix Epoxy was mixed under a fume hood and applied to the sample, which had been warmed to ca 40ºC on a hot plate. A glass plate, grinded with 500 grit sandpaper, was placed carefully on the sample, drying for 24 hours (Fig. 9a).

Vacuum attached the glass plate to a sample holder in the Struers Accutom 50 saw, allowing for thinning of the sample to a few millimetres (Fig. 9b). The samples were further grinded on glass plates (Fig. 9c) using one teaspoon of Struers Silicon Carbide Powder and tap water, through the grit steps of 220, 320, 600 and 1000. Samples were controlled in a Zeiss Stemi DV4 binocular between each step. Finally, the thin sections were polished using a Struers RotoPol-35, to achieve the desired thickness of 25-30 µm.
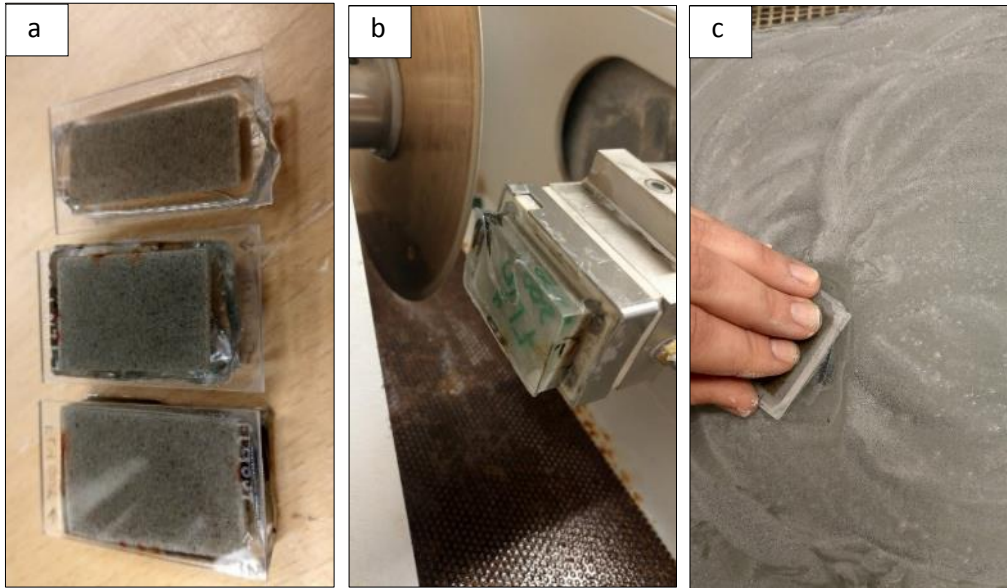
Figure 9. Preparing thin sections. a) Epoxy glued the glass plate to the rock sample. c) Vacuum allowed for cutting the sample. c) Grinding the thin section on glass plates with silicon carbide powder and water.

3.2.2 Methodology

At the UiS, Zeiss Stemi DV4 binoculars and Zeiss Axio Lab 1a light microscope was utilized. An optical light microscope is based on the reflection and transmission of visible light, providing magnifications of the sample up to 20 times. The objective lens collects the light diffracted from the sample placed on the rotating stage, through a series of lenses, forming a magnified image near the oculars (Murphy, 2001). Objective lenses for this microscope are 2,5x, 5x, 10x and 20x. The condenser lens focuses light from the illuminator to the sample, and the condenser diaphragm gathers wave fronts from the light source, illuminating the thin section. The microscope is equipped with a polariser oriented 90° to the light source, making it possible to determine phase differences of the minerals depending on the birefringence.

3.3 X-ray diffraction analysis (XRD)

3.3.1 Preparing for XRD

The XRD-analysis requires milled samples to provide good results. Eight samples were prepared - seven of flooded and unflooded core material, and one of dried SS + HCl + DW from flooding #4. A Struers Accutom 50 cut slices of the cores according to the area of interest; close to inlet and outlet of the flooded cores, and close to the flooded equal of the unflooded core.

A simple manual tool (Fig. 10a) cut fragments off the slices, which were collected in an agate-mortar and milled to the texture of icing sugar (Fig. 10b). Samples were put into small plastic containers. The mortar was thoroughly cleaned with water and ethanol, and finally dried with compressor air.

Further, the samples were evenly distributed and lightly compacted into sample holders (Fig. 10c) by spreading the milled powder with a spatula. This technique is to ensure that the particles lie in a random orientation. A glass plate was pressed evenly down on the sample (Fig. 10d), and excess material was removed. Finally, samples were loaded into the machine (Fig. 10e).
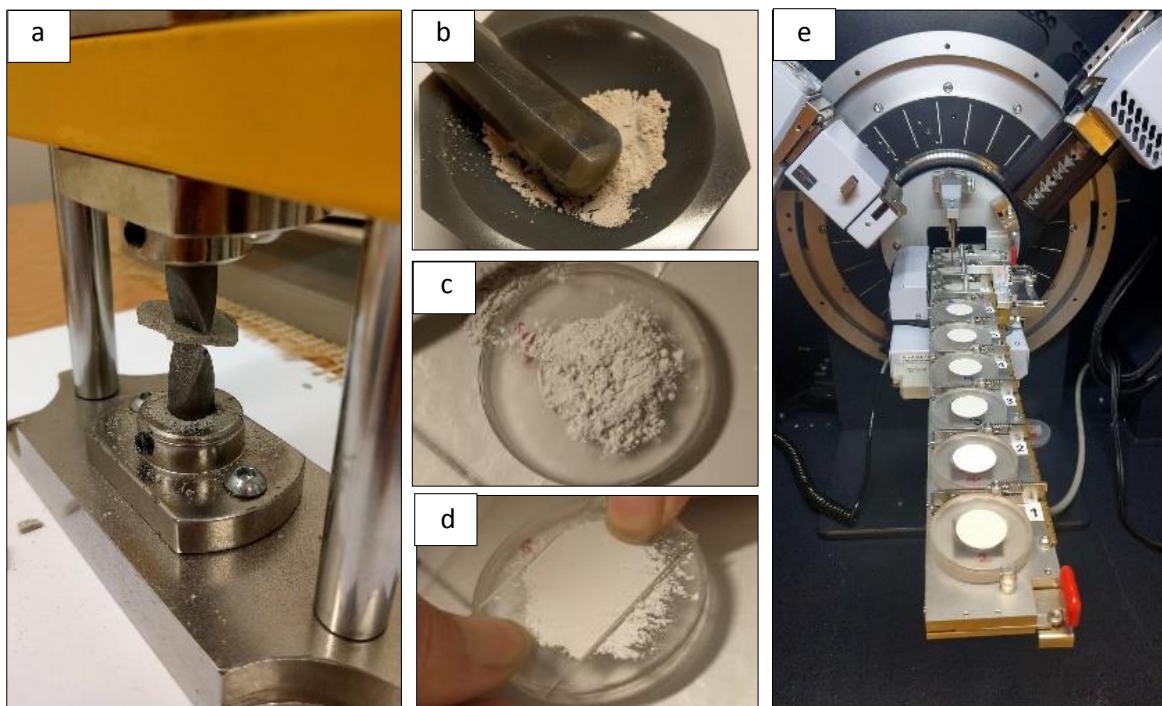
Figure 10. Preparation for XRD. a) Tool used for crushing sample material. b) Agate mortar to mill the samples. c) Milled sample in sample holder. d) Putting even pressure on the milled sample and removing excess material. e) Ready for analysis.

3.3.2 Methodology

XRD-analysis was conducted at UiS, using a Bruker D8 ADVANCE Eco and the software DIFFRAC.SUITE EVA for mineral identification (Robinson, 2009). When a powdered sample is hit by an electron beam, the electrons of the material decelerate and produce electromagnetic radiation; X-rays. The relationship between X-ray wavelength in relation to the diffraction-angle and the lattice spacing which is characteristic for each mineral, is called Bragg's law (Robinson, 2009). This is the principle which XRD analysis and interpretation is based on, illustrated in Figure 11. The electron beam increases the angle of diffraction from $0° - 70°$ during the analysis, resulting in crystallographic planes diffracting X-rays at certain angles, shown as distinctive peaks. The peaks makes it possible to differentiate minerals with similar chemical composition, as each mineral has its own "signature" based on individually unique structures (Robinson, 2009).
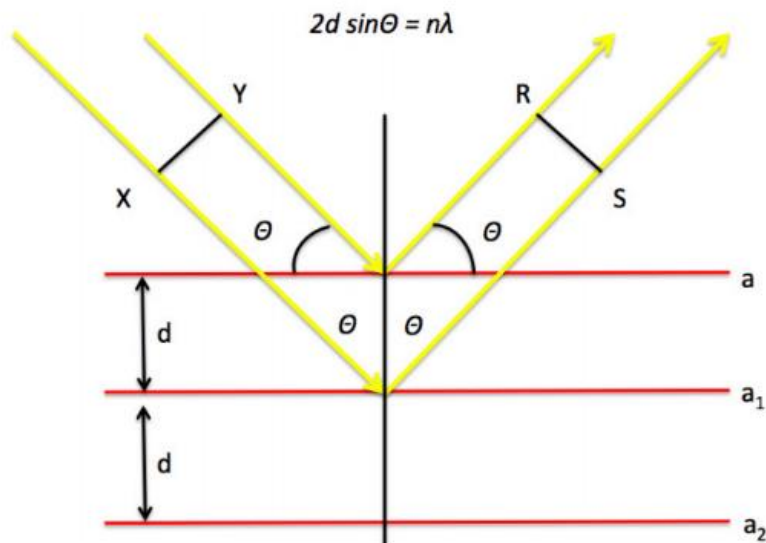
Figure 11. The principle of Bragg's law. X/Y are the emitted X-rays, and R/S are reflected X-rays. a, a_1 and a_2 are crystallographic planes from where X-rays diffract. d is the lattice spacing, and Θ is the diffraction angle. Modified after (Robinson, 2009).

3.4 Geochemistry (GC)

3.4.1 Sample preparation at UiS

According to Table 1, eight core samples- flooded and unflooded- were prepared for GC analysis. In addition, dried SS and SS + HCl + DW from flooding #1 were analysed.

Approximately 1 cm thick slices of the cores were cut with a Struers Accutom 50 saw, using tap water to cool the saw blade (due to the hard epoxy) before cleaning all samples with distilled water. Next, the slices were cut into halves (Fig. 12a), resulting in samples weighing between 11 and 16 grams (Fig. 12b). The SS and SS + HCl + DW were dried according to Chapter 3.1.1, and hard-gelled samples were put in plastic bags for further preparation in Canada (Fig. 12c). SS-sample weighed 4,4 grams and SS + HCl + DW 0,6 grams.
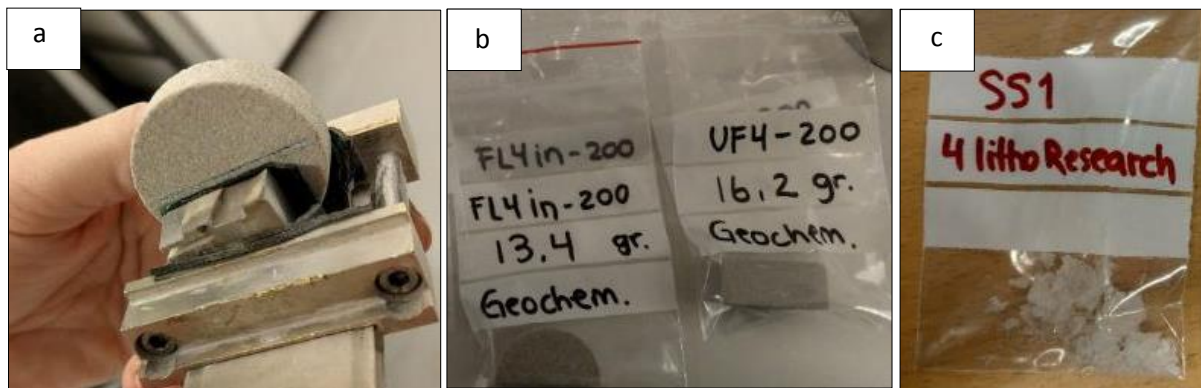
Figure 12. Preparation for GC analysis. a) Core slice in the holder for Accutom 50. b) Double bagged samples ready for further preparation in Canada. c) Bagged sample of SS.

3.4.2 Further preparations (Canada) and methodology

Core samples were sent to Bureau Veritas (former ACME Laboratories) in Vancouver (Canada), for further preparation and analysis. The dried samples of SS and of SS + HCl + DW were sent to ACTLAB, Ontario (Canada). Equipment for preparation of the latter was more appropriate in Canada, due to very limited amount of sample material.

At Bureau Veritas, the core samples were dried at 60° C, before individually crushed to 85%, passing a 200 mesh (75µm). The final stage was to pulverize the samples in a ceramic bowl. The ceramic bowl could add contaminants: Al (up to 0,2%), Ba, Trace rare earth elements (REE).

The samples were then mixed with $LiBO_2/Li_2B_4O_7$ flux in crucibles and fused in a furnace. The cooled beads were dissolved in ACS grade nitric acid and analysed by inductively coupled plasma mass spectroscopy (ICP-MS). Loss on ignition (LOI) was determined by igniting a sample split then measured the weight loss. The samples were weighed into a tarred crucible and ignited to 1000°C for one hour, then cooled and weighed again. The loss in weight is the LOI of the sample. Total Carbon and Sulphur were determined by the LECO® method. Here, induction flux was added to the prepared sample then ignited in an induction furnace. A carrier gas sweeps up released carbon to be measured by adsorption in an infrared spectrometric cell. Results are total concentrations and attributed to the presence of carbon and sulphur in all components. An additional 14 elements were measured after dilution in Aqua Regia. The prepared samples were digested with a modified Aqua Regia solution of equal parts concentrated HCl, HNO_3, and DI-H_2O for one hour in a heating block or hot water bath. The sample volume was increased with dilute HCl- solutions and splits of 0,5g were analysed. None of the measured concentrations was too far above the possible detection limit, but in standard range, and accuracy and precision are between 1-2%.

"4Lithoresearch" analysis was performed by ACTLABS, on the dried SS and SS + HCl + DW from flooding #1. At their preparation laboratory in Canada, the samples were first pulverized by hand, and then mixed together with lithium metaborate and lithium tetraborate, before melting in a furnace. The melt was mixed until dissolved in a solution of 5% nitric acid.

Major oxides and trace elements of the fused samples were analysed on an Agilent 700 Series Inductively coupled plasma optical emission spectrometry (ICP-OES). CANMET (Canada Centre for Mineral and Energy Technology) and USGS (U. S. Geological Survey) reference materials were used for calibration for every ten samples. The fused samples were diluted and analysed by Perkin Elmer Sciex ELAN 6000, 6100 or 9000 ICP/MS, with instrument calibration every 40 samples.

3.5 Scanning electron microscopy (SEM) and Energy dispersive x-ray spectrometry (EDS)

3.5.1   Sample preparation

A variety of samples were studied in the SEM and EDS (Fig. 13a): thin sections, core fragments and dried SS solution. For EDS-analysis, polished surfaces were preferred; however, fresh surfaces were favoured for imaging the gel on a micron- and nano-scale, as the surface was not corrupted by grinding and polishing.

The thin sections were prepared as described in Chapter 3.2.1. With double sided carbon tape, the samples were attached to sample holders. Core fragments with approximate size of 1 x 0,5 cm were simply chopped off the core material and mounted onto sample holders with double sided carbon tape. The dried samples of SS and SS + HCl + DW were dismembered into small pieces and placed carefully on double sided carbon tape on a sample holder (Fig. 13b).

Palladium (Pd) or carbon (C) coating was applied on all samples prior to analysis, using Emitech K550X, with TK8885 Palladium 60 mm Dia x 0,1 mm x1 (Fig. 13c). This conductive layer is a necessity to enable good quality imaging of samples, as well as to avoid charging of the sample. After cleaning the chamber thoroughly with ethanol and placing the samples inside, argon gas was used to create a vacuum and the coating of Pd was finalised.

Figure 13. Sample preparation for SEM and EDS. a) A sample holder containing 3 samples: dried SS (upper left corner), core fragment (lower left corner) and thin section (right side). b) A close-up of the mounted dried SS + HCl + DW. c) Pd coating.

3.5.2 Methodology

At UiS, the Zeiss Supra 35VP Scanning electron microscope was utilized for SEM analysis (Fig. 14). EDAX Octane Elite 25 is the Energy dispersive X-ray spectrometer used for measuring chemical compositions.
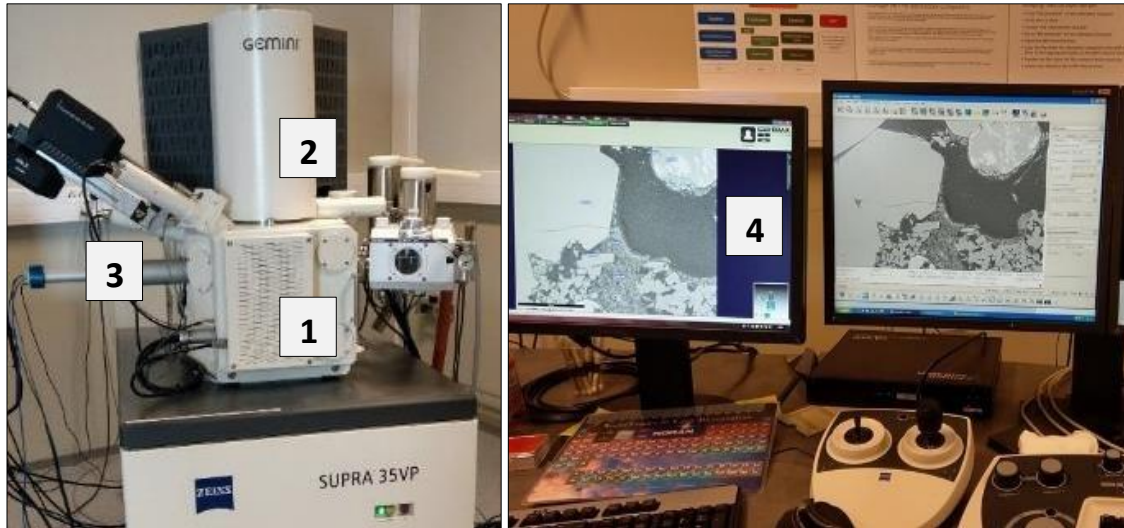
Figure 14. The set-up of a SEM at UiS. 1: sample chamber, 2: electron gun, 3: detectors. 4: Imaging and results shown on a computer screen connected to the SEM.

The sample is exposed to vacuum in the SEM-chamber, where an electron gun beams the sample with accelerated high intensity electrons from a field emission gun, providing good resolution and a small spot size down to 1-2 μm. Before the electrons hit the sample surface, they are sent through different lenses, which focus the beam. Figure 15 shows a schematic set up for a SEM, where the electron gun in placed above two condenser lenses, an objective lens, the detector system and a set of deflectors (Khursheed, 2010).

The machine can simultaneously measure X-rays, cathodoluminescence light, augur electrons, and the more commonly used electrons for SEM analysis, which are backscattered electrons (BSE) and secondary electrons (SE). The energy of secondary electrons varies and provide varying images depending on topography and composition of the sample. High-resolution images are created when the secondary electrons are gathered in the SE-detector. Backscattered electrons are scattered from a deeper level of the sample than secondary electrons, which escape from closer to the sample surface (Khursheed, 2010). The BSE image display a change in greyscale depending on the variation of atomic number in the sample surface, as showed in Figure 16. This is valuable when distinguishing phases of a sample and when identifying areas of interest for EDS-analysis.
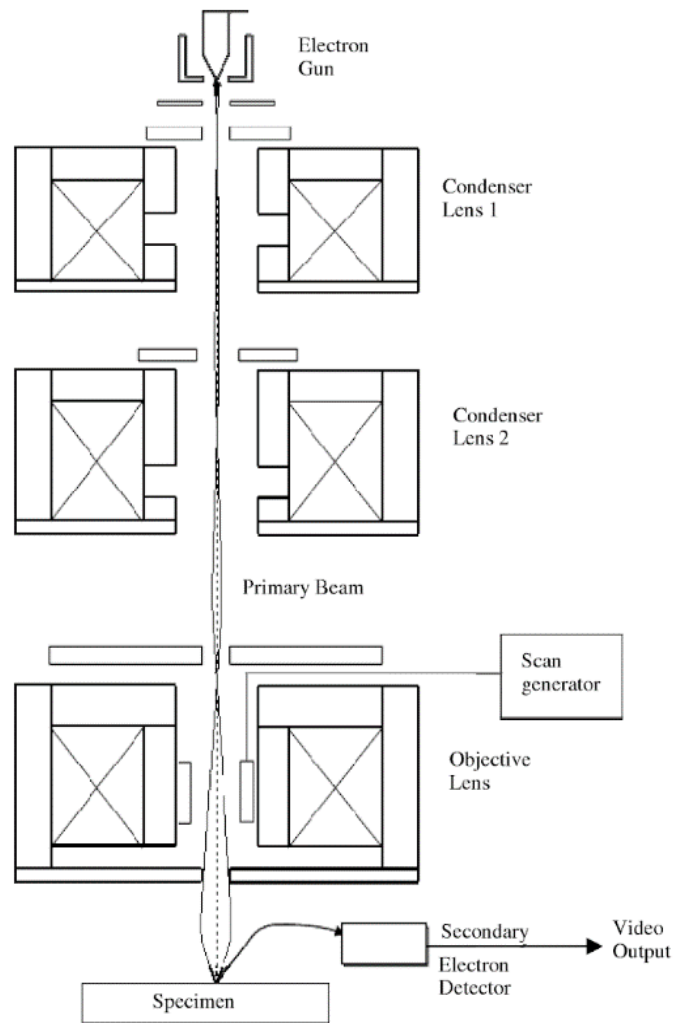
Figure 15. A schematic set up of the SEM (Khursheed, 2010).
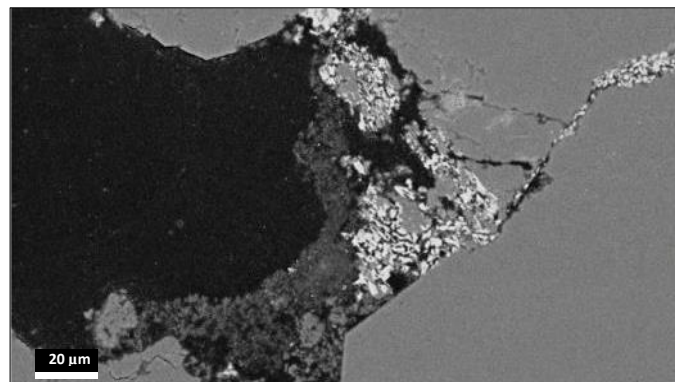
Figure 16. Example of a BSE image, providing information about the different minerals atomic number, according to levels of greyscale.

X-rays are produced when an electron moves from the outer to the inner shell of an atom, and they can be detected by the EDS which is coupled with the SEM. Each element has a different specific energy level of X-rays. The chemical composition is analysed by a 2 μm wide beam or the average of a selected area. Abundance of elements present in the sample is given either as a spectrum, or as a map of the elements of interest. The EDS is equipped with a software, which aids identifying the elements in the spectrum, based on standard values. Ideally, standards should be used for assuring precise measurements, however, there are no available standard for SS.

For this study, the standard acceleration voltage was set to 15 kV, working distance 10 mm, and aperture size 15-30 μm. For the EDS point analysis, live seconds was mainly set to 100 seconds, and for mapping, approximately 100 frames were mapped at a resolution of 1024 x 800.

3.6 Transmission electron microscopy (TEM)

3.6.1 Sample preparation

A FIB/SEM sample was prepared at the Norwegian University of Science and Technology (NTNU), Trondheim, using a FEI Helios G4 UX. The area of interest was in advance located in a polished thin section of the flooded 500 mD core, using SEM (Fig. 17).
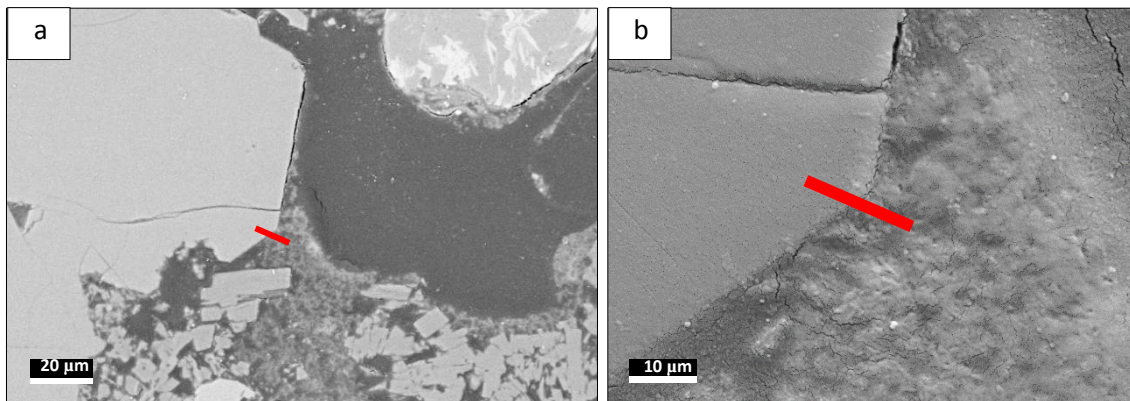
Figure 17. SEM-image of FIB/SEM sampling area. a) The red line illustrates where the sample was retrieved, in the transition between a quartz grain and gelled SS (BSE image). b) Magnification of the sampled area (SE image).

The thin section was initially coated with carbon. Protection layers of carbon were deposited on the selected area from where the sample would be extracted. The material on each side of the protection layers was removed by a Ga^+ ion-beam sputtering (Fig. 18a), leaving a sample with a size of approximately 14 μm x 14 μm x 2 μm (Fig. 18b). A wolfram-needle was welded to the sample by carbon (Fig. 18c), as the precursor gas Naphthalene ($C_{10}H_8$) was injected into the chamber. The ion-beam was used to break the atomic bonds in the precursor gas, leaving carbon material at the location where the ion-beam was hitting the sample surface. The FIB/SEM-sample was further attached to an omniprobe copper grid, so that it could easily be detected in the TEM (Fig. 18d), despite the microscopic size. Sample thickness needed to be reduced from 2 μm to ideally 100 nm for good quality TEM-results. Thinning of the sample was achieved by beaming it while gradually tilting to 52° in the chamber, and by gradually lowering the acceleration voltage from 30 kV to 2 kV.
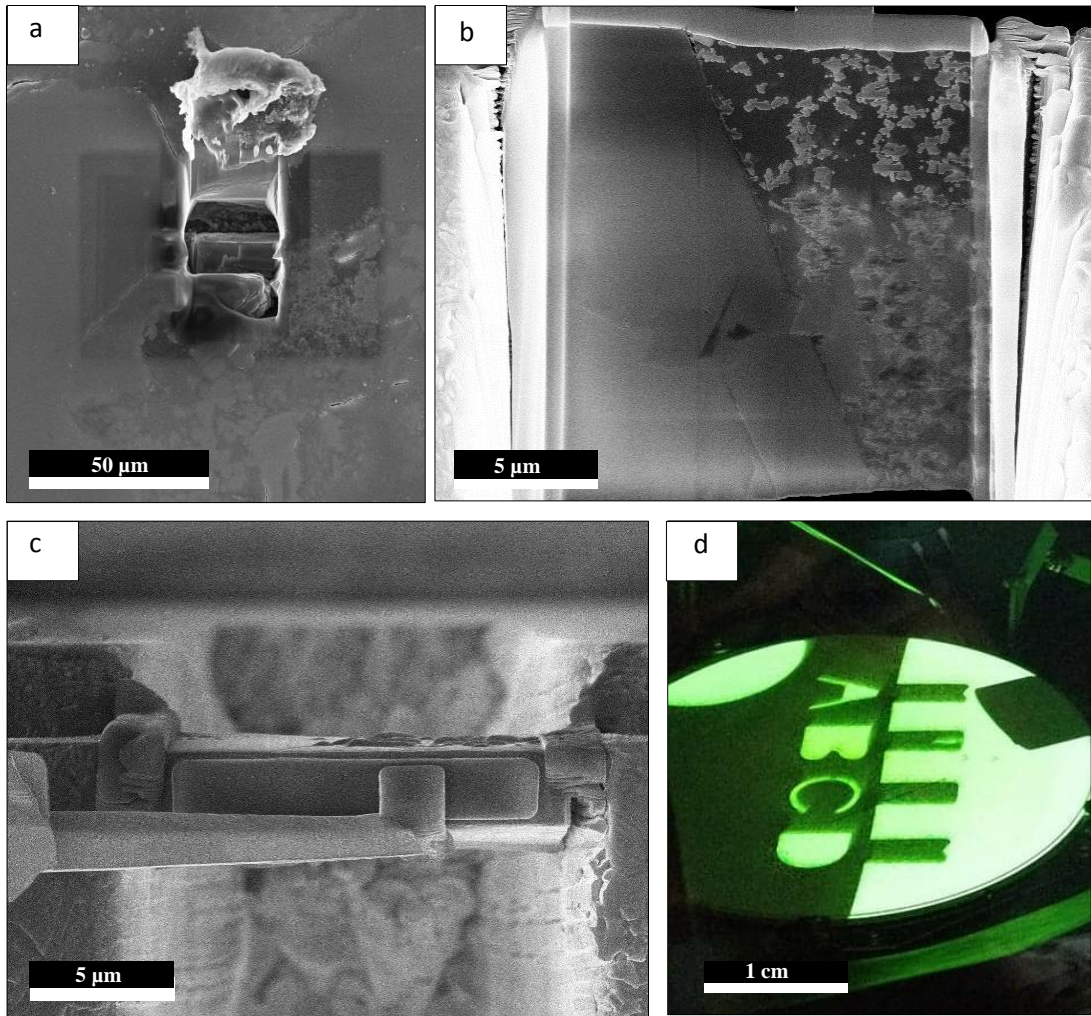
Figure 158. FIB/SEM sample preparation for TEM. a) BSE overview-image of the hole in the thin section where the FIB/SEM-sample was to be retrieved. b) Wolfram needle welded to the carbon on top of the FIB/SEM-sample. c) 14 µm x 14 µm FIB/SEM-sample. d) The omniprobe, here shown magnified in the TEM. For Figure a) – c), BSE-images, 15 kV, WD: 4 mm.)

3.6.2 Methodology

The FIB/SEM sample arrived from NTNU in a box, attached to the omniprobe (Fig. 19a). The omniprobe is carefully removed with a tweezer and placed onto the double tilt TEM-sample holder (Fig. 19b). Two copper-rings are secured on top of the sample to prevent it from being able to move. Next, the sample holder is placed into the sample chamber in the TEM (Fig. 19c).
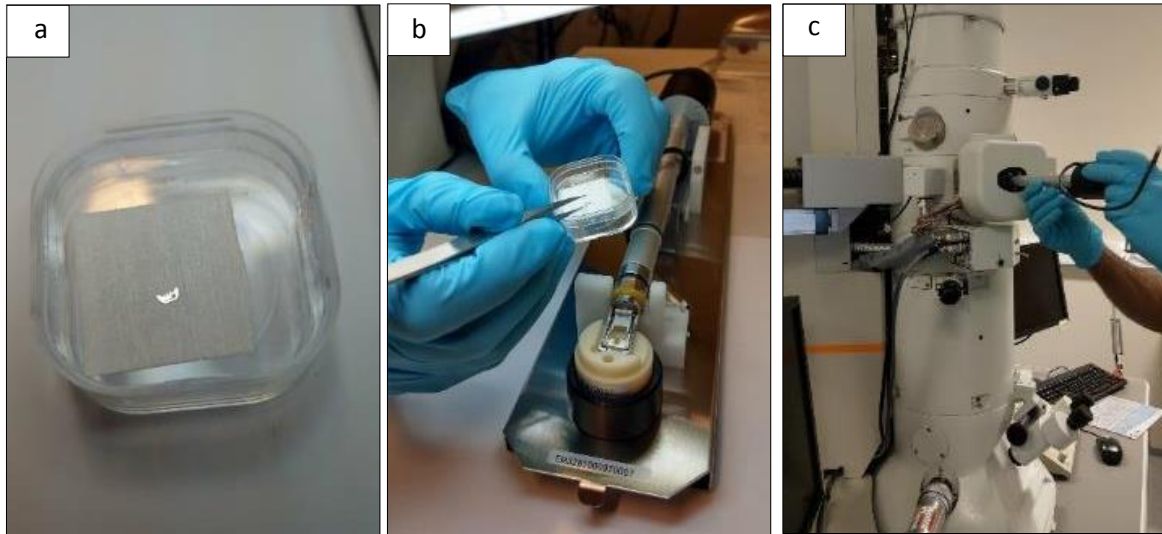
Figure 169. FIB/SEM-sample. a) The sample is attached to an omniprobe, the small shiny object. b) Carefully moving the omniprobe to the sample holder. c) Sample holder is placed in the sample chamber in the TEM.

On the top of the Jeol JEM-2100 Transmission electron microscope (Fig. 20), the illumination system consisting of a filament (LaB$_6$) is heated up, generating an electric field of 200kV (Solberg and Hansen, 2007). The electrons are directed towards the sample, using a condenser lens below the filament. The condenser lens is a magnetic field produced by a magnetic current, which condenses the beam. When the primary beam interacts with the atoms in the sample, it releases several signals. For the TEM, the most significant signals are the ones which transmit through the sample, unlike in the SEM, where BSE, X-ray or SE is used. These signals are also detected in the TEM, though not frequently used.

Figure 20 shows the arrangement of the TEM. From the top, the illumination system consists of a filament generating the electrons, and a condenser lens, directing the beam towards the sample. Below is the sample chamber and the objective - this generates and magnifies the

image. Located underneath are the intermediate lenses and projector lenses which magnifies further. Finally, the viewing system displaying the magnified image of the sample with or without binoculars, as well as sending the image to the computer screen using a camera.

At the rear of the machine, an EDS detector is installed for analysing chemical composition based on X-ray measurements.
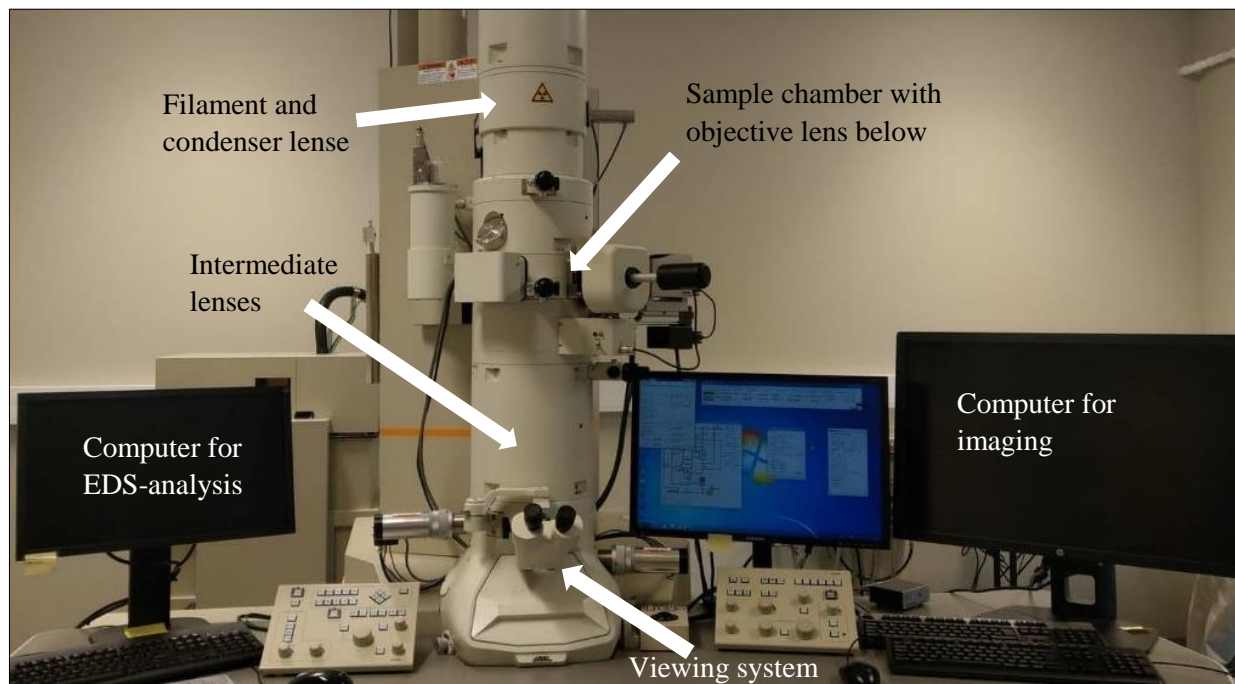
Figure 20. The set-up of the Jeol JEM-2100 Transmission electron microscope at UiS.

4 Results

4.1 Optical light microscopy (OLM)

4.1.1 Binoculars

Fragments of the **unflooded 200 mD core** are used to determine the texture of the rocks. The Berea sandstone is in average a well to very well sorted, medium sized sandstone (200-600 µm), grains are sub-rounded to rounded with medium to high sphericity. Distribution is uniform with no visible alignment. The easy breakable material indicates poor consolidation and/or weak cementation. Kaolinite fills most of the pore spaces of the unflooded 200 mD core (Fig. 21a). The pore space of the **flooded 200 mD core** is also filled with a white, relatively soft substance (Fig. 21b), however, less amounts than in the unflooded. There was no noticeable change in hardness after flooding; grains could easily be scratched off with a finger.
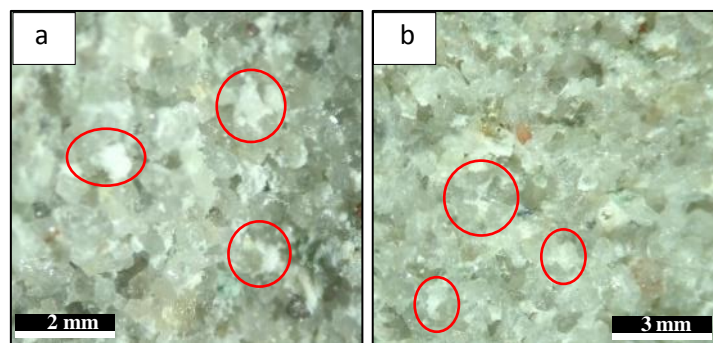
Figure 21. A white substance within the pore space in both a) the unflooded 200 mD core and in b) inlet of the flooded 200 mD core. Marked with red circles.

4.1.2 Light microscope

Thin sections of **unflooded 500 mD and 200 mD core samples** are studied for mineralogical composition, determined by the relief, birefringence and other optical properties of each mineral. In general, the Berea Sandstone is composed of mainly quartz, feldspar- both completely dissolved, partly dissolved (Fig. 22a) and well-preserved (plagioclase with lamellar twinning and microcline with crosshatched twinning), kaolinite (Fig. 22b), heavy minerals (e.g. zircon, tourmaline, rutile), muscovite, meta-psammitic rock fragments of layered quartz and muscovite, and carbonate cement. Hematite, pyrite and pseudo matrix of dissolved feldspar or sericite (fine grained mica) are observed. There are only minor varieties observed when comparing 500 mD and 200 mD cores, for instance the degree of roundness of

tourmaline (very well-rounded grains in 200 mD, Fig. 22c), not observed in the 500 mD core), and less amount of carbonate cement in 200 mD compared to 500 mD. The pore space in the unflooded thin sections is homogenous and dark in cross polarized light, except from the pores containing cement, kaolinite, matrix or pseudo-matrix.
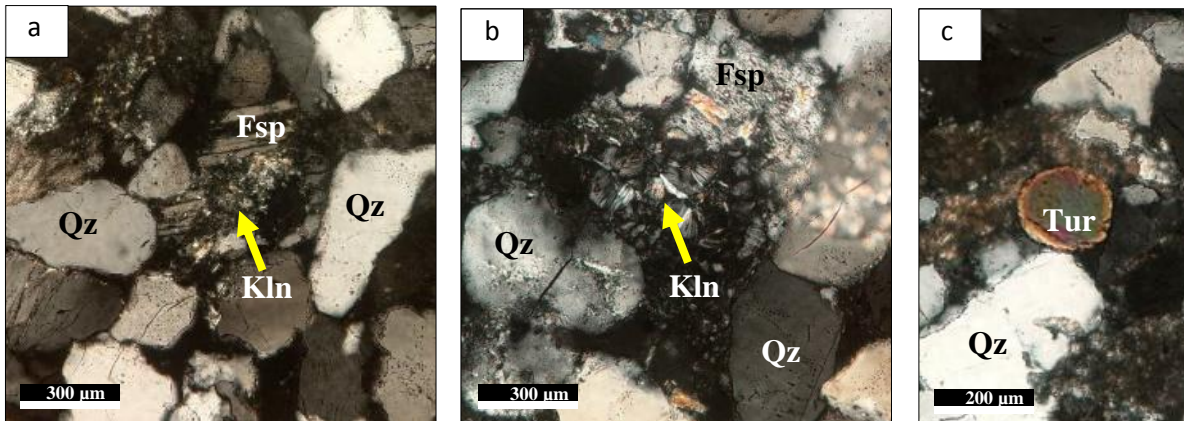
Figure 172. Thin section of flooded 200 mD core. a) Partly dissolved feldspar with kaolinite filling in the pore space. b) Kaolinite in the pore space next to a dissolved feldspar. c) Very well rounded tourmaline. Fsp= feldspar, Qz= quartz, Kln= kaolinite. Tur=

Thin sections of **flooded 500 mD and 200 mD cores** are investigated at high magnifications to detect the gelled SS. Observations indicating gel is made in several pores in the flooded 500 mD core. In cross polarized light, one can observe a rim-less undulose extinction from the surrounding grains into the pore space (Fig. 23), not a typical feature for the thin section resin. However, the gel can not be located in thin sections of the flooded 200 mD.
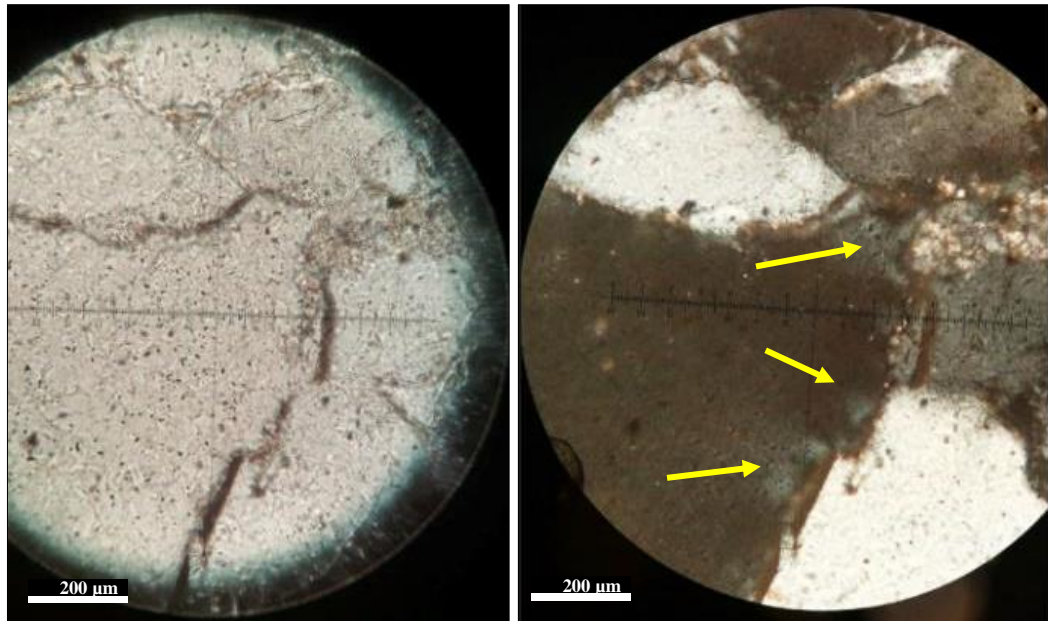
Figure 183. Thin section of flooded 500 mD core. In cross polarized light, the yellow arrows point to the undulose extinction indicating SS gel precipitating on the nearby grain surfaces.

4.2 X-ray diffraction analysis

To best identify the gel in the flooded cores, the SS + HCl + DW from flooding #4 are scanned on its own as a reference line to compare with the flooded 200 mD core material. The flooded and unflooded 500 mD and 200 mD core samples are scanned (see Table 1, Chapter 3.1.1), showing close to identical mineralogy.

The limited amount of dried SS + HCl + DW from flooding #1 hinders an XRD-analysis of this sample; however the flooded and unflooded 500 mD cores are presented together in Figure 24. Comparing the flooded (black line) and unflooded (red line), it is obvious that there are no significant changes in mineralogy despite them being of two separate cores. The minimal variation between flooded and unflooded can only be seen by magnification, as seen in the inset-image uppermost right corner and could be either due to minor mineralogical changes or the presence of SS gel.

Four peaks are detected in the XRD when analysing the SS + HCl + DW, however, none of these phases are recognised nor identified by the software mineral library. The line is
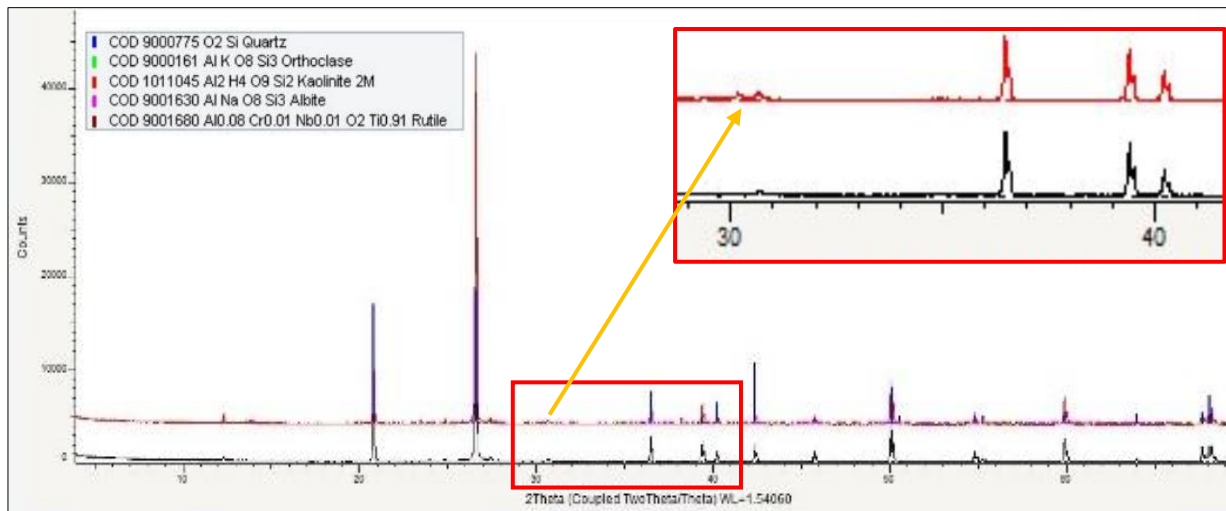
Figure 194. XRD of 500 mD core. Main minerals are compiled in the upper left corner. The red square marks the magnification where a minor variation (orange arrow) from flooded to unflooded can be observed.

displayed on top of the flooded and unflooded samples of the 200 mD in Figure 25, showing the inconsistency between the flooded core containing gel, and the actual gel which was injected into it. None of the SS + HCl + DW peaks matches with the flooded core sample. Comparing the flooded and unflooded 200 mD core samples in the same figure, no visible changes has occurred subsequently to the flooding.
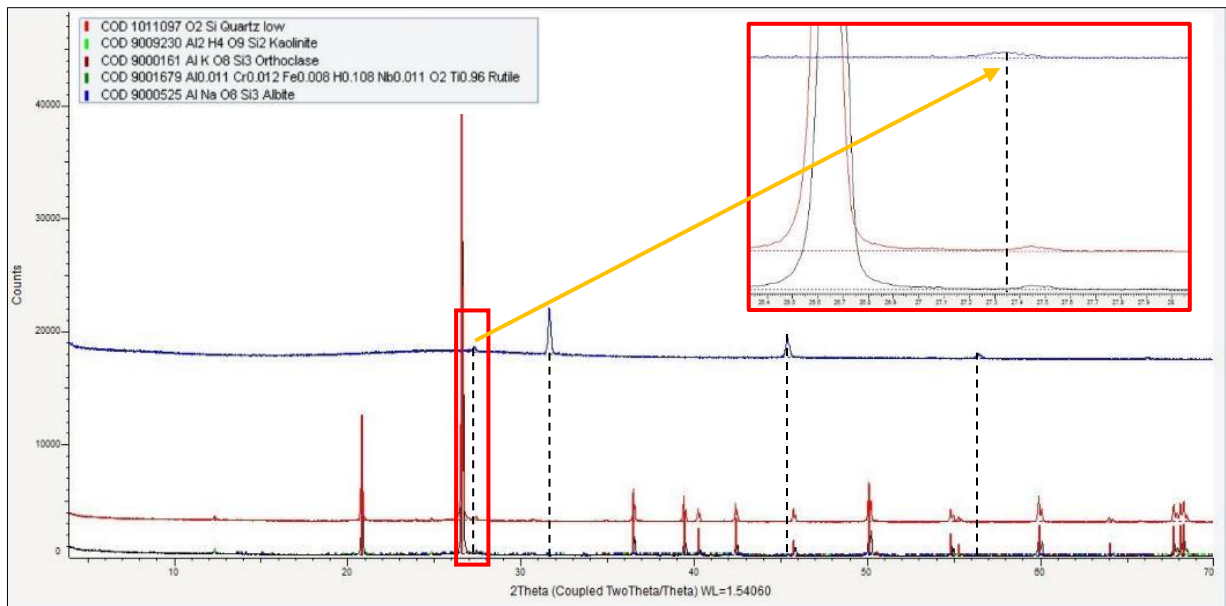
Figure 205. XRD of 200 mD core. Main minerals of the samples compiled on the left side. The red square marks the magnification of a SS + HCl + DW peak, showing inconsistency between gel (blue line), and flooded sample containing gel (lowermost black line). Dashed black lines are added to underline that there is no direct match between any of the SS + HCl + DW peaks and the peaks in the flooded core sample.

4.3 Geochemistry

GC data of the Berea Sandstone cores before and after flooding differ in very few aspects. Generally, the rock is geochemically dominated by silica and few wt% of Al_2O_3. All other elements are strongly depleted besides some trace elements such as Zr, Hf and Yb.

The unflooded 500 mD and 200 mD core samples have low Na_2O concentrations with 0,13 and 0,14 wt%, respectively. In the experiment with the 500 mD sample the Na_2O concentration increase nearly about 100% to 0,22 wt% for the inlet, and the outlet is less affected by the polymer with 0,18 wt%. Also, Zr has a notable doubling of content, from 142 ppm (flooded) till 281 ppm (unflooded). A similar trend can be observed in the 200 mD sample where the inlet has 0,27 wt% Na_2O and the outlet nearly the same abundance with 0,30 wt%. The most relevant major elements are listed in Table 2.

The composition of dried SS and SS + HCl + DW from flooding # 1 are dominated by SiO_2 (58,6% and 56,5%, respectively) and Na_2O (17,9% and 15,3%, respectively). The analysis however, shows a major variance in the Fe_2O_3 content. Prior to mixing the SS with HCl, the abundance was 0,8 wt%, and after mixing it ascends to 15,8 wt%. All trace elements increase after adding HCl to the SS solution, e.g. Cr (40 to 280 ppm), Co (less than 1 to 4 ppm) Cu (<10 to 60 ppm), Rb (1 to 4 ppm), and Mo (less than 2 to 9 ppm).

Table 2. Relevant major element GC data of all samples. MDL = method detection limit. % = weight percentage. N/A= not applicable

Elements	SiO_2	Al_2O_3	Fe_2O_3	Na_2O	K_2O	LOI
Unit	%	%	%	%	%	%
MDL	0,01	0,01	0,04	0,01	0,01	
Unflooded 500 mD	93,4	3,0	0,5	0,13	0,8	1,2
Inlet 500 mD	93,9	2,8	0,5	0,22	0,7	1,0
Outlet 500 mD	94,0	2,8	0,5	0,18	0,7	1,2
Unflooded 200 mD	93,6	3,0	0,5	0,14	0,8	1,3
Inlet 200 mD	93,1	3,2	0,6	0,27	0,9	1,4
Outlet 200 mD	93,2	3,1	0,5	0,30	0,8	1,3
SS (flooding #1)	58,6	0,5	0,8	17,9	0,1	20,9
SS + HCl + DW (flooding #1)	56,5	1,4	15,8	15,3	0,3	N/A

For the complete overview of GC results of all samples, see Appendix B.

4.4 Scanning electron microscopy (SEM) and Energy X-ray dispersive spectrometry (EDS)

Three dried samples of the solutions are studied first; SS and SS + HCl + DW from flooding #1 as well as SS + HCl + DW from flooding #4. Following, the unpolished core fragment of the flooded 500 mD, and finally two thin sections of the flooded 500 mD core are investigated. Thin sections of the flooded 200 mD (flooding #4) are studied, however, no SS gel is found in the pore space. No sample of the unflooded material is investigated with this method.

Dried SS from flooding #1

The sample of the SS solution was retrieved before HCl and DW was added, then dried according to Chapter 3.1.1. The surface of the dried sample (Fig. 26) appeared rough and rugged yet relatively low grown (red point), with relatively large areas (tens of μm) of smooth-skinned surfaces (blue point). EDS-measurements identify Na, O and Si. The two measured points show these elements with a variation in content of in particular Si and Na, with an increased amount of Na in the smooth-skinned area (blue point).
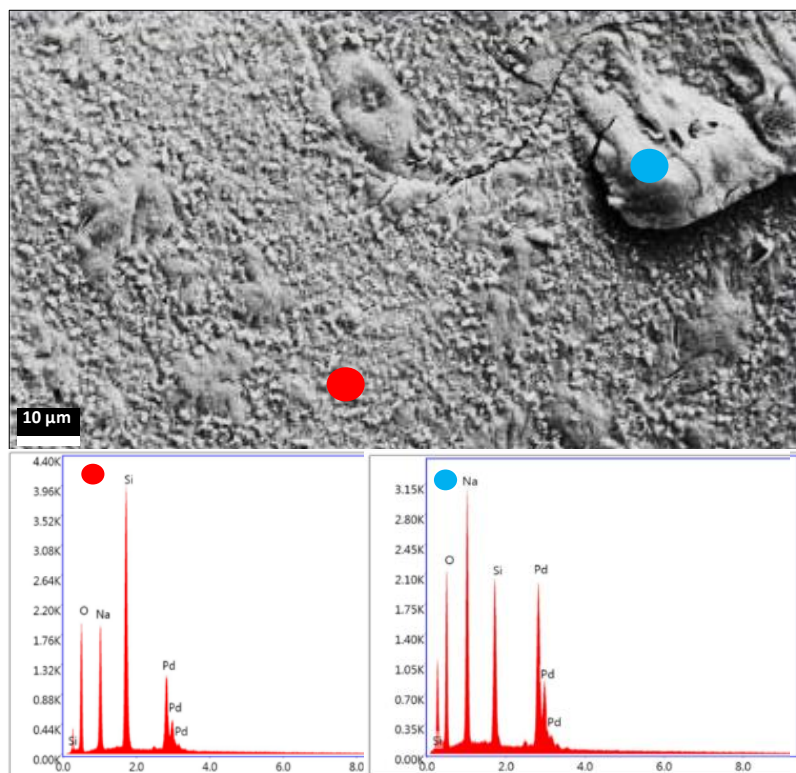
Figure 216. SE-image of dried SS (flooding #1). Two EDS-measurements show the content of Si, O and Na. Pd due to coating.

Dried SS + HCl + DW from flooding #1

As HCl is added to the solution, the dried surface appears more topographic (Fig. 27a), with completely dissimilar structures. In the loose fragment of dried SS + HCl + DW in Figure 27b), smooth pillow-like structures dominate (blue point) with 2-6 µm long needles attached. Figures 27c) to e) show other areas of the underlying surface of the dried sample, covered in acicular crystals, approximately 80 - 200 nm thick individual "tubes", 4 µm or longer. The EDS detects two types of phases for the SS gel in this specific sample; a pillow-structured precipitation with Cl, and acicular precipitation without Cl.
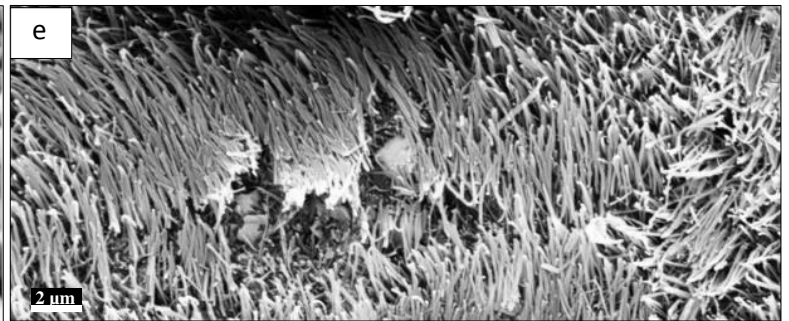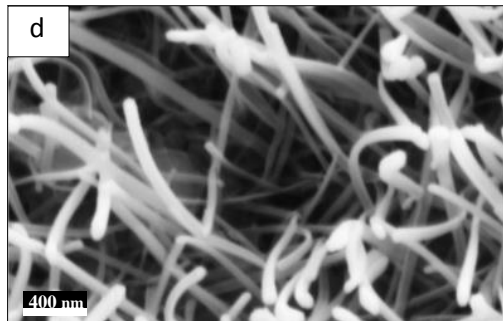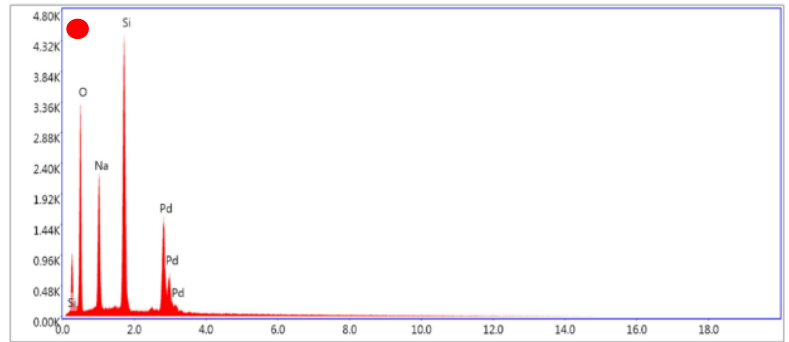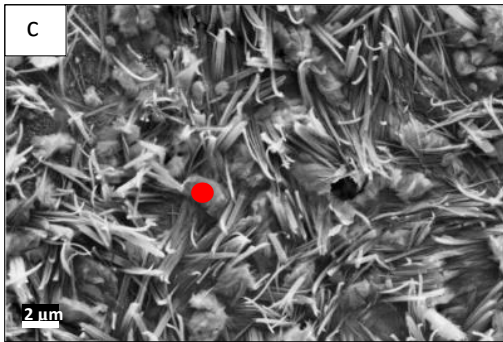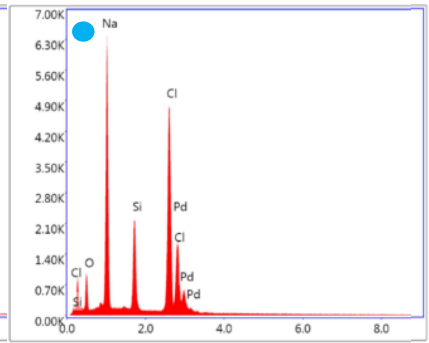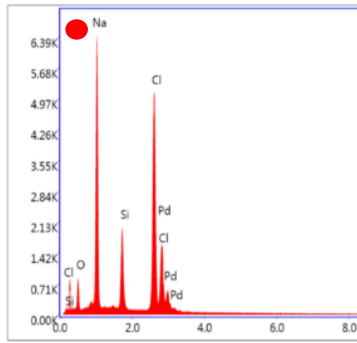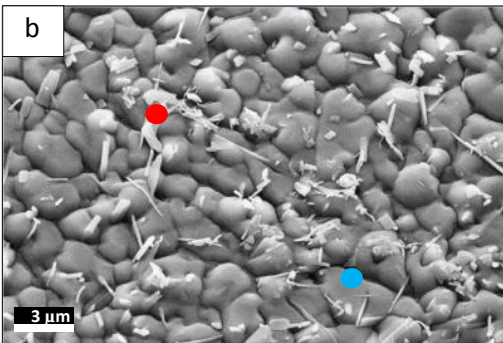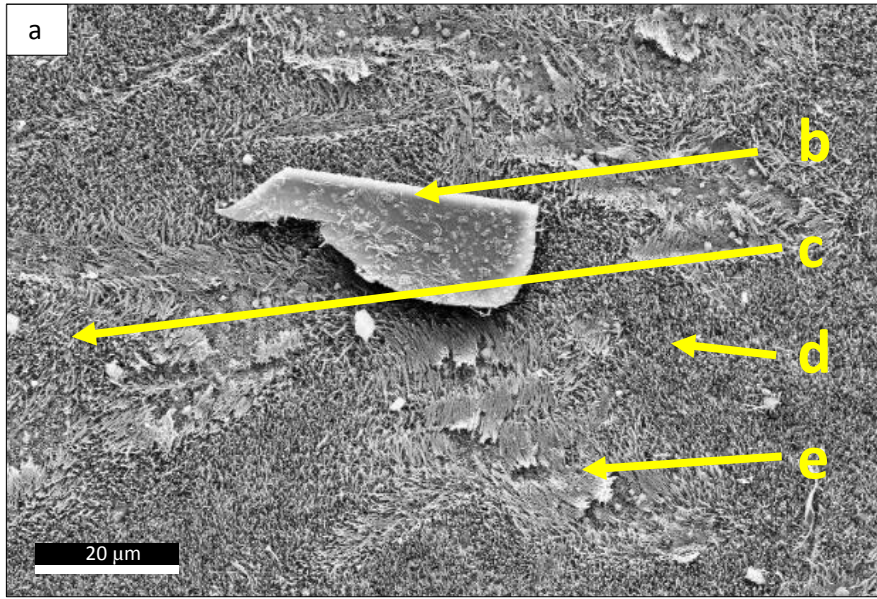
Figure 227. SE-images of dried SS + HCl + DW from flooding #1. a) An overview of the sample, showing the locations of figures b) to e). b) EDS-measurements show high peaks of Cl and Na. c) The surface in this location is dominated by acicular crystal "tubes", with a high content of Na and no Cl. d) and e) are further magnifications of the "tubes", for imaging. No EDS analysis preformed.

Dried SS + HCl + DW from flooding #4

A wide diversity of NaCl-crystals (red points in figures 28a) to c)) has precipitated on the surface of the dried sample, whereas Si seemingly has fractionated on the "floor" (blue points in figures 28b) and c)). The crystal habits are irregular, layered or cubic – the latter being more similar to a euhedral NaCl-crystal.
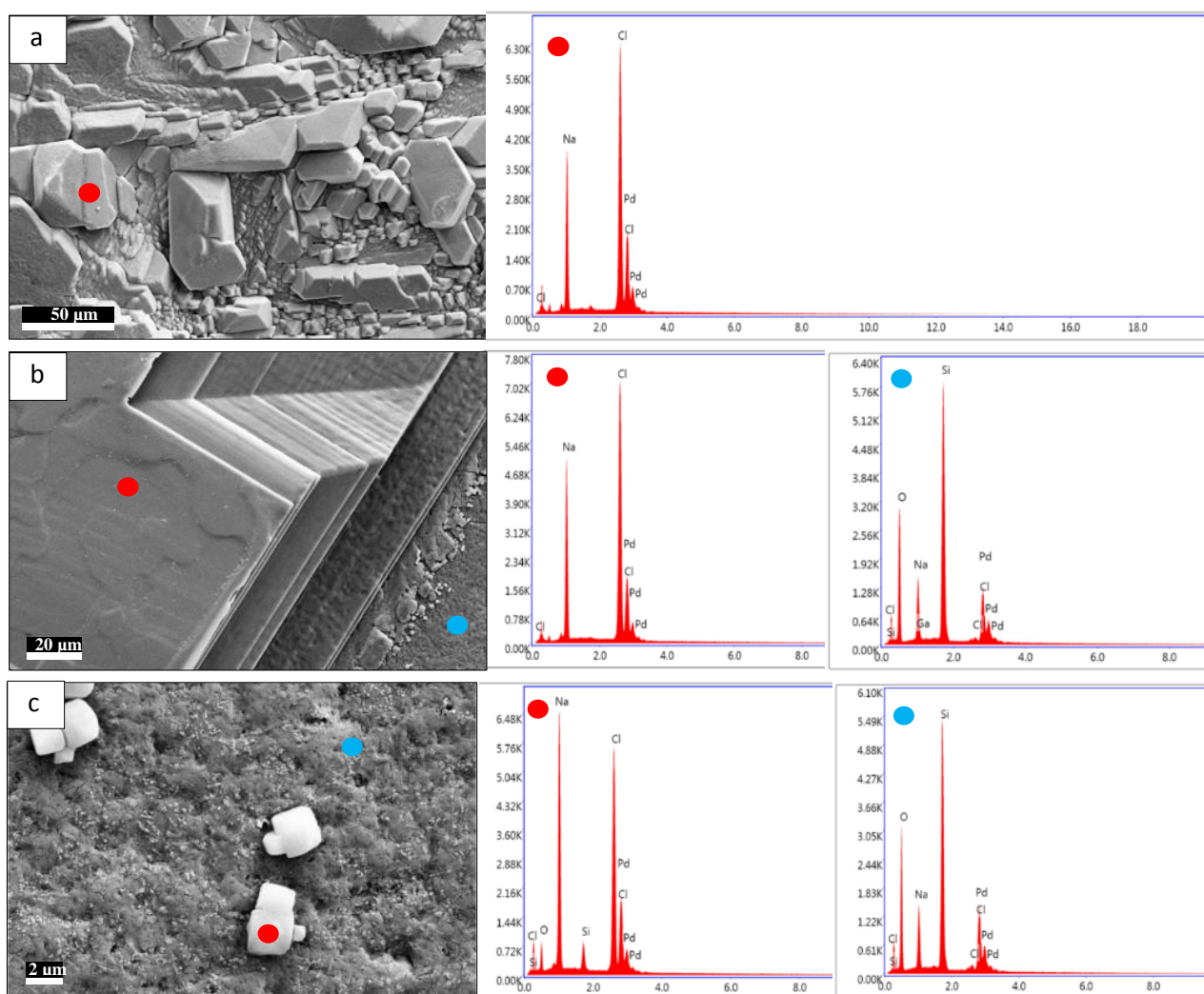
Figure 238. NaCl-precipitation on the surface of SS + HCl + DW (flooding #4). a) Irregular NaCl crystals with no visible "floor" to measure Si and Cl abundance. b) A sharp boundary between the relatively wide layer of NaCl (red point) and the surface of the gelled SS (blue point). c) Cubic NaCl crystals (red point) spread on the Si-enriched surface (blue point).

Fragment of flooded 500 mD core

In this unpolished sample, the gel is visual in three dimensions, revealing precipitation on the grain surfaces both as visible agglomerations with a globular habit (figures 29a) to c)) as well as acicular structures (Fig. 29d) as seen in Figure 27. The gel grows on both kaolinite ($Al_2(Si_2O_5)(OH)_4$) and on quartz (SiO_2). EDS detects Cl and Al in gel precipitated on kaolinite, however in the neighbouring gel, both Cl and Al are absent.
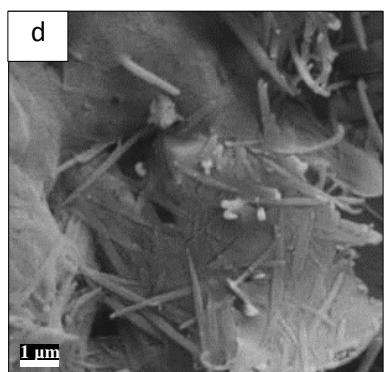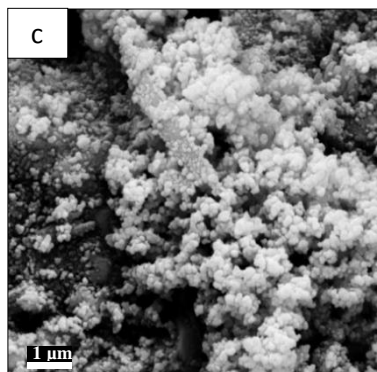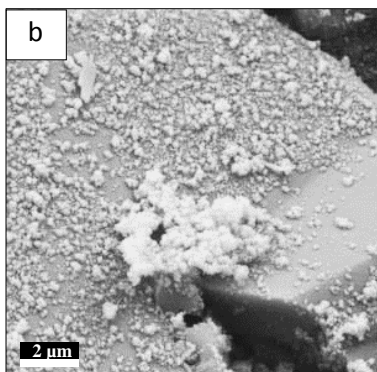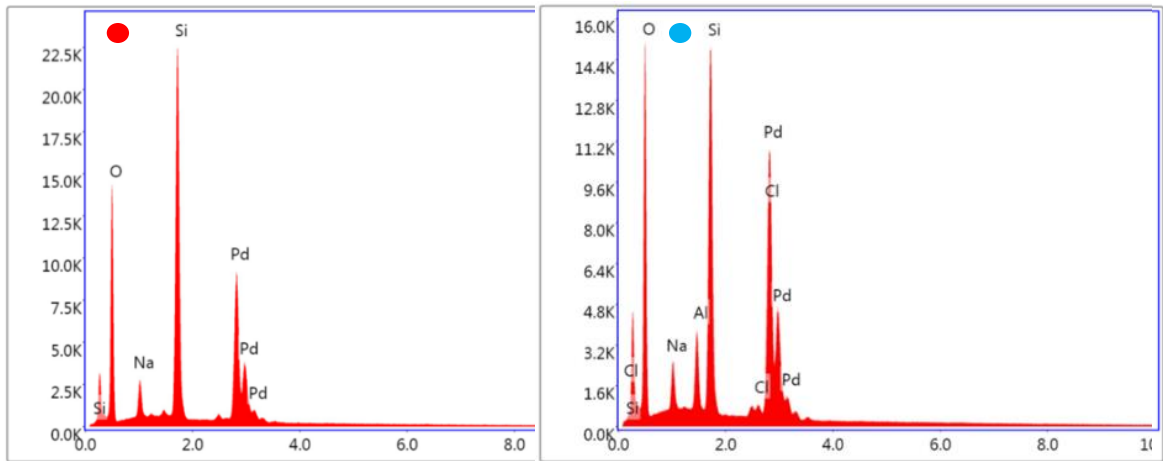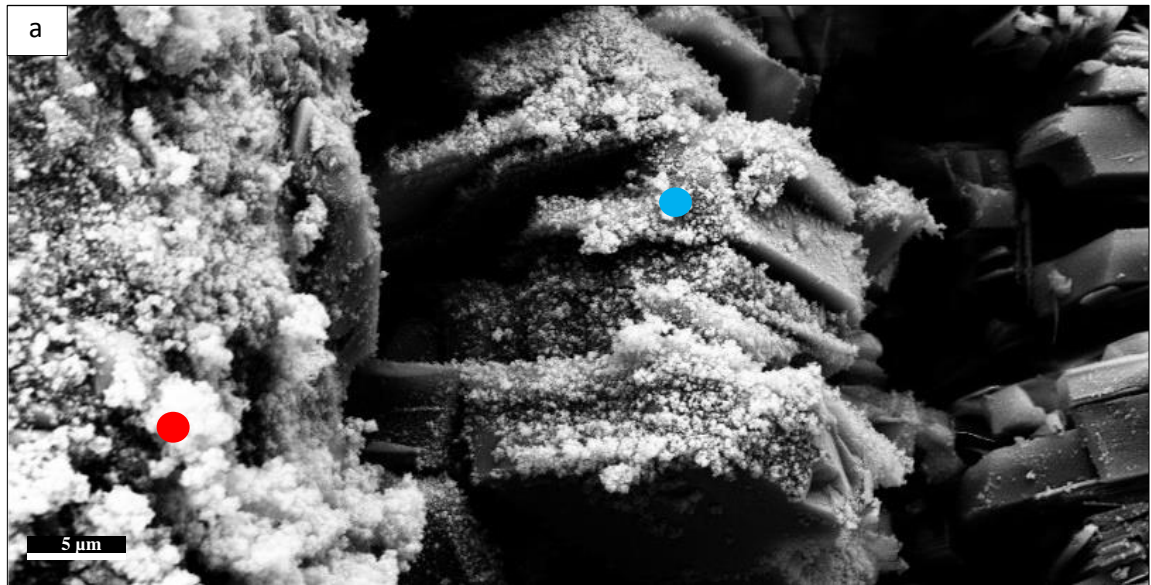
Figure 249. Gelled SS in 500 mD core fragment, in three dimensions. a) SS agglomerated on the surface of kaolinite minerals. EDS-measurements detect presence of Al and Cl in the blue point, and absence in the red point. b) and c) show agglomeration on quartz surfaces. d) Acicular growth, as seen in the dried SS + HCl + DW of flooding #1.

Thin section of flooded 500 mD core

SEM-images of the gel in the thin section demonstrate a variety of shapes and patterns. In some cases, it develops directly on grain surfaces, and in other cases, seemingly into "thin air" with no visible connection to any surface. The common visual feature is that the gel has a solid centre, surrounded by a more distal, seemingly thinner and less solid SS, as seen in Figure 30a) (blue point). Figure 30b) shows a remarkable growth of SS- solid where it assumingly started to grow close to an unknown mineral (marked with a yellow point), and SS thinning into the pore space. No acicular growth has been observed in a thin section. The EDS-spectra of SS in Figure 30 (red and blue points) are characteristic for all measurements of the gel in this thin section, showing only a minor Na-peak. Even lower amounts of Na have been detected, with signature corresponding with that of quartz (Si and O), but with visual appearance identical to SS. 48 EDS-measurements were made of SS in this sample, and no more than 25 of them detected Na. The remaining were hardly detectable Na-peaks of SS growing on kaolinite (high Al, Si, O and only minor Na).
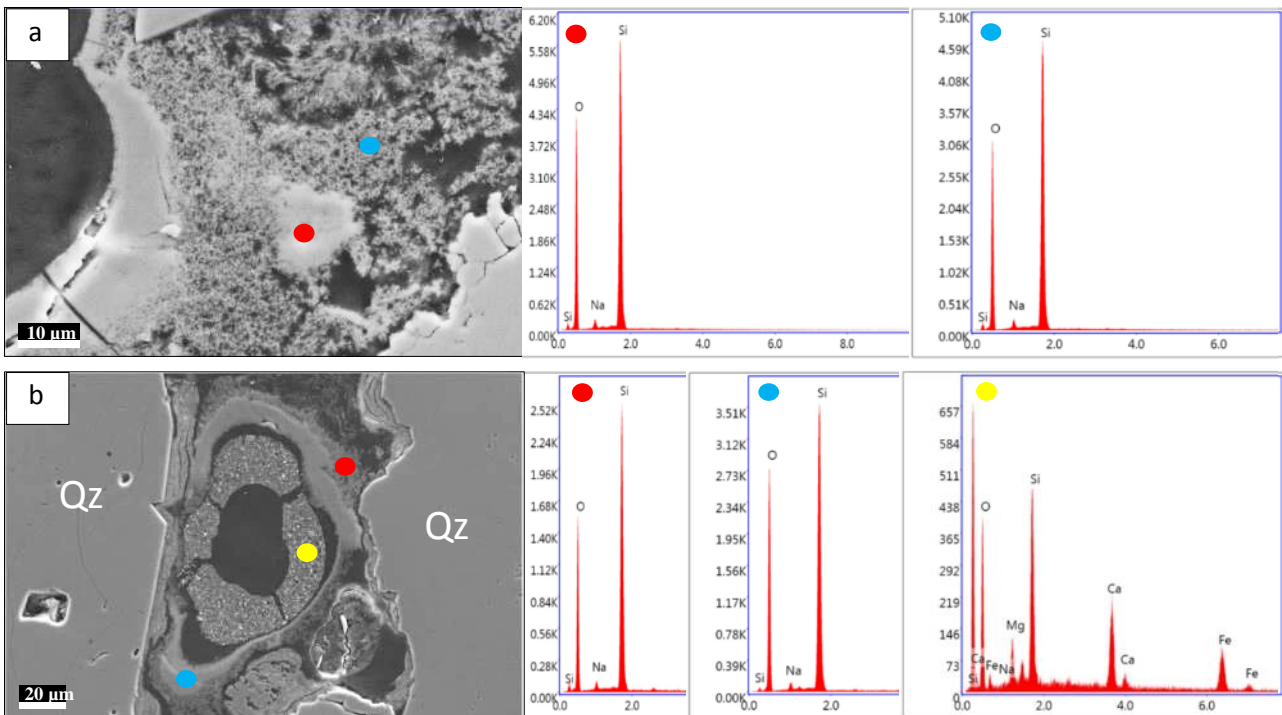
Figure 30. Thin section of flooded 500 mD core. a) The red point is placed in the solid centre of SS, and the blue point in the surrounding, less solid SS. No difference shown in EDS. b) SS growing on an unknown mineral, with a transition from solid SS growing on the unknown mineral, to less solid SS.

Mapping: thin section of flooded 500 mD core

An EDS-mapping (Fig. 31) of SS between quartz grains and kaolinite display the Na-content of the SS (yellow arrow in Fig. 31b)), as well as the presence of Al-rich kaolinite (red arrows in Fig. 31c)). According to this map, there is no variation in the Na-distribution from solid SS centre to the thinner distal SS.
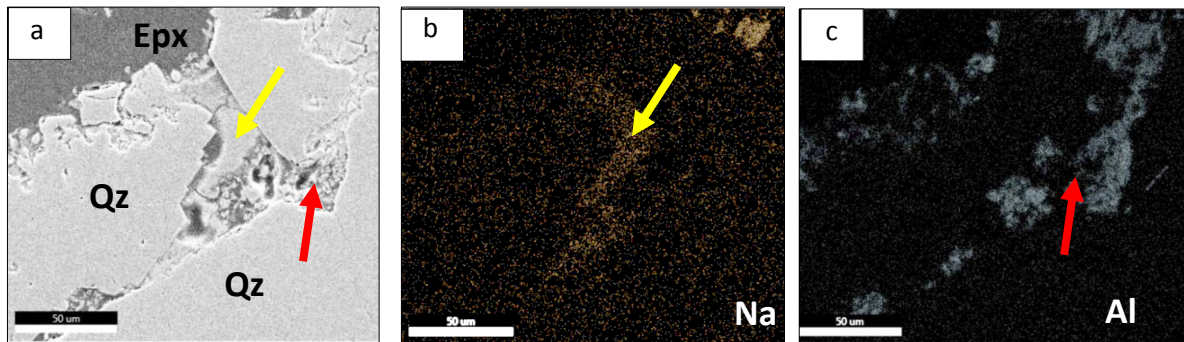
Figure 31. A mapped area in thin section of the flooded 500 mD core. a) SEM-image of SS, (yellow arrow), kaolinite (red arrow), surrounded by quartz and epoxy. b) Na is present in the SS, yellow arrow. c) Kaolinite is rich in alumina, red arrow.

Additional EDS-results and SEM-images of the samples are compiled in Appendix C.

4.5 Transmission electron microscopy

The FIB/SEM sample (Fig. 32) contains a cut quartz grain and adjacent a fraction of pore space filled with epoxy and SS-particles. The quartz grain has a smooth surface, and in several locations, the SS is attached to the quartz. TEM-analysis reveals a fractionation within a single SS-particle; a dark core and a brighter rim. The changes in greyscale could simply be due to the sample thickness; however, chemical results demonstrate a difference in abundance of Na from the centre to the rim.
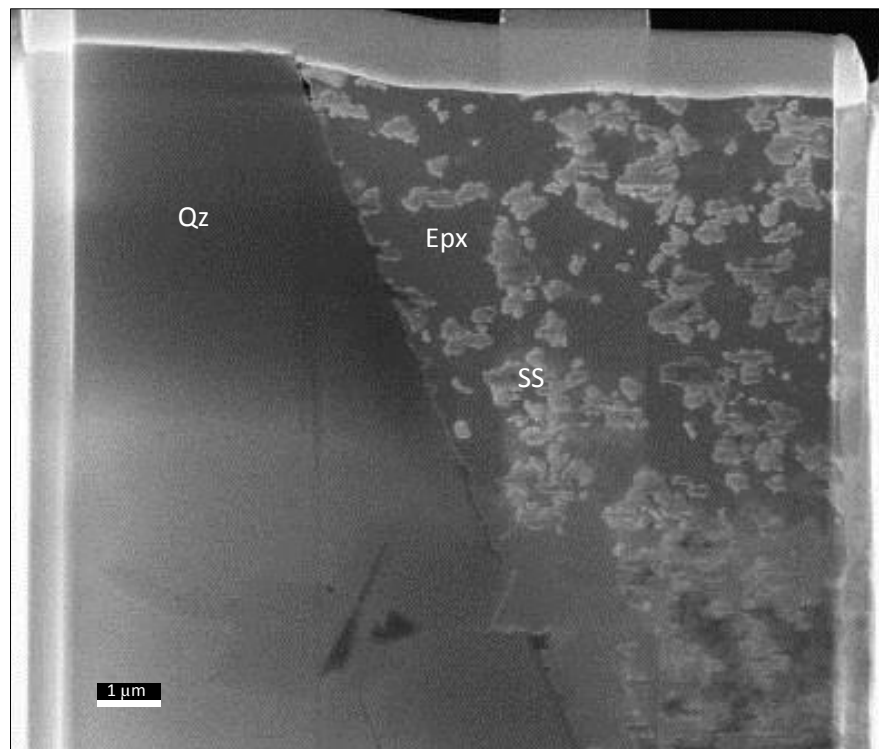
Figure 32. FIB/SEM sample showing quartz (Qz) grain and a pore filled with SS surrounded by epoxy (Epx).

On the FIB/SEM sample, one area scan is carried out, one line-scan is performed, in addition to several point analyses. The area scan (Fig. 33) covers SS growing on the quartz surface, where Si and Na distributions are mapped. The result underlines the fractionation; higher content of Na in the rim compared to the centre of the SS particle.
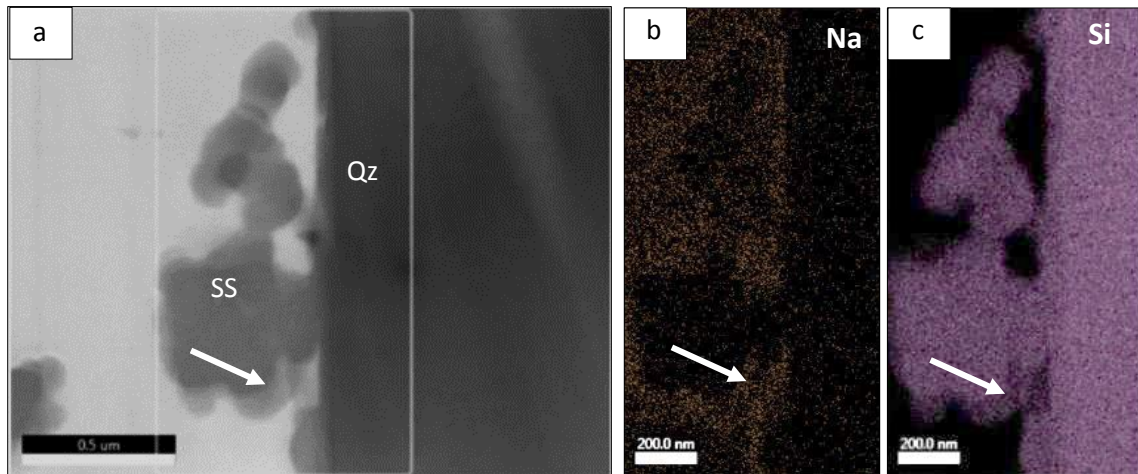
Figure 33. The mapped area of FIB/SEM: SS gel on quartz surface. a) TEM-image of mapping area. b) Na distribution mapped c) Si distribution mapped. The white arrow in a) – c) indicates the bright SS, showing an increased content of Na, and decrease of Si.

The line scan (Fig. 34) is preformed to determine whether the chemical transition of Si and Na from the quartz grain into the SS is gradual or abrupt. The scan shows a gradual decrease in Si from Qz to the dark SS, and a dramatic decrease moving into the bright SS. Sodium increases slightly from being absent in the dark SS to being steadily present in the bright SS. From bright SS to epoxy, the C (epoxy) dramatically increases and Si, O and Na decrease.
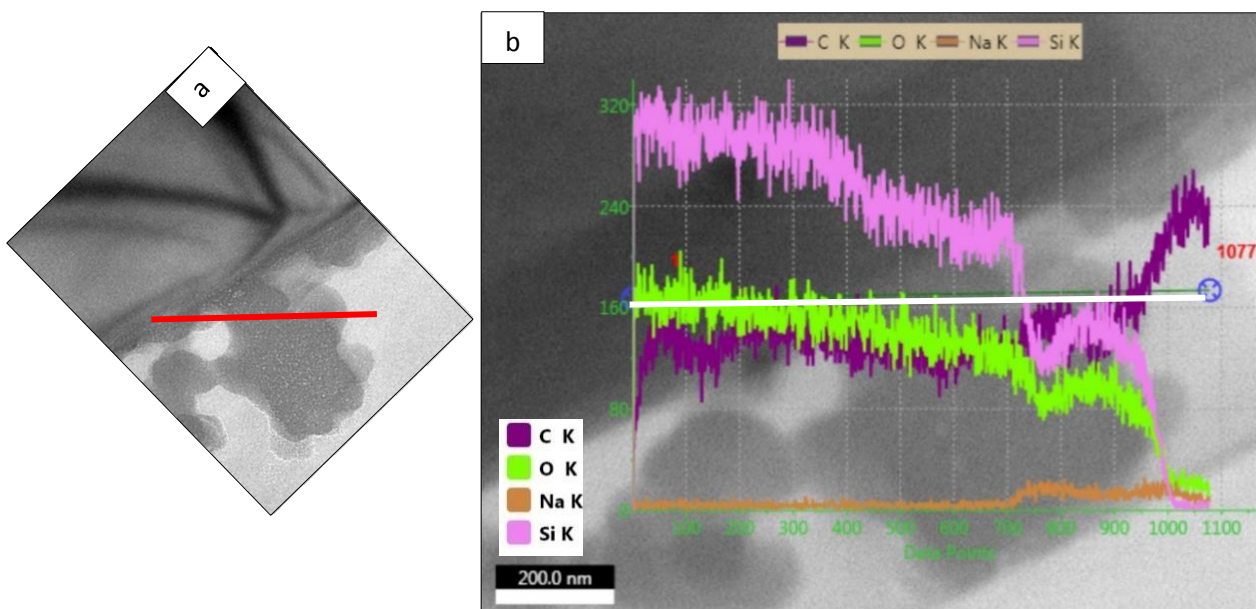
Figure 254. Line scan of FIB/SEM. a) The scan is preformed along the red line. b) The result shows a dramatic decrease in Si and an increase of Na as the scan moves from dark SS into the bright SS. C= carbon. O = oxygen. Na = sodium. Si = silicon.

Point scans (Fig. 35) indicate a difference in Na-content from the dark SS to the bright SS. EDS-measurements of the quartz-grain (yellow point) and of the dark SS (red points) is practically identical with absence of Na, while the bright SS (blue points) contains Na.
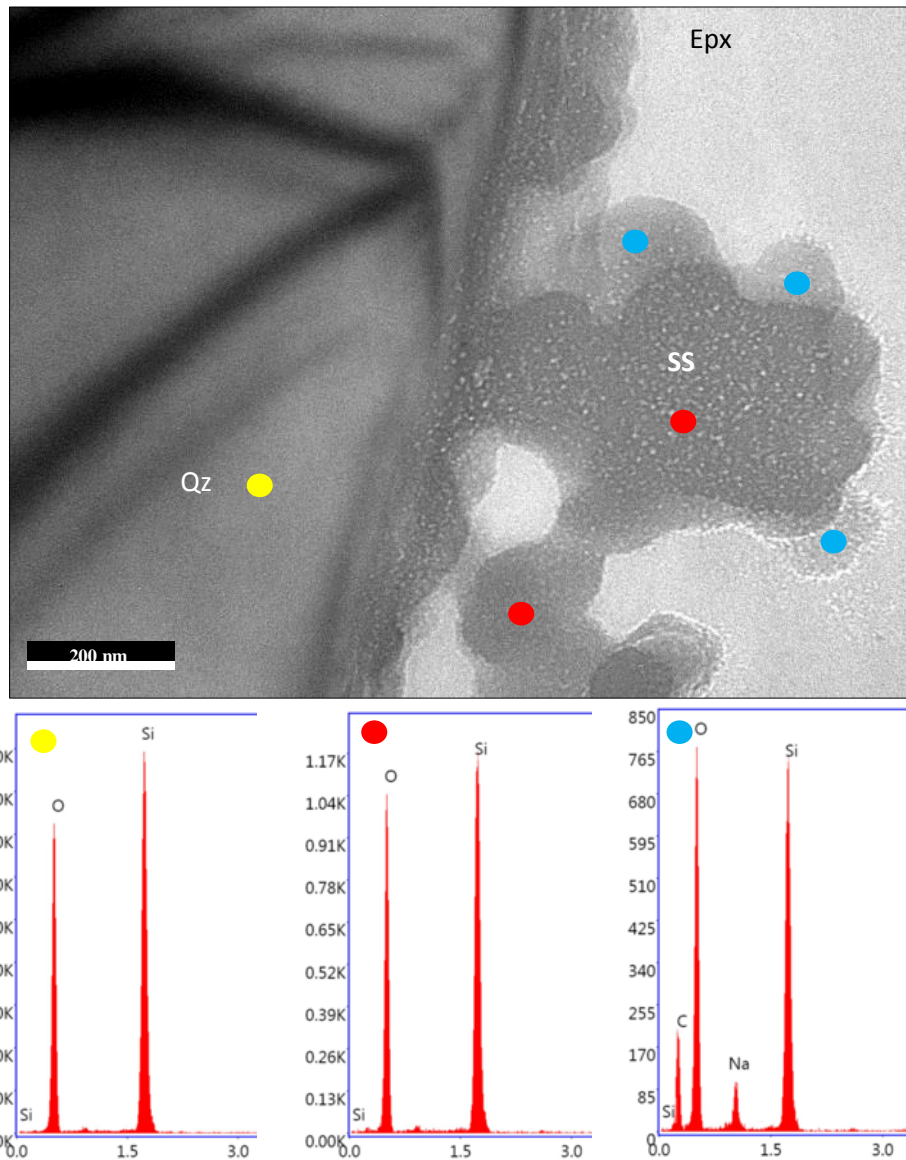
Figure 265. Point scan of FIB/SEM sample. Noticeable similarity between dark SS (red points) and Qz (yellow point), both lacking Na. However, Na is detected in the bright SS (blue points).

Additional EDS-results and TEM-images are compiled in Appendix D.

5 Discussion

5.1 Berea Sandstone cores

The Berea Sandstone cores were homogenous and mature in composition, and therefore beneficial to use in this study. A less mature material would have contained a larger variety of minerals which the gel could potentially react with. However, the relatively high abundance of kaolinite could have an impact due to its powder-like texture. It may dissolve and interact with the liquid SS solution, causing impurities and altering the composition and crystal habit of the SS, as seen in figures 28a) and b).

Comparing the flooded and the unflooded 500 mD cores, the doubling of Zr indicates a change in provenance. These two samples originate from two individual cores, so they may have been deposited from two different sediment sources (see Chapter 2.2), sampled from different depths or areas of the quarry.

5.2 Sodium silicate gel

The major increase in Fe_2O_3 after mixing with HCl may be explained by either contamination from the piston cell from where it was sampled prior to flooding, or contamination in the laboratory. This iron oxide was, however, never detected in any of the methods utilized for studying the gel in the core samples. The variations of Si, O, Na and Cl content in EDS-measurements of the gel (dried samples as well as injected SS) presumably reflect the small EDS-spot size, the varying parameters of the flooding experiments (e.g. connate water), as well as sample preparation.

5.3 Gel after injection

The Na content of the gel in the 500 mD core thin section was drastically lower than that of the gel in the 500 mD core fragment. The maximum thickness of the gel in a thin section is 25-30 μm, however, the gel in the fragment has not been thinned in a grinding process, and is subsequently thicker, and could therefore produce a higher element count of Na. In addition, the thin section has been saturated with epoxy, sawed, grinded and polished; therefore some gel material might have fallen out. No SS was observed or detected by EDS in the 200 mD core thin sections, probably due to more advanced preparation techniques at Bureau Veritas' laboratory, better preserving the material, compared to the laboratory at UiS.

5.4 Fractionation of Na

The TEM line scan revealed that the core of the SS-particle (referred to as "dark SS") and the quartz grain on which it was growing, were compositionally the same. Seemingly, the SS entered the core, SiO started to crystallize on the quartz, and the Na precipitated on the rim. This fractionation was not reflected in the SEM, which could be explained by a two dimensional sample or thin section preparation issues.

5.5 Sodium liberation during flooding

As explained in Chapter 2.1, Na^+ is released during the polymerization, and the counterion is Cl^- when hydrochloric acid is used as activator. NaCl is soluble in the effluent, whereas the less soluble silicate polymer remains in the pore space. However, since the effluent was not preserved during the flooding experiment, this can only be assumed. The analyses indicated no noticeable increase of sodium in the pores after the flooding; on the contrary, the EDS results clearly showed a significant decrease in sodium after injection, underlining this assumption.

5.6 Sodium diffusion in electron microscopes

A study conducted by Nielsen and Sigurdsson (1981) proves the time-dependent element diffusion of sodium during electron bombardment of volcanic and synthetic glasses. To be able to attain sufficient element counts of Na during a microprobe electron analysis, the sample needs to be bombarded over a certain time, leading to intensity loss of Na. This study emphasizes that sample size matters; a thin sample (e.g. thin section) heats faster, leading to diffusion. The result of experimenting with decreasing temperature is given in Figure 36 (Nielsen and Sigurdsson, 1981). A sample (20-200 µm thick glass fragments, containing 5,68% Na_2O) was cooled down to -90°C using a "cryogenic cold-finger" - equipment used for localized cooling in laboratories, and the result was dramatic. At -90°C, direct quantitative measurements could be made with no Na diffusion, whereas the Na X-ray intensity decreased with 50% in just 15 seconds using a room temperature sample.
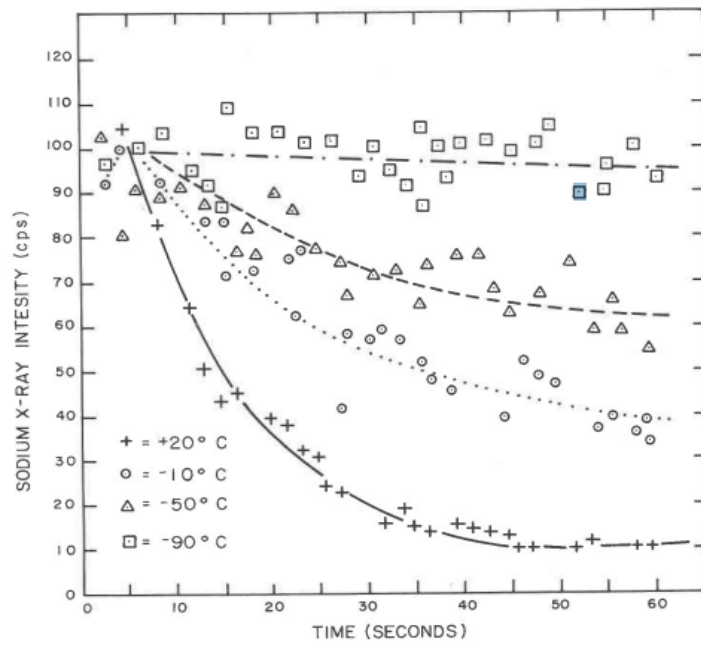
Figure 36. The effect of decreasing sample temperature on Na-diffusion during electron bombardment. Sodium loss measured in a sample of rhyolitic glass fragments mounted in epoxy, coated with carbon. (Nielsen and Sigurdsson, 1981)

5.7 Morphology

Comparing the tabular crystals of the dried SS + HCl + DW to the globular particles of the gelled SS in the core, the appearance is undeniably dissimilar. Precipitation of SS gel within a pore of a saturated core (SSW/DW (flooding #1) or NaCl (flooding #24)) represents a far more limited process than precipitation by evaporation in an open glass beaker in a heating cabinet. Sizes of the globular gel-particles range from a few tens of nm to 100 nm before they start to agglomerate and form larger clasts of particles. Figure 37 show the globular gel growth in a thin section and a core fragment, comparing the thin section and fragment of the 500 mD core.
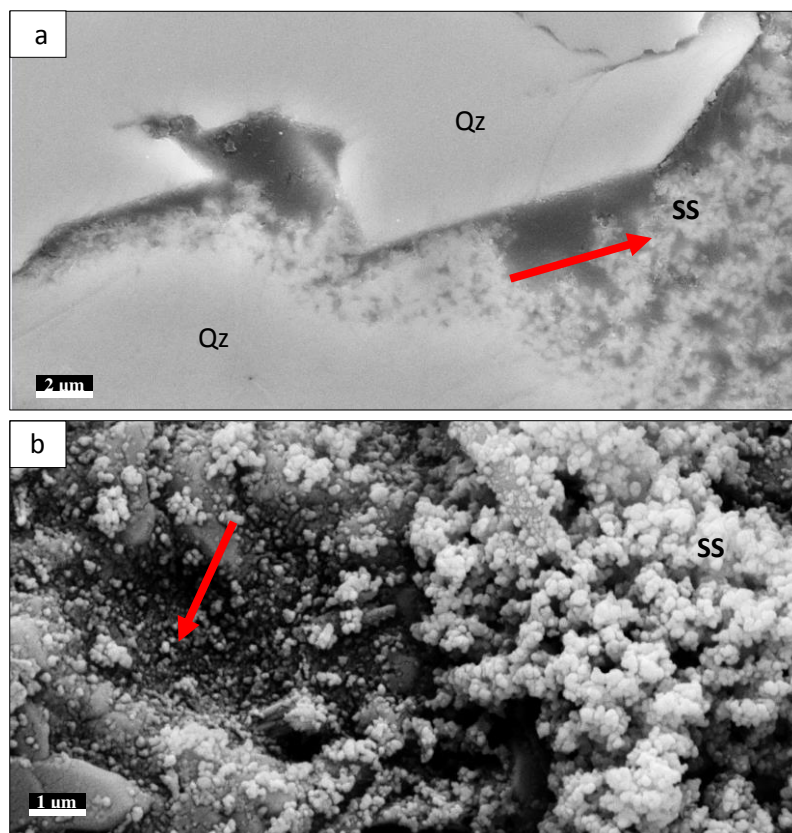
Figure 37. Comparing particle size of gel in thin section and fragment of 500 mD core. a) The smallest gel particles visible in the thin section are 200 nm, however, these may be agglomerated particles, not single. b) Gel particles in the fragment are measured to approx. 100 nm. Red arrows point to the measured particles.

5.8 Methods

Utilizing methods which are based on electron beaming of the sample has proven to be a challenge du to Na diffusion, in particular for thin samples. When bombarding a sample in the SEM, the element count of Na decreases in under a second, while other elements such as O or Si increased. It is important that the EDS detector is highly sensitive to light elements, to improve the detection of Na. GC and XRD were useful to get an overview of bulk composition, however, for a micron- and nano-scale study, the detailed information provided by TEM regarding chemical transitions in a single SS particle or SEM imaging of how SS grows onto a grain surface was key. Also, a downside of the bulk information is that it is not possible to differentiate the diagenetic and the detrital phases (Robinson, 2009).

5.9 Reliability of the data

One needs to be highly aware of possible sources of contamination and the reliability of data throughout a research project, especially during such a small-scale study. A simple grain of dust could potentially affect the TEM-analysis immensely. However, every step of the laboratory work has been performed with focus on mitigating the risk of contamination.

6 Conclusion

This study was successful, and further knowledge was gained about gelled SS. Understanding the micron- and nano-scale changes in the host rock is significant for IOR-porposes. The fractionation of Na in a single SS-particle could impact reservoir wettability and the surface charge interactions. Despite the Na diffusion during electron beaming of the samples, SEM-EDS and TEM-EDS proved to be useful methods to study the SS on this scale, with chemical compositions measured down to a spot size of 1 μm. Measuring on a nano-scale the fractionation of a single SS-particle in the TEM gave extraordinary results.

The crystallization of the SS has been examined, and no solid, porefilling gel has been observed at any stage or in any sample. On the contrary, the globular precipitation of SS on the grain surfaces represent merely a fraction of the total porespace. Still, the difference in parameters from flooding experiments to field-scale operations allow for plugging, water diversion and an increase in oil production.

Scientific data needs to be reproducible, however in this case, the sample material was not provided in a manner to make a minimum of experiments for further interpretations. For further studies, collecting and studying the chemical composition of the effluent will be key in fully understanding the low content of Na in the gelled SS.

7 References

ClevelandQuarries, 2018, Berea Sandstone™ Petroleum Cores, Volume 2018.

Hamouda, A. A., and Amiri, H. A. A., 2014, Factors affecting alkaline sodium silicate gelation for in-depth reservoir profile modification: Energies, v. 7, no. 2, p. 568-590.

Khursheed, A., 2010, Scanning Electron Microscope Optics And Spectrometers, World Scientific.

Madland, M. V., Flornes, K. M., Hiort, A., Valestrand, R., Skjæveland, S. M., and Viig, S. O., 2016, The National IOR Centre of Norway- Annual Report 2016.

Murphy, D. B., 2001, Fundamentals of light microscopy and electronic imaging, John Wiley & Sons.

Nielsen, C. H., and Sigurdsson, H., 1981, Quantitative methods for electron microprobe analysis of sodium in natural and synthetic glasses: American Mineralogist, v. 66, p. 547-552.

Omekeh, A., Hiorth, A., Stavland, A., and Lohne, A., Silicate Gel for In-depth Placement-Gelation Kinetics and Pre-flush Design, *in* Proceedings IOR 2017-19th European Symposium on Improved Oil Recovery, University of Stavanger, Norway, 2017.

Pepper, J. F., De Witt, W., and Demarest, D. F., 1954, Geology of the Bedford Shale and Berea Sandstone in the Appalachian basin: Science, v. 119, no. 3094, p. 512-513.

Robinson, A. G., 2009, Inorganic geochemistry: Applications to petroleum geology, John Wiley & Sons.

Skrettingland, K., Dale, E. I., Stenerud, V. R., Lambertsen, A. M., Nordaas Kulkarni, K., Fevang, O., and Stavland, A., Snorre In-depth Water Diversion Using Sodium Silicate-Large Scale Interwell Field Pilot, *in* Proceedings SPE EOR Conference at Oil and Gas West Asia2014, Society of Petroleum Engineers.

Skrettingland, K., Ulland, E., Ravndal, O., Tangen, M., Kristoffersen, J., Stenerud, V., Dalen, V., Standnes, D., Fevang, Ø., and Mevik, K., Snorre In-Depth Water Diversion-New Operational Concept for Large Scale Chemical Injection from a Shuttle Tanker, *in* Proceedings SPE Improved Oil Recovery Conference2016, Society of Petroleum Engineers.

Solberg, J. K., and Hansen, V., 2007, Innføring i transmisjon elektronmikroskopi, NTNU and Universitet I Stavanger.

Stavland, A., Jonsbraten, H. C., Vikane, O., Skrettingland, K., and Fischer, H., In-depth water diversion using sodium silicate on snorre-factors controlling in-depth placement, *in*

Proceedings SPE European Formation Damage Conference2011, Society of Petroleum Engineers.

Stenerud, V., Håland, K., Skrettingland, K., Fevang, Ø., and Standnes, D., Snorre In-depth Water Diversion Using Sodium Silicate-Evaluation of Interwell Field Pilot, *in* Proceedings IOR 2017-19th European Symposium on Improved Oil Recovery, University of Stavanger, Norway, 2017.
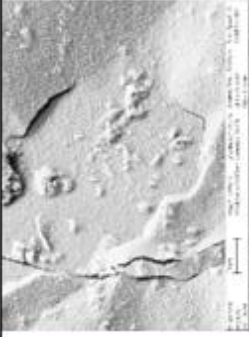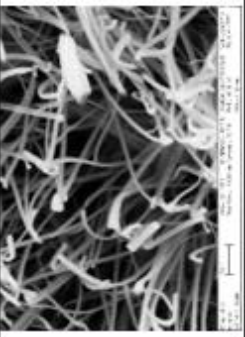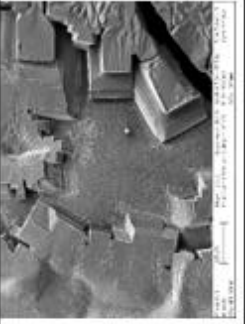
Wright, A. F., and Dupuy, J., 2012, Glass... current issues, Springer Science & Business Media.

Appendix A
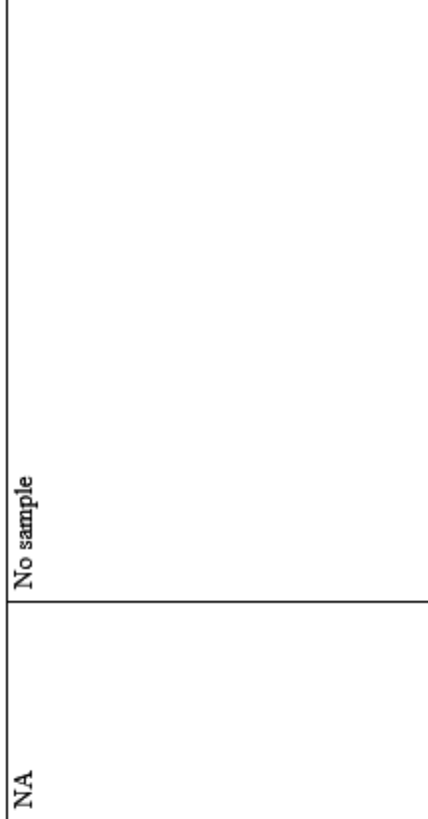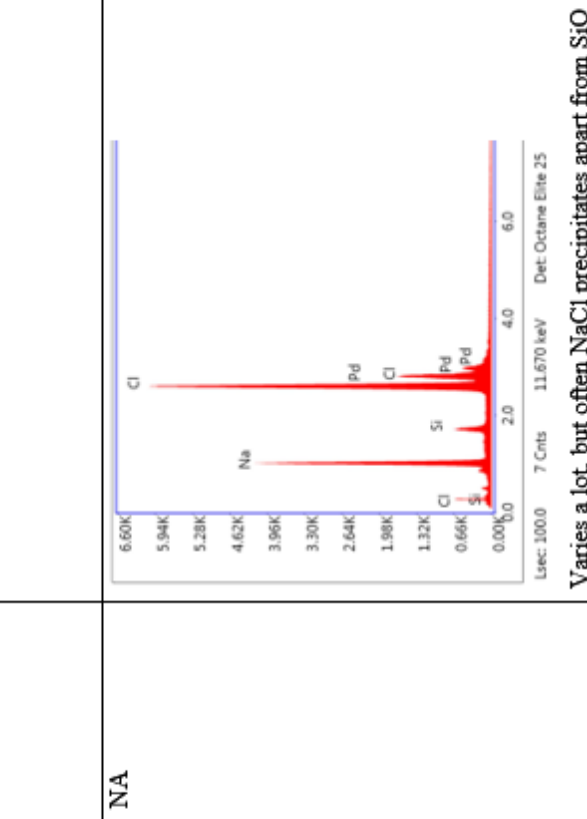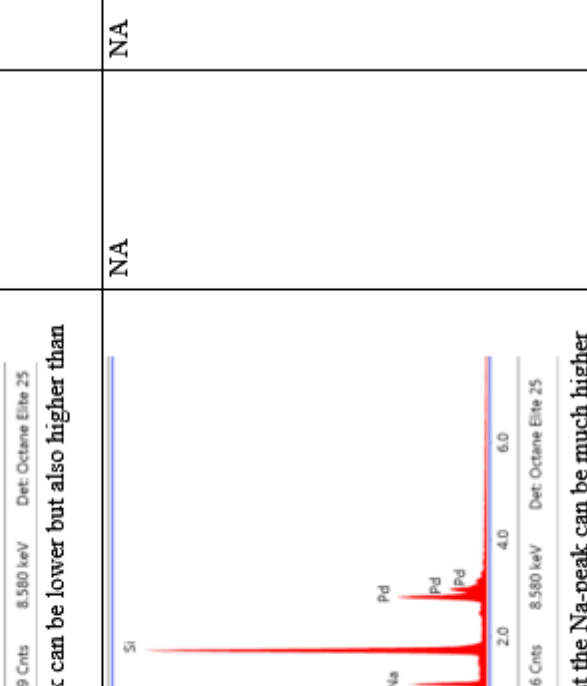
Table 1. An overview of the flooding parameters for floodings #1 – #4, and of the dried SS and the SS + HCl + DW samples. Continues for three pages with a short summary of results for SS and SS + HCl + DW.

Information	Flooding #1 (success)	Flooding #2 (failure)	Flooding #3 (failure)	Flooding #4 (success)
Core permeability	500 mD	200mD	200mD	200mD
Length/diameter of core	7,2 cm/3,7 cm	24,9 cm/3,7 cm	Ca 12 cm/3,7 cm	NA
Connate water	50/50 SSW/DW	50/50 SSW/DW	50/50 SSW/DW	2500 ppm NaCl
Age of SS-solution	August 2013	August 2013	August 2013	August 2013
Silicate-solution	5%	5%	5%	5%
SS-solution filtered pre-flooding	5 µm	5 µm	5 µm	5 µm
HCl-solution	14%, 1 molar-solution	14%, 1 molar-solution	14%, 1 molar-solution	14%, 1 molar-solution
Total mix	92 gr SS, 70 gr HCl, 337 gr DW	92 gr SS, 70 gr HCl, 337 gr DW	92 gr SS, 70 gr HCl, 337 gr DW	92 gr SS, 70 gr HCl, 337 gr DW
Injected at temperature	Room temperature, then heating cabinet, 60°C	60°C, then heating cabinet, 60°C	Room temp., then heating cab. 60°C	Room temperature, then heating cabinet, 60°C
Rate	1 ml/min	NA	2 ml/min	NA
Gelation time	2 days	NA	NA	3 days
pH	11,08	NA	NA	11,08 +/-
CAS-number	NA	NA	NA	NA
Liquid sampled from	Piston cell	No SS-sample	No SS-sample	Piston cell
Process for drying sodium silicate and sodium silicate +HCl	In glass beaker at 55°C in a heating cabinet SS+HCl+DW (small sample,0,59 gr) dried in a few hours. SS (bigger sample: 4,38 gr) needed 3 days. Removed from the beaker with a steel spatula.	No SS-sample	No SS-sample	SS+HCl+DW in a hard-plastic cup in heating cabinet, 40°C, 4 days. No sample of only SS.

SEM (UiS): SS		Smooth surface, not much happening.	NA	NA	No sample	
SEM (UiS): SS+HCl+DW		Looks like grass/tubes.	NA	NA		NaCl precipitates on the surface, and SiO$_2$ concentrated in the centre of the sample.
SEM (UiS): SS+HCl+DW in the core (FL_500)		Looks like powder.	NA	NA	No SS+HCl+DW detected in the sample.	

Continues on next page

54
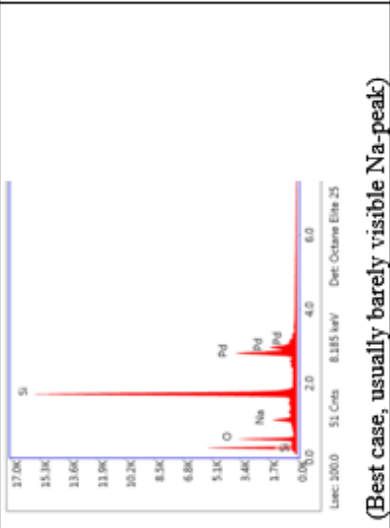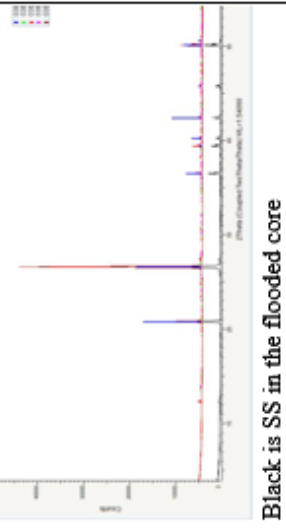
| EDS (UiS): SS |
Lsec: 100.0 19 Cnts 8.580 keV Det: Octane Elite 25
The Na peak can be lower but also higher than Si and O | NA | NA | No sample |
| EDS (UiS): SS+HCl+DW |
Lsec: 100.0 16 Cnts 8.580 keV Det: Octane Elite 25
Average, but the Na-peak can be much higher | NA | NA |
Lsec: 100.0 7 Cnts 11.670 keV Det: Octane Elite 25
Varies a lot, but often NaCl precipitates apart from SiO |

EDS (UiS): SS+HCl+DW in the core (FL_500)	(Best case, usually barely visible Na-peak)	NA	NA	NA	Had to give up, didn't find any SS in the thin section.
XRD (UiS): SS	No sample	NA	NA	No sample
XRD (UiS): SS+HCl+DW	No sample	NA	NA	Blue is SS+HCl4
XRD (UiS): SS+HCl+DW in the core	Black is SS in the flooded core	NA	NA	Black is SS in the flooded core

Appendix B

Table 1. GC results of dried SS and of SS + HCl + DW, both from flooding # 1.
Analysis conducted at Actlabs, Canada.

Analyte Symbol	SiO2	Al2O3	Fe2O3(T)	MnO	MgO	CaO	Na2O
Unit Symbol	%	%	%	%	%	%	%
Detection Limit	0,01	0,01	0,01	0,001	0,01	0,01	0,01
Analysis Method	FUS-ICP	FUS-ICP	FUS-ICP	FUS-ICP	FUS-ICP	FUS-ICP	FUS-ICP
SS1+HCL	56,49	1,37	15,83	0,104	0,05	0,06	15,31
SS1	58,55	0,52	0,76	0,007	0,06	0,1	17,89

K2O	TiO2	P2O5	LOI	Total	Sc	Be	V
%	%	%	%	%	ppm	ppm	ppm
0,01	0,001	0,01		0,01	1	1	5
FUS-ICP	FUS-ICP	FUS-ICP	FUS-ICP	FUS-ICP	FUS-ICP	FUS-ICP	FUS-ICP
0,26	0,03	< 0.01		89,51	< 1	< 1	< 5
0,09	0,028	< 0.01	20,88	98,89	< 1	< 1	< 5

Cr	Co	Ni	Cu	Zn	Ga	Ge	As
ppm	ppm	ppm	ppm	ppm	ppm	ppm	ppm
20	1	20	10	30	1	0,5	5
FUS-MS	FUS-MS	FUS-MS	FUS-MS	FUS-MS	FUS-MS	FUS-MS	FUS-MS
280	4	40	60	< 30	2	1,4	< 5
40	< 1	< 20	< 10	< 30	1	0,6	< 5

Rb	Sr	Y	Zr	Nb	Mo	Ag
ppm	ppm	ppm	ppm	ppm	ppm	ppm
1	2	0,5	1	0,2	2	0,5
FUS-MS	FUS-ICP	FUS-MS	FUS-ICP	FUS-MS	FUS-MS	FUS-MS
4	15	2,3	39	0,6	9	< 0.5
1	9	1,4	35	0,3	< 2	< 0.5

In	Sn	Sb	Cs	Ba	La	Ce
ppm	ppm	ppm	ppm	ppm	ppm	ppm
0,1	1	0,2	0,1	2	0,05	0,05
FUS-MS	FUS-MS	FUS-MS	FUS-MS	FUS-ICP	FUS-MS	FUS-MS
< 0.1	2	< 0.2	0,1	34	2,18	4,51

< 0.1	< 1	< 0.2	< 0.1	27	1,54	3,07
Pr	Nd	Sm	Eu	Gd	Tb	Dy
ppm	ppm	ppm	ppm	ppm	ppm	ppm
0,01	0,05	0,01	0,005	0,01	0,01	0,01
FUS-MS	FUS-MS	FUS-MS	FUS-MS	FUS-MS	FUS-MS	FUS-MS
0,54	2,07	0,4	0,081	0,32	0,05	0,36
0,4	1,56	0,31	0,062	0,21	0,04	0,24

Ho	Er	Tm	Yb	Lu	Hf	Ta
ppm	ppm	ppm	ppm	ppm	ppm	ppm
0,01	0,01	0,005	0,01	0,002	0,1	0,01
FUS-MS	FUS-MS	FUS-MS	FUS-MS	FUS-MS	FUS-MS	FUS-MS
0,08	0,25	0,038	0,24	0,037	0,8	0,02
0,05	0,14	0,023	0,15	0,022	0,7	0,02

W	Tl	Pb	Bi	Th	U
ppm	ppm	ppm	ppm	ppm	ppm
0,5	0,05	5	0,1	0,05	0,01
FUS-MS	FUS-MS	FUS-MS	FUS-MS	FUS-MS	FUS-MS
1,3	0,13	< 5	< 0.1	0,57	0,25
0,6	< 0.05	< 5	< 0.1	0,41	0,15

Table 2. GC results of eight core samples. Analysis conducted at Bureau Veritas, Canada.

Method	WGHT	LF200	LF200	LF200	LF200	LF200	LF200	LF200	LF200	LF200	LF200	LF200	LF200	LF200	LF200	LF200	LF200	LF200	LF200	LF200
Analyte	Wgt	SiO2	Al2O3	Fe2O3	MgO	CaO	Na2O	K2O	TiO2	P2O5	MnO	Cr2O3	Ba	Ni	Sc	LOI	Sum	Be	Co	Cs
Unit	kg	%	%	%	%	%	%	%	%	%	%	%	ppm	ppm	ppm	%	%	ppm	ppm	ppm
MDL	0	0.01	0.01	0.04	0.01	0.01	0.01	0.01	0.01	0.01	0.01	0.002	1	20	1	-5.1	0.01	1	0.2	0.1
FLout-500 Rock	0.012	93.99	2.77	0.50	0.18	0.28	0.18	0.67	0.21	0.02	<0.01	<0.002	80	<20	1	1.2	99.98	<1	3.4	0.5
FLin-500 Rock	0.012	93.88	2.82	0.54	0.21	0.31	0.22	0.72	0.21	0.02	0.01	<0.002	75	<20	2	1.0	99.98	<1	3.4	0.6
UF-500 Rock	0.011	93.38	2.95	0.54	0.22	0.41	0.13	0.75	0.31	0.02	0.01	0.003	85	<20	2	1.2	99.95	<1	3.8	0.5
UF2-200 Rock	0.014	92.03	3.80	0.63	0.19	0.23	0.41	1.04	0.22	0.03	<0.01	0.002	113	<20	2	1.4	99.97	<1	3.4	0.8
FL2-200 Rock	0.015	92.56	3.72	0.68	0.19	0.19	0.27	1.00	0.22	0.03	<0.01	0.003	107	<20	2	1.1	99.97	<1	4.2	0.8
FL4in-200 Rock	0.014	93.06	3.23	0.55	0.18	0.21	0.27	0.85	0.23	0.02	<0.01	<0.002	92	<20	2	1.4	99.97	<1	4.6	0.5
FL4out-200 Rock	0.011	93.24	3.13	0.51	0.17	0.21	0.30	0.81	0.23	0.02	<0.01	<0.002	86	<20	1	1.3	99.97	<1	3.9	0.5
UF4-200 Rock	0.016	93.59	3.01	0.53	0.17	0.21	0.14	0.80	0.24	0.01	<0.01	<0.002	81	<20	2	1.3	99.97	2	4.4	0.5

Method	LF200	LF200	LF200	LF200	LF200	LF200	LF200	LF200	LF200	LF200	LF200	LF200	LF200	LF200	LF200	LF200	LF200	LF200	LF200	LF200
Analyte	Ga	Hf	Nb	Rb	Sn	Sr	Ta	Th	U	V	W	Zr	Y	La	Ce	Pr	Nd	Sm	Eu	Gd
Unit	ppm	ppm	ppm	ppm	ppm	ppm	ppm	ppm	ppm	ppm	ppm	ppm	ppm	ppm	ppm	ppm	ppm	ppm	ppm	ppm
MDL	0.5	0.1	0.1	0.1	1	0.5	0.1	0.2	0.1	8	0.5	0.1	0.1	0.1	0.1	0.02	0.3	0.05	0.02	0.05
FLout-500 Rock	3.4	3.7	3.5	20.6	2	12.7	0.3	3.2	0.7	15	<0.5	142.6	5.5	8.8	17.5	1.86	6.8	1.22	0.21	1.02
FLin-500 Rock	3.3	3.9	3.9	21.4	1	11.5	0.3	3.0	0.8	17	<0.5	142.0	6.2	8.5	17.4	1.91	7.2	1.31	0.25	1.07
UF-500 Rock	3.4	7.0	4.6	22.5	2	13.4	0.3	4.4	1.1	20	0.5	281.6	6.9	10.7	22.9	2.47	9.2	1.59	0.31	1.31
UF2-200 Rock	3.5	3.8	3.2	30.3	<1	15.1	0.3	3.6	1.0	19	0.6	142.0	7.5	10.9	25.0	2.75	11.2	2.01	0.43	1.83
FL2-200 Rock	3.8	3.6	3.7	30.3	1	14.9	0.3	3.5	1.0	19	0.7	135.7	7.7	11.4	25.5	2.89	11.1	2.13	0.43	1.62
FL4in-200 Rock	3.3	4.6	3.9	26.2	1	13.9	0.3	3.1	1.1	17	<0.5	189.3	6.7	9.5	21.3	2.25	8.3	1.57	0.31	1.30
FL4out-200 Rock	3.2	5.3	3.3	24.1	<1	12.4	0.3	3.4	1.0	17	<0.5	205.0	7.3	9.0	18.8	1.94	8.0	1.24	0.28	1.13
UF4-200 Rock	3.0	4.9	3.4	23.3	2	12.0	0.4	3.3	1.2	17	<0.5	193.2	7.2	9.2	19.7	2.13	7.8	1.56	0.30	1.22

Method	LF200	LF200	LF200	LF200	LF200	LF200	LF200	TC000	TC000	AQ200	AQ200	AQ200	AQ200	AQ200	AQ200	AQ200	AQ200	AQ200	AQ200	AQ200
Analyte	Tb	Dy	Ho	Er	Tm	Yb	Lu	TOT/C	TOT/S	Mo	Cu	Pb	Zn	Ni	As	Cd	Sb	Bi	Ag	Au
Unit	ppm	ppm	ppm	ppm	ppm	ppm	ppm	%	%	ppm	ppm	ppm	ppm	ppm	ppm	ppm	ppm	ppm	ppm	ppb
MDL	0.01	0.05	0.02	0.03	0.01	0.05	0.01	0.02	0.02	0.1	0.1	0.1	1	0.1	0.5	0.1	0.1	0.1	0.1	0.5
FLout-500 Rock	0.15	0.97	0.23	0.63	0.09	0.67	0.10	0.16	0.02	0.1	16.4	3.3	7	5.3	1.7	<0.1	0.2	<0.1	<0.1	2.1
FLin-500 Rock	0.18	0.98	0.22	0.73	0.11	0.76	0.13	0.15	<0.02	0.2	10.3	4.8	6	5.2	1.3	<0.1	0.2	<0.1	<0.1	1.1
UF-500 Rock	0.19	1.22	0.24	0.79	0.12	0.86	0.14	0.17	0.03	0.2	14.4	6.1	5	5.2	2.4	<0.1	0.6	<0.1	<0.1	0.7
UF2-200 Rock	0.25	1.49	0.26	0.75	0.11	0.82	0.13	0.09	0.04	0.1	3.8	2.4	7	4.0	1.2	<0.1	0.1	<0.1	<0.1	<0.5
FL2-200 Rock	0.25	1.38	0.29	0.73	0.12	0.78	0.13	0.10	0.11	0.1	5.7	4.1	7	5.8	2.1	<0.1	0.2	<0.1	<0.1	1.5
FL4in-200 Rock	0.20	1.23	0.23	0.74	0.12	0.91	0.13	0.13	0.03	<0.1	8.1	2.2	6	5.3	1.3	<0.1	<0.1	<0.1	<0.1	0.6
FL4out-200 Rock	0.19	1.16	0.26	0.80	0.13	0.77	0.14	0.13	0.03	<0.1	9.4	2.6	7	5.3	1.5	<0.1	<0.1	<0.1	<0.1	1.4
UF4-200 Rock	0.19	1.27	0.27	0.92	0.12	0.84	0.15	0.12	0.03	<0.1	12.5	2.2	5	4.4	1.1	<0.1	<0.1	<0.1	<0.1	1.5

Method	AQ200	AQ200	AQ200
Analyte	Hg	Tl	Se
Unit	ppm	ppm	ppm
MDL	0.01	0.1	0.5
FLout-500 Rock	<0.01	<0.1	<0.5
FLin-500 Rock	<0.01	<0.1	<0.5
UF-500 Rock	<0.01	<0.1	<0.5
UF2-200 Rock	<0.01	<0.1	<0.5
FL2-200 Rock	0.01	<0.1	<0.5
FL4in-200 Rock	<0.01	<0.1	<0.5
FL4out-200 Rock	<0.01	<0.1	<0.5
UF4-200 Rock	<0.01	<0.1	<0.5

Appendix C

Additional SEM- and EDS results of dried sample of SS (flooding #1), before injection (500 mD).

EDS Spot 1

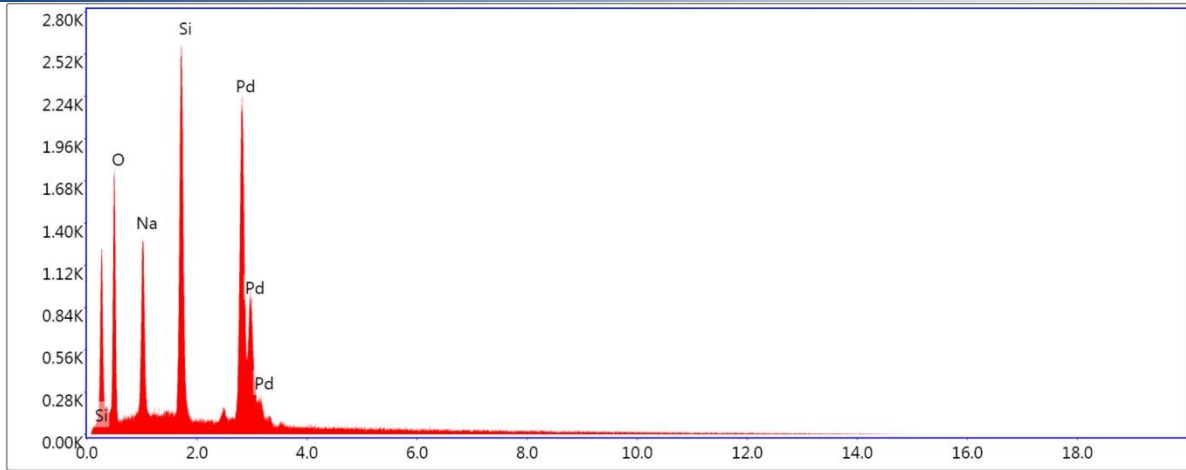Lsec: 100.0   13 Cnts   8.580 keV   Det: Octane Elite 25

Element	Weight %	Atomic %	Net Int.	Error %	Kratio	Z	A	F
O K	31.55	42.21	251.17	7.14	0.0800	1.0707	0.4993	1.0000
NaK	33.24	30.95	308.75	5.41	0.1031	0.9675	0.6743	1.0021
SiK	35.21	26.84	417.99	4.15	0.1270	0.9644	0.7879	1.0007

EDS Spot 2

Lsec: 100.0   10 Cnts   8.580 keV   Det: Octane Elite 25

Element	Weight %	Atomic %	Net Int.	Error %	Kratio	Z	A	F
O K	31.29	42.58	173.37	7.89	0.0600	1.0710	0.4606	1.0000
NaK	24.22	22.94	167.36	5.92	0.0608	0.9680	0.6647	1.0025
SiK	44.48	34.48	417.62	3.78	0.1380	0.9650	0.8262	1.0005

EDS Spot 3
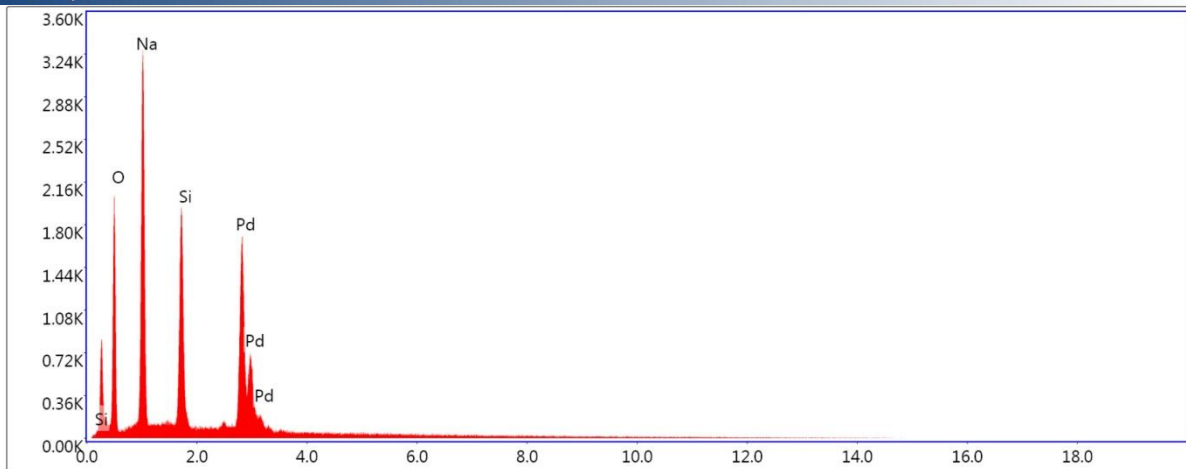
Lsec: 100.0   7 Cnts   8.580 keV   Det: Octane Elite 25

Element	Weight %	Atomic %	Net Int.	Error %	Kratio	Z	A	F
O K	25.12	34.13	201.16	7.02	0.0739	1.0779	0.5161	1.0000
NaK	46.16	43.65	448.07	4.69	0.1726	0.9740	0.7246	1.0017
SiK	28.72	22.22	314.05	4.72	0.1101	0.9709	0.7460	1.0007

EDS Spot 4
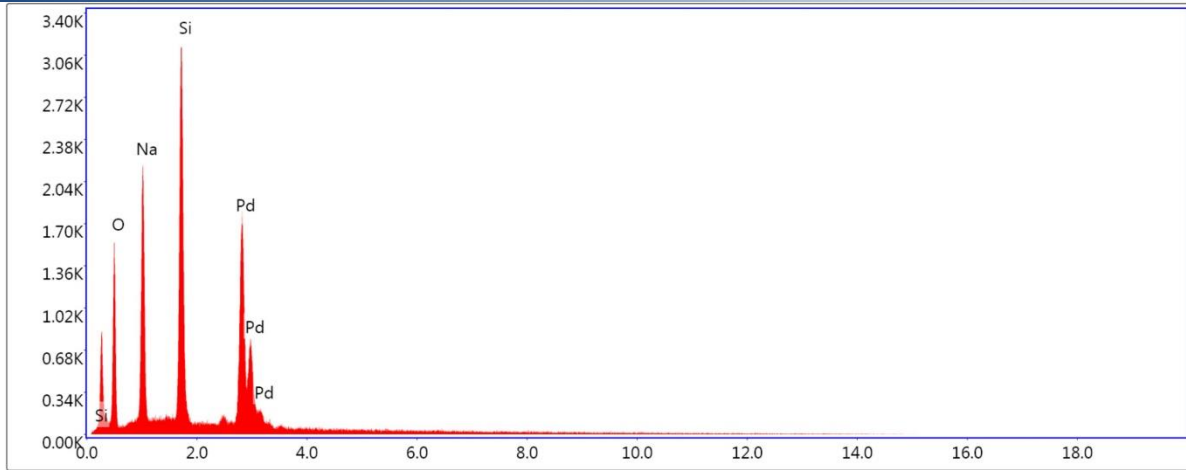
Lsec: 100.0   11 Cnts   8.580 keV   Det: Octane Elite 25

Element	Weight %	Atomic %	Net Int.	Error %	Kratio	Z	A	F
O K	22.49	31.85	143.76	8.16	0.0539	1.0810	0.4405	1.0000
NaK	31.46	31.00	283.54	4.96	0.1114	0.9771	0.7186	1.0024
SiK	46.05	37.15	510.96	3.86	0.1827	0.9742	0.8090	1.0005

EDS Spot 5
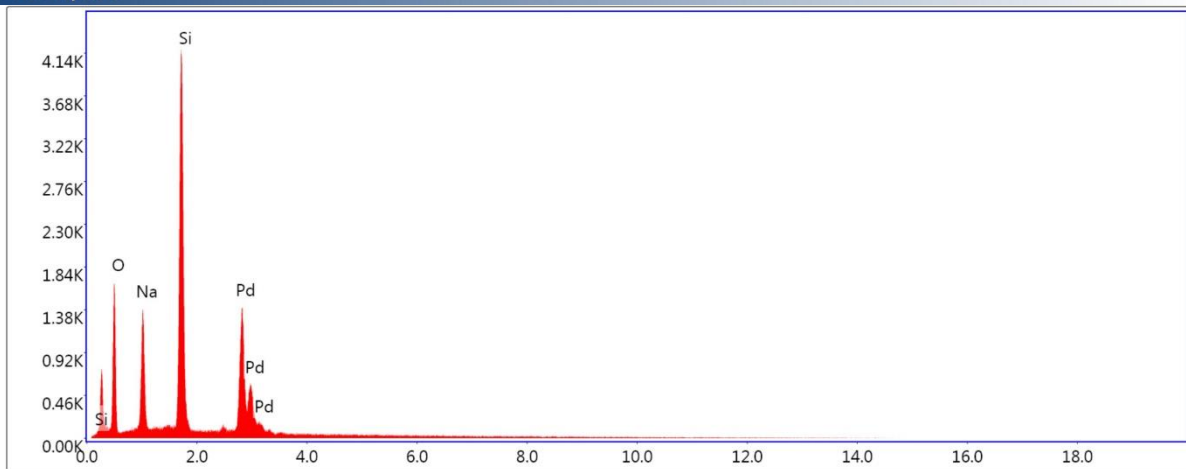
Lsec: 100.0   11 Cnts   8.580 keV   Det: Octane Elite 25

Element	Weight %	Atomic %	Net Int.	Error %	Kratio	Z	A	F
O K	26.04	36.91	162.90	8.31	0.0678	1.0771	0.4149	1.0000
NaK	18.80	18.55	167.69	5.67	0.0732	0.9737	0.6840	1.0030
SiK	55.16	44.54	675.22	3.22	0.2683	0.9708	0.8589	1.0004
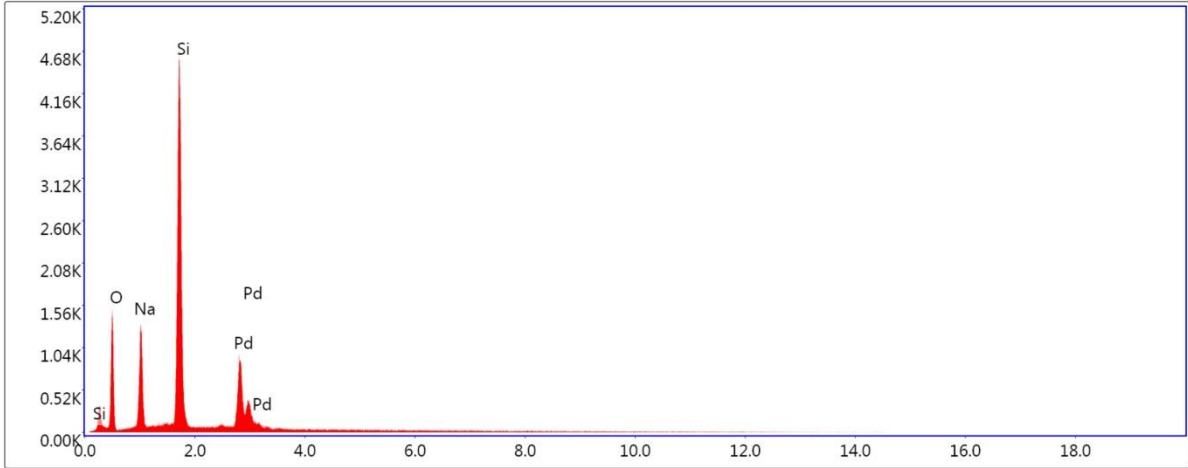
62

EDS Spot 6

Lsec: 100.0   14 Cnts   8.580 keV   Det: Octane Elite 25

Element	Weight %	Atomic %	Net Int.	Error %	Kratio	Z	A	F
O K	23.22	33.58	140.53	8.54	0.0689	1.0803	0.3978	1.0000
NaK	17.29	17.40	158.44	5.56	0.0815	0.9767	0.6963	1.0031
SiK	59.49	49.02	744.89	3.06	0.3486	0.9739	0.8705	1.0003
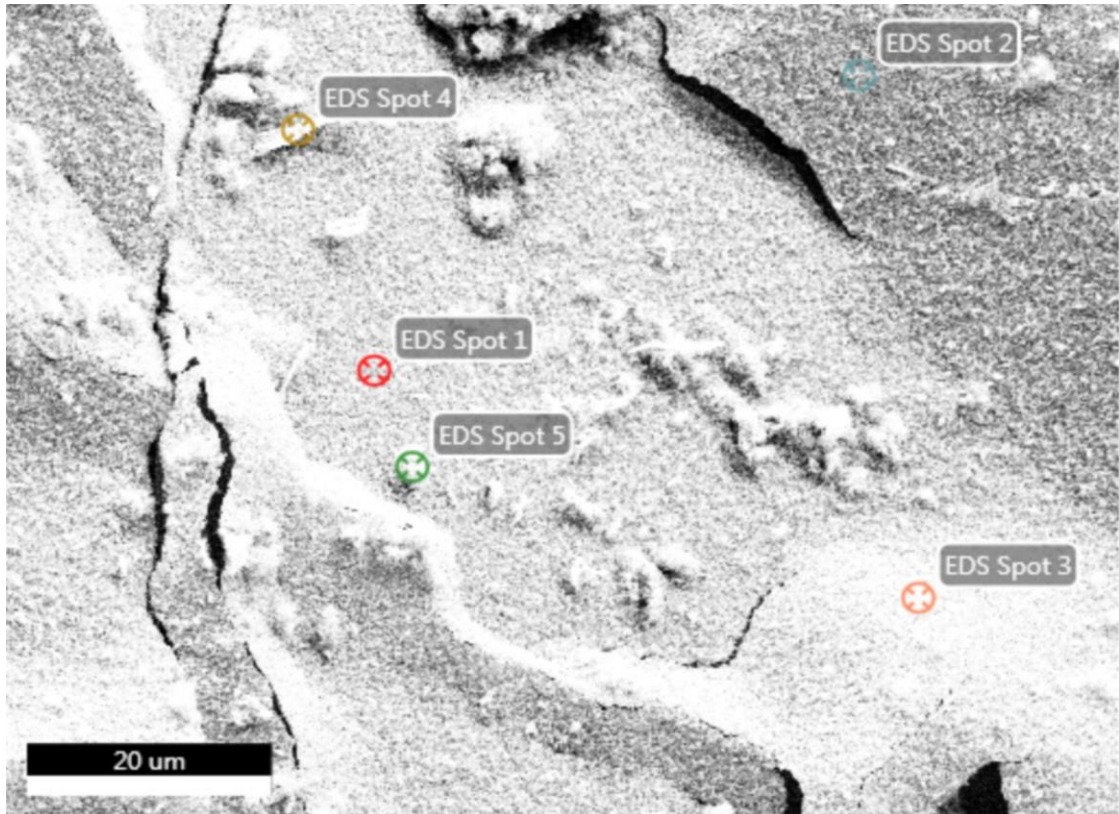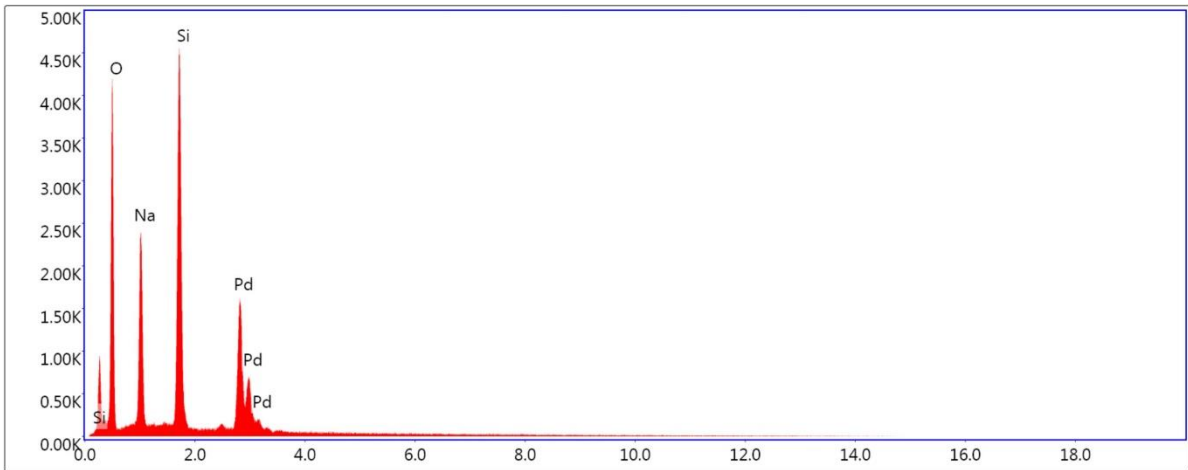
Lsec: 100.0   20 Cnts   8.580 keV   Det: Octane Elite 25

Element	Weight %	Atomic %	Net Int.	Error %	Kratio	Z	A	F
O K	36.65	48.34	438.53	6.85	0.1234	1.0651	0.4944	1.0000
NaK	24.37	22.37	326.53	5.69	0.0965	0.9624	0.6417	1.0024
SiK	38.98	29.29	727.76	3.62	0.1959	0.9594	0.8184	1.0006

EDS Spot 2
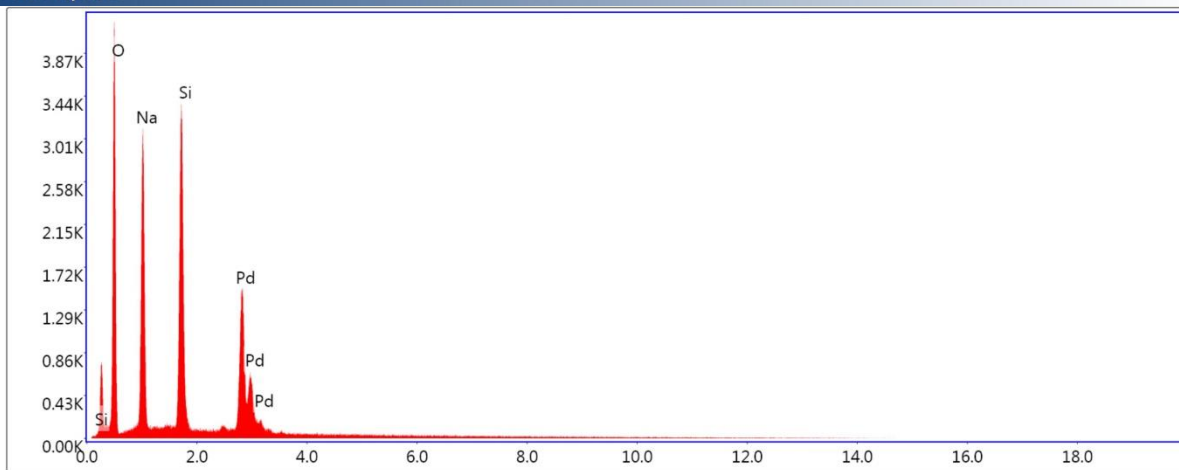
Lsec: 100.0   19 Cnts   8.580 keV   Det: Octane Elite 25

Element	Weight %	Atomic %	Net Int.	Error %	Kratio	Z	A	F
O K	35.98	47.02	439.01	6.54	0.1288	1.0657	0.5261	1.0000
NaK	32.31	29.38	422.30	5.44	0.1301	0.9629	0.6537	1.0020
SiK	31.71	23.60	545.12	4.02	0.1529	0.9598	0.7865	1.0008

EDS Spot 3
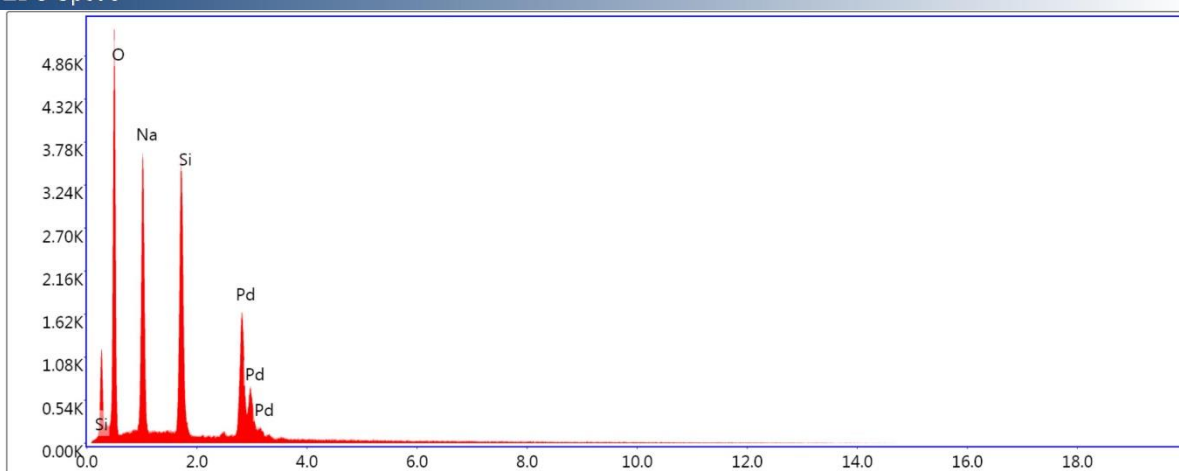
Lsec: 100.0   20 Cnts   8.580 keV   Det: Octane Elite 25

Element	Weight %	Atomic %	Net Int.	Error %	Kratio	Z	A	F
O K	38.14	49.18	566.30	6.28	0.1461	1.0633	0.5450	1.0000
NaK	33.05	29.66	500.27	5.43	0.1355	0.9607	0.6445	1.0019
SiK	28.81	21.16	577.19	4.06	0.1424	0.9575	0.7803	1.0008
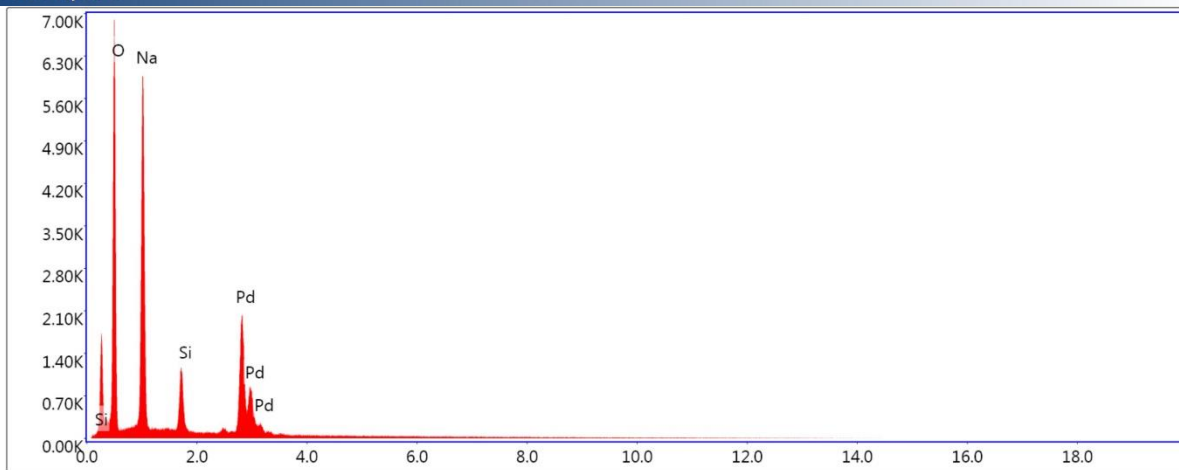
65

EDS Spot 4

Lsec: 100.0   21 Cnts   8.580 keV   Det: Octane Elite 25

Element	Weight %	Atomic %	Net Int.	Error %	Kratio	Z	A	F
O K	39.51	49.14	785.55	5.05	0.1763	1.0617	0.6638	1.0000
NaK	50.91	44.07	865.00	5.17	0.2039	0.9589	0.6589	1.0008
SiK	9.58	6.79	192.21	5.49	0.0413	0.9554	0.7107	1.0013

EDS Spot 5
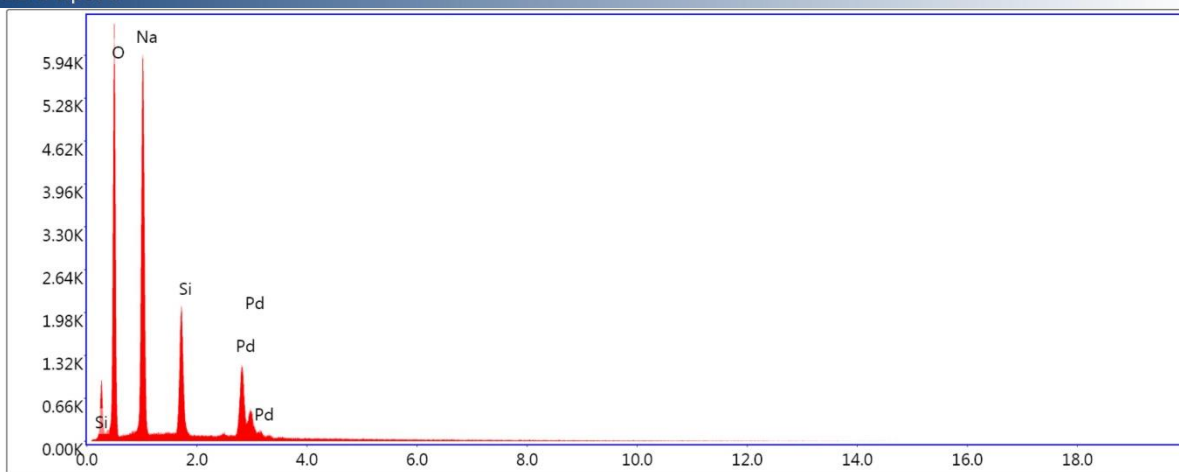
Lsec: 100.0   19 Cnts   8.580 keV   Det: Octane Elite 25

Element	Weight %	Atomic %	Net Int.	Error %	Kratio	Z	A	F
O K	36.97	46.88	704.40	5.52	0.1846	1.0645	0.6161	1.0000
NaK	47.34	41.78	840.77	5.03	0.2314	0.9615	0.6668	1.0011
SiK	15.70	11.34	332.63	4.85	0.0834	0.9582	0.7270	1.0011

Additional SEM- and EDS results of dried sample of SS + HCl + DW from flooding #1, before injection (500 mD).
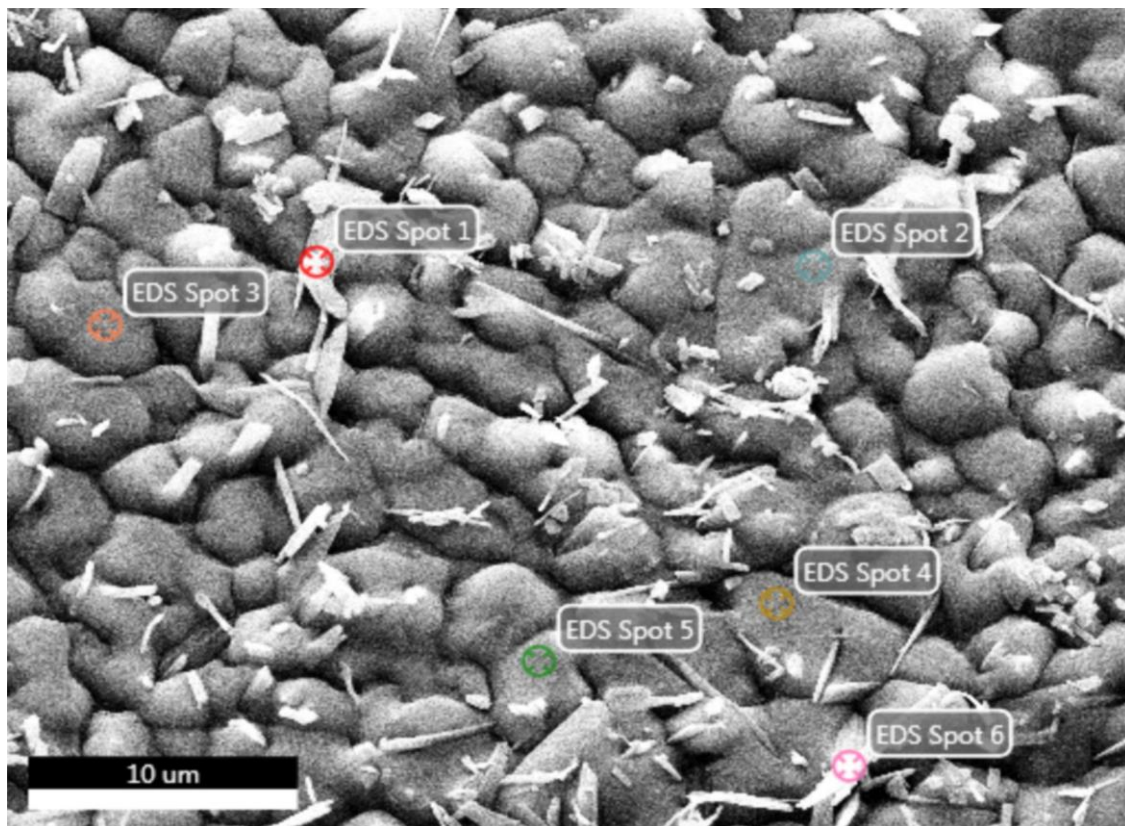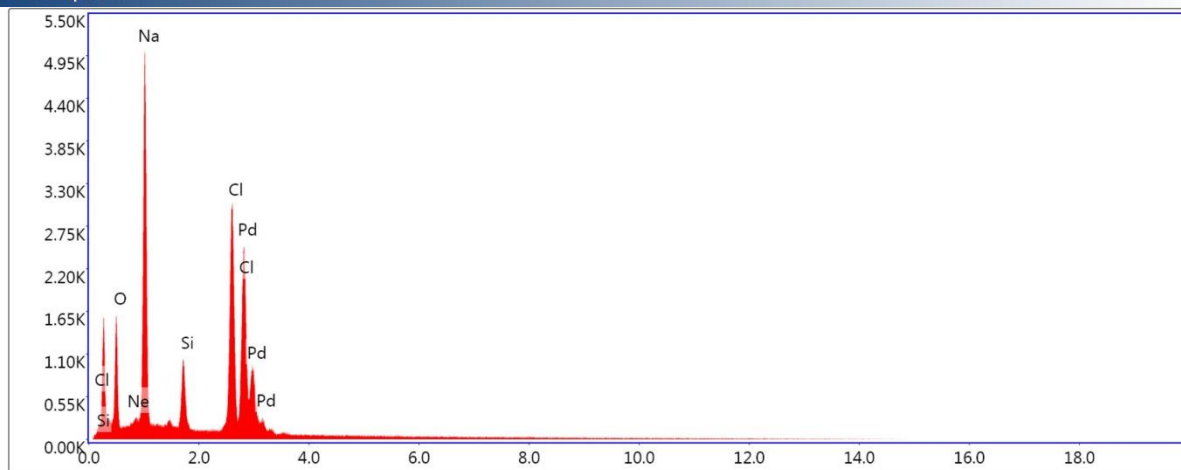
EDS Spot 1

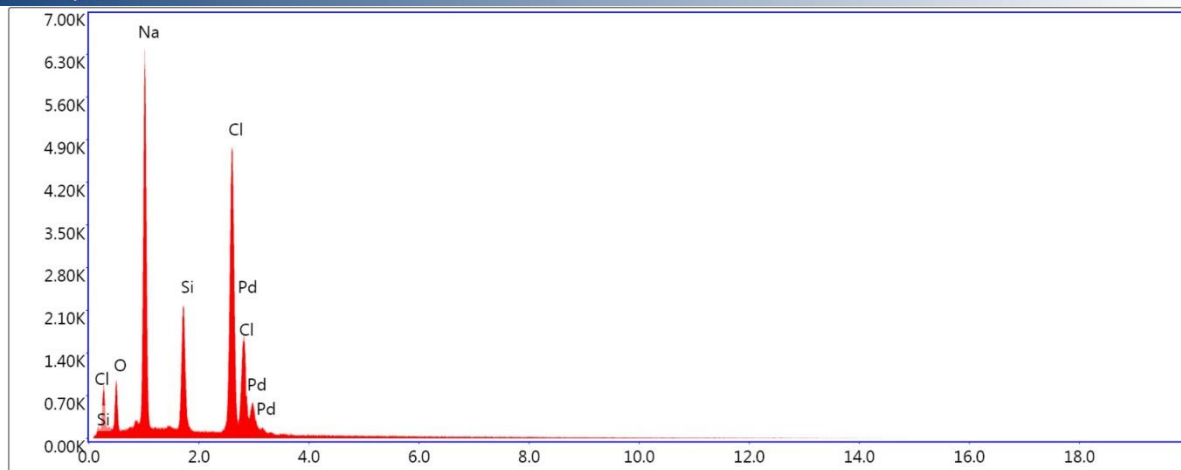

Lsec: 100.0   19 Cnts   8.580 keV   Det: Octane Elite 25

Element	Weight %	Atomic %	Net Int.	Error %	Kratio	Z	A	F
O K	17.72	27.06	168.09	9.48	0.0375	1.1119	0.3037	1.0000
NeK	0.74	0.89	18.08	16.23	0.0025	1.0595	0.5183	1.0000
NaK	39.01	41.45	706.23	5.05	0.1655	1.0057	0.6724	1.0014
SiK	7.10	6.18	160.18	5.13	0.0342	1.0031	0.7606	1.0071
ClK	35.43	24.42	583.51	2.82	0.1900	0.9316	0.9171	1.0018

EDS Spot 2

Lsec: 100.0   28 Cnts   8.580 keV   Det: Octane Elite 25

Element	Weight %	Atomic %	Net Int.	Error %	Kratio	Z	A	F
O K	8.80	14.64	88.66	10.20	0.0202	1.1298	0.2554	1.0000
NaK	35.84	41.50	857.98	4.65	0.2055	1.0223	0.7032	1.0016
SiK	11.70	11.09	343.51	4.29	0.0749	1.0200	0.7828	1.0073
ClK	43.66	32.78	902.01	2.71	0.3003	0.9476	0.9102	1.0013

EDS Spot 3
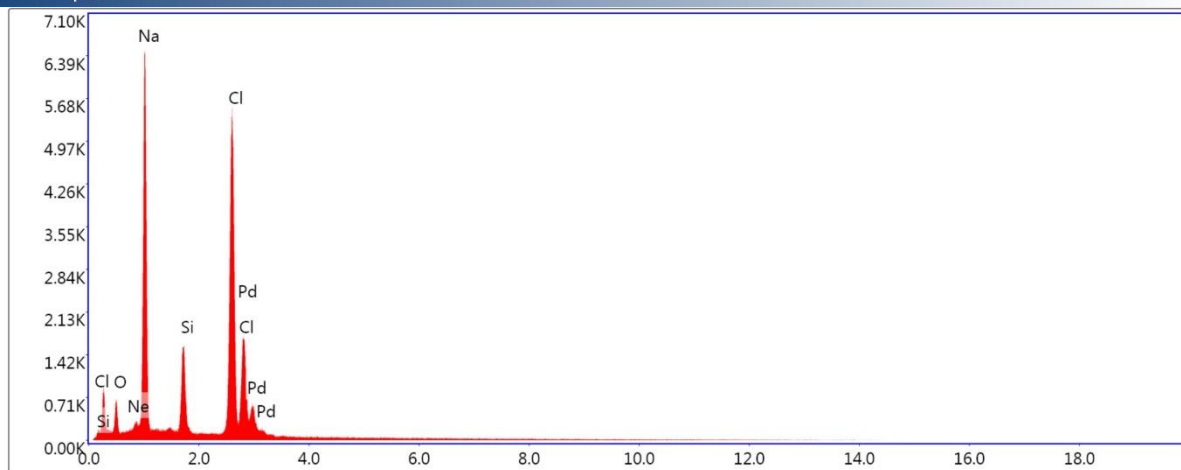
Lsec: 100.0   28 Cnts   8.580 keV   Det: Octane Elite 25

Element	Weight %	Atomic %	Net Int.	Error %	Kratio	Z	A	F
O K	5.97	10.20	57.50	11.05	0.0131	1.1371	0.2409	1.0000
NeK	0.38	0.52	12.81	19.50	0.0018	1.0839	0.5494	1.0000
NaK	36.48	43.43	887.11	4.63	0.2129	1.0290	0.7041	1.0016
SiK	8.51	8.29	252.65	4.48	0.0552	1.0269	0.7799	1.0079
ClK	48.66	37.56	1030.19	2.59	0.3436	0.9540	0.9193	1.0012
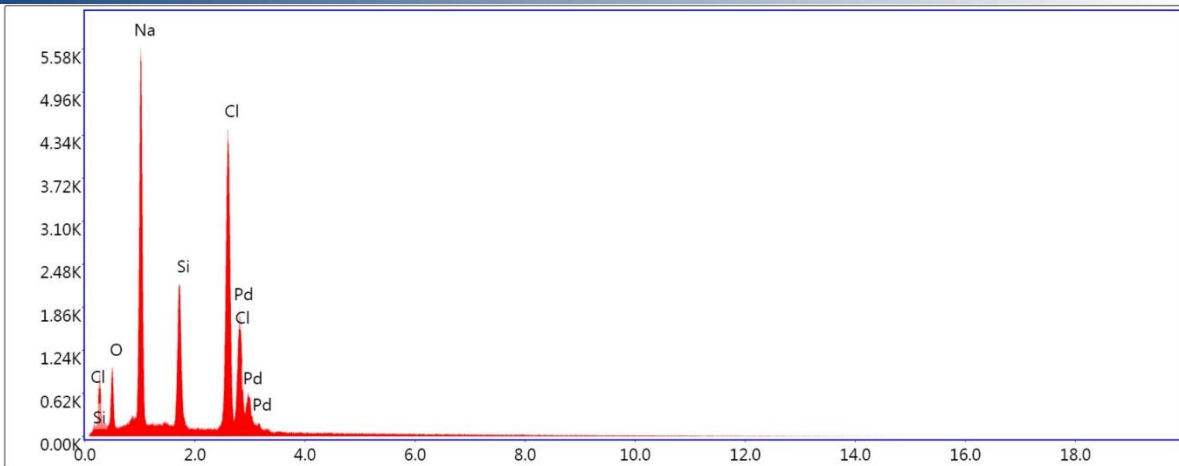
68

EDS Spot 4

Lsec: 100.0   16 Cnts   8.580 keV   Det: Octane Elite 25

Element	Weight %	Atomic %	Net Int.	Error %	Kratio	Z	A	F
O K	9.84	16.26	94.65	10.14	0.0222	1.1276	0.2584	1.0000
NaK	34.76	39.95	779.66	4.73	0.1925	1.0203	0.6988	1.0016
SiK	12.82	12.06	356.58	4.21	0.0802	1.0180	0.7864	1.0072
ClK	42.58	31.73	827.52	2.78	0.2839	0.9457	0.9081	1.0013

EDS Spot 5
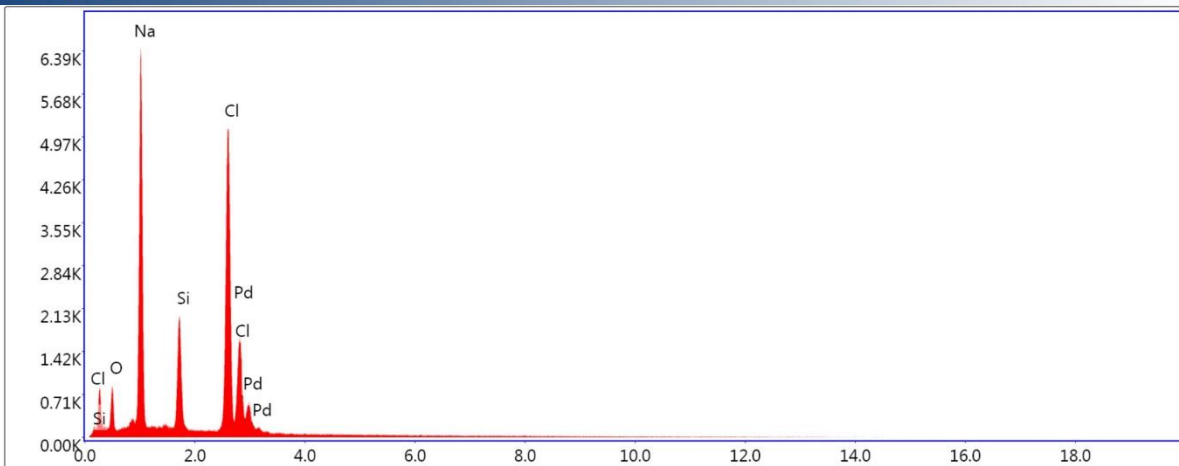
Lsec: 100.0   9 Cnts   8.580 keV   Det: Octane Elite 25

Element	Weight %	Atomic %	Net Int.	Error %	Kratio	Z	A	F
O K	7.69	12.96	77.57	10.76	0.0176	1.1329	0.2486	1.0000
NaK	35.92	42.10	885.42	4.64	0.2111	1.0252	0.7043	1.0016
SiK	10.53	10.10	317.80	4.37	0.0690	1.0230	0.7827	1.0076
ClK	45.86	34.85	978.09	2.66	0.3241	0.9503	0.9139	1.0012

EDS Spot 6
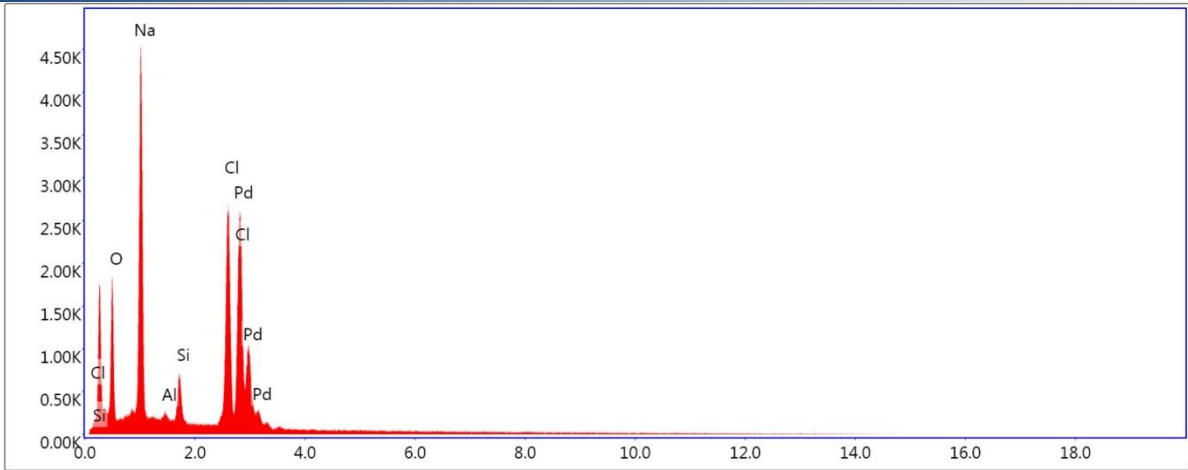
Lsec: 100.0   16 Cnts   8.580 keV   Det: Octane Elite 25

Element	Weight %	Atomic %	Net Int.	Error %	Kratio	Z	A	F
O K	21.49	31.97	202.93	9.04	0.0444	1.1064	0.3203	1.0000
NaK	38.57	39.94	652.93	5.17	0.1500	1.0005	0.6660	1.0014
AlK	1.68	1.48	31.32	12.27	0.0063	0.9776	0.6514	1.0049
SiK	5.20	4.41	109.38	5.64	0.0229	0.9979	0.7512	1.0070
ClK	33.07	22.21	515.41	2.84	0.1645	0.9267	0.9193	1.0020
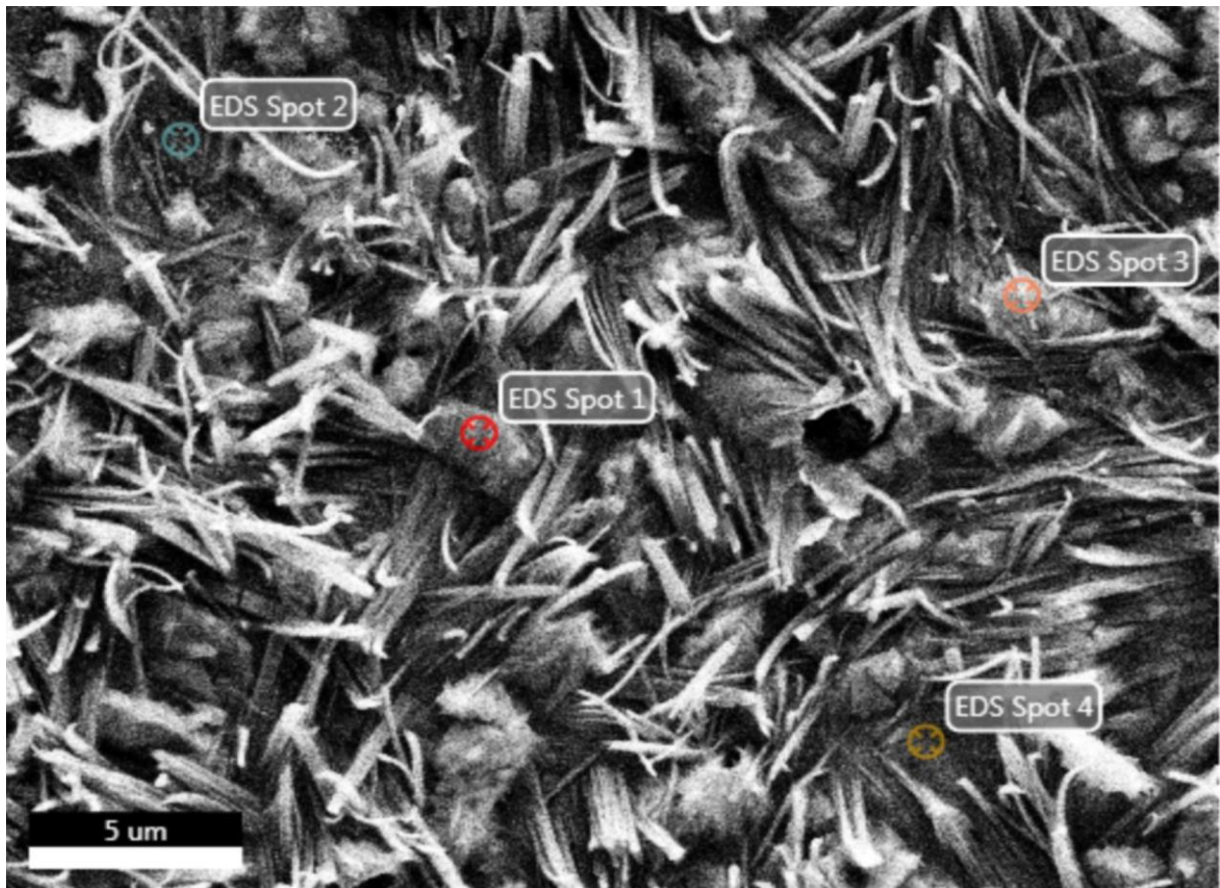
EDS Spot 1
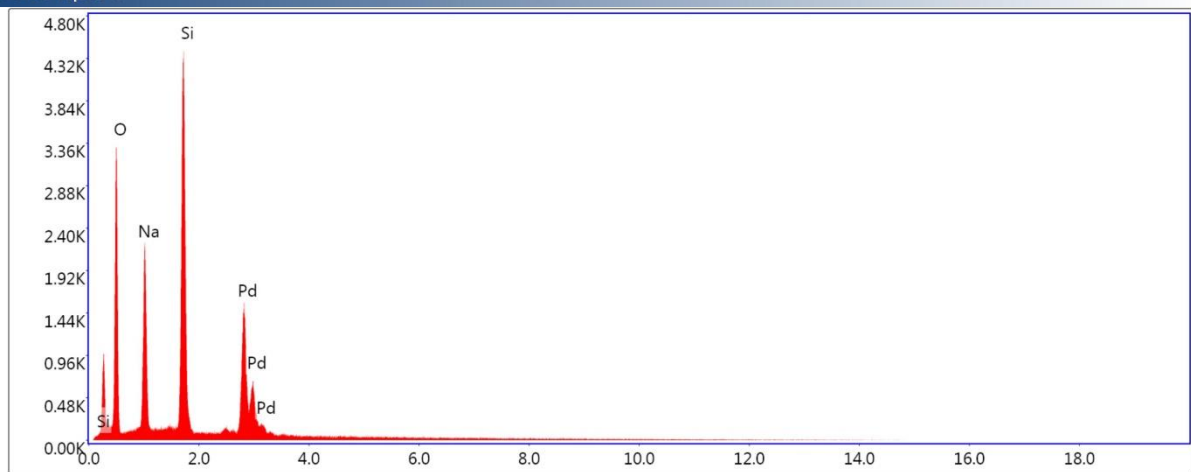
Lsec: 100.0   21 Cnts   8.580 keV   Det: Octane Elite 25

Element	Weight %	Atomic %	Net Int.	Error %	Kratio	Z	A	F
O K	34.32	45.92	356.01	7.18	0.1104	1.0677	0.4772	1.0000
NaK	23.75	22.12	290.17	5.63	0.0944	0.9649	0.6512	1.0025
SiK	41.93	31.96	708.82	3.57	0.2100	0.9618	0.8243	1.0006

EDS Spot 2
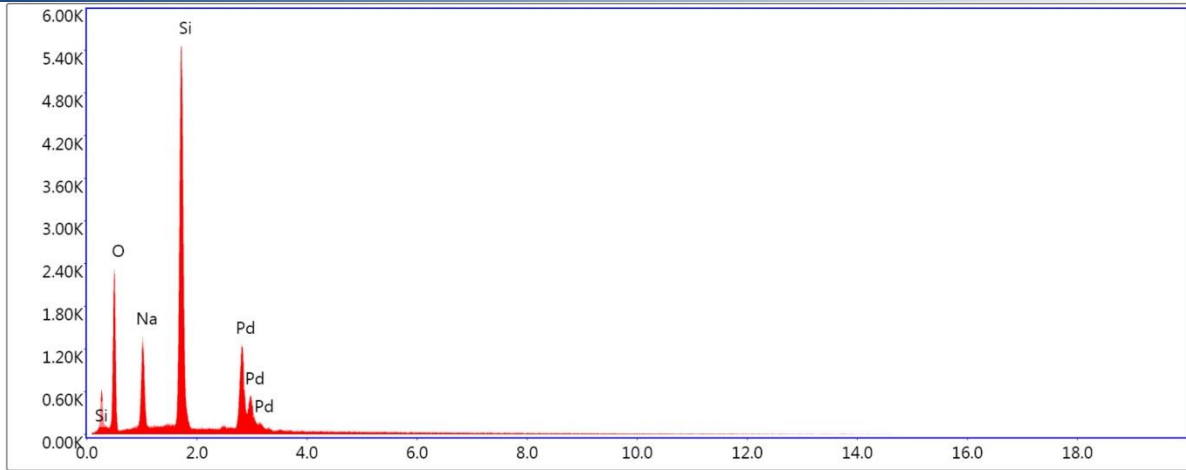
Lsec: 100.0   14 Cnts   8.580 keV   Det: Octane Elite 25

Element	Weight %	Atomic %	Net Int.	Error %	Kratio	Z	A	F
O K	29.31	41.04	235.66	7.90	0.0874	1.0733	0.4182	1.0000
NaK	14.66	14.28	161.73	5.90	0.0630	0.9703	0.6643	1.0031
SiK	56.03	44.68	887.55	3.00	0.3145	0.9674	0.8731	1.0004

EDS Spot 3
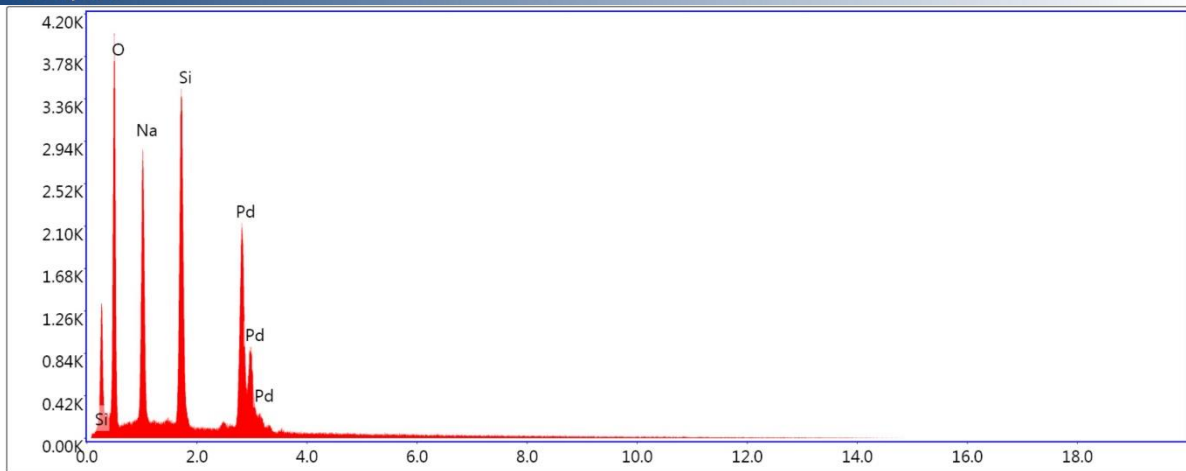
Lsec: 100.0   24 Cnts   8.580 keV   Det: Octane Elite 25

Element	Weight %	Atomic %	Net Int.	Error %	Kratio	Z	A	F
O K	36.49	47.69	435.89	6.60	0.1128	1.0652	0.5204	1.0000
NaK	30.50	27.74	391.75	5.51	0.1064	0.9624	0.6487	1.0021
SiK	33.01	24.57	566.46	3.95	0.1401	0.9593	0.7927	1.0007

EDS Spot 4
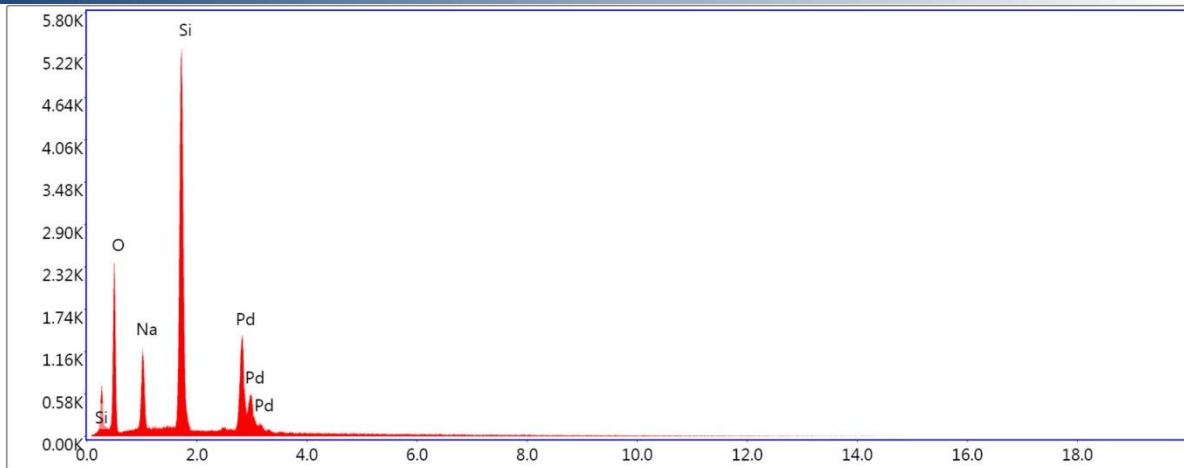
Lsec: 100.0   16 Cnts   8.580 keV   Det: Octane Elite 25

Element	Weight %	Atomic %	Net Int.	Error %	Kratio	Z	A	F
O K	30.57	42.58	235.49	7.90	0.0869	1.0719	0.4192	1.0000
NaK	13.15	12.75	137.14	6.20	0.0531	0.9690	0.6567	1.0032
SiK	56.28	44.67	856.89	2.96	0.3020	0.9662	0.8779	1.0004

Additional SEM- and EDS results of dried sample of SS + HCl + DW from flooding #4, before injection (200 mD).

Element	Weight %	Atomic %	Net Int.	Error %	Kratio	Z	A	F
NaK	28.94	38.14	528.85	4.96	0.1640	1.0496	0.6860	1.0017
SiK	5.09	5.49	120.81	5.03	0.0340	1.0478	0.8049	1.0096
ClK	65.97	56.37	1106.01	2.36	0.4750	0.9737	0.9405	1.0006

Lsec: 100.0   1 Cnts   14.260 keV   Det: Octane Elite 25

Element	Weight %	Atomic %	Net Int.	Error %	Kratio	Z	A	F
NaK	34.71	45.05	774.27	4.78	0.2038	1.0490	0.6948	1.0016
ClK	65.29	54.95	1331.29	2.23	0.4854	0.9730	0.9488	1.0007

EDS Spot 3
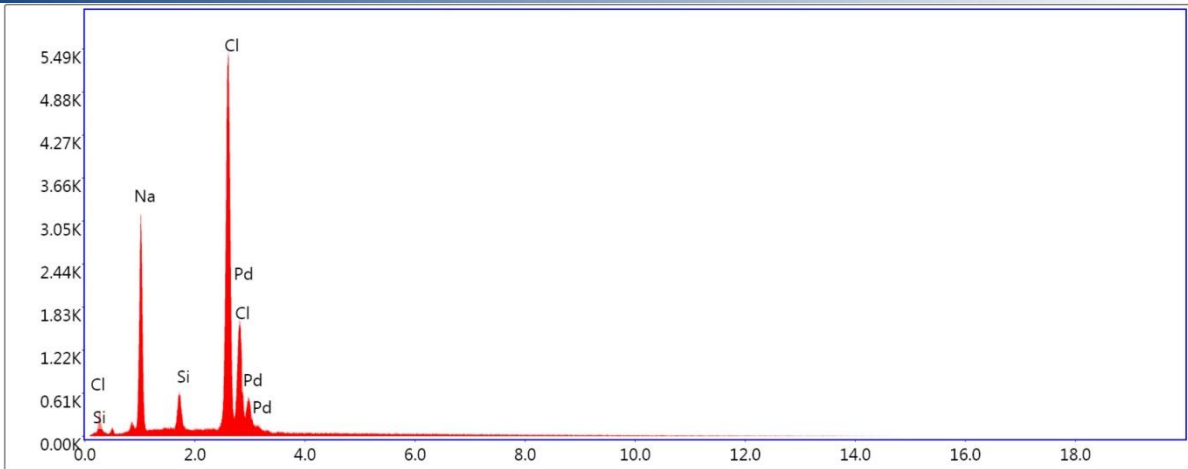
Lsec: 100.0   3 Cnts   14.260 keV   Det: Octane Elite 25

Element	Weight %	Atomic %	Net Int.	Error %	Kratio	Z	A	F
NaK	25.48	34.20	395.00	5.21	0.1378	1.0531	0.6722	1.0018
SiK	4.01	4.41	83.77	6.08	0.0266	1.0514	0.8167	1.0102
ClK	70.51	61.38	1032.53	2.28	0.4990	0.9772	0.9489	1.0005

EDS Spot 4
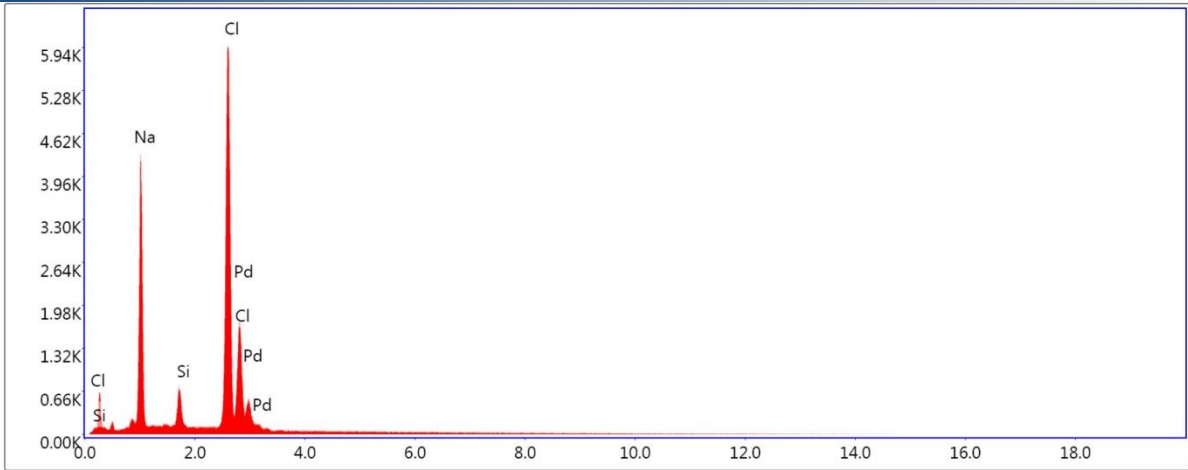
Lsec: 100.0　　0 Cnts　　14.260 keV　　Det: Octane Elite 25

Element	Weight %	Atomic %	Net Int.	Error %	Kratio	Z	A	F
NaK	29.63	39.00	561.31	4.94	0.1695	1.0497	0.6863	1.0017
SiK	4.15	4.47	101.71	5.31	0.0279	1.0480	0.8018	1.0097
ClK	66.22	56.53	1153.07	2.33	0.4823	0.9739	0.9425	1.0006
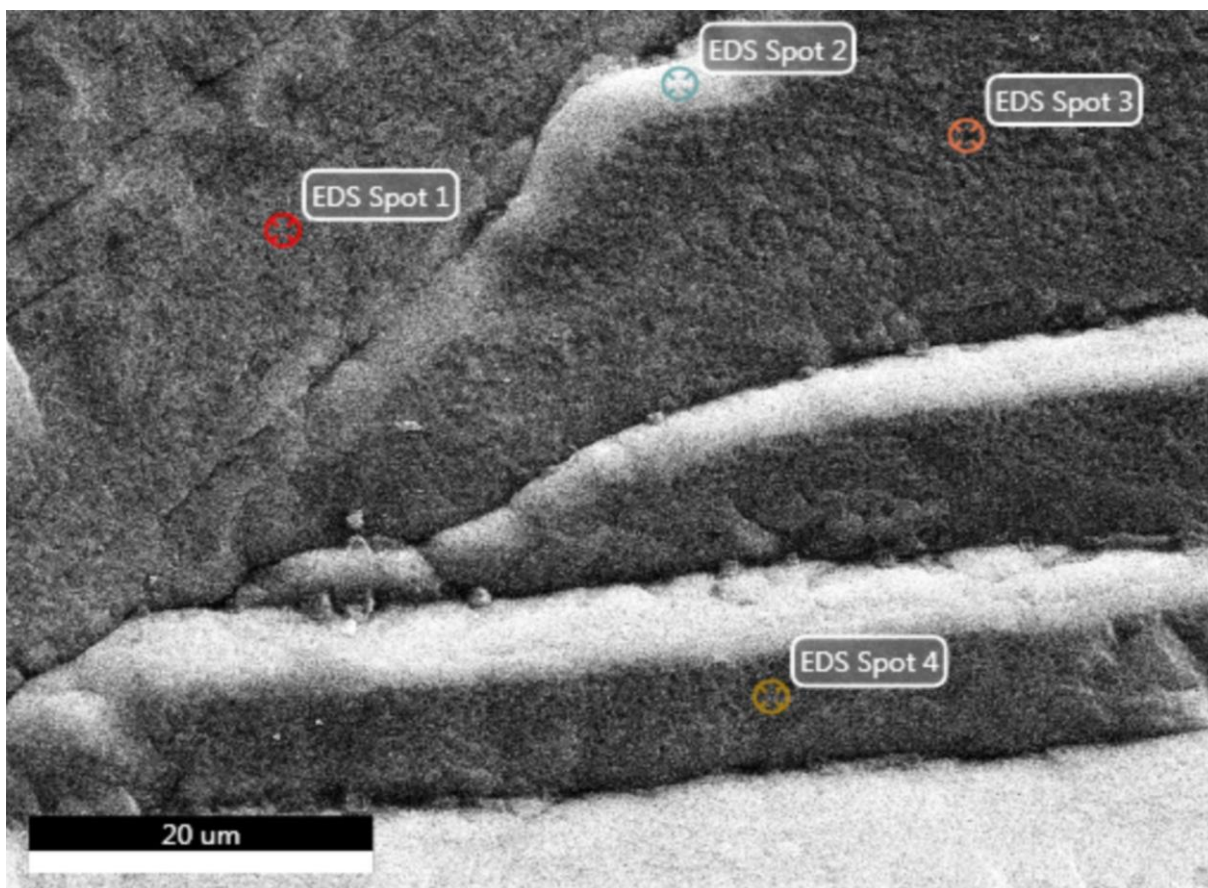
EDS Spot 1
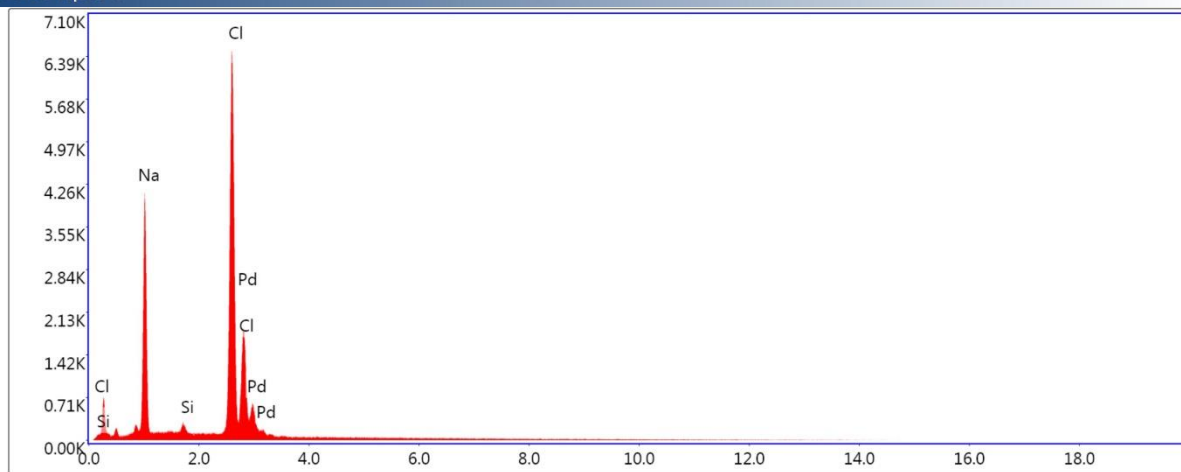
Lsec: 100.0   148 Cnts   1.595 keV   Det: Octane Elite 25

Element	Weight %	Atomic %	Net Int.	Error %	Kratio	Z	A	F
NaK	28.89	38.42	531.30	5.03	0.1601	1.0525	0.6786	1.0017
SiK	1.24	1.35	29.80	11.24	0.0082	1.0508	0.8030	1.0104
ClK	69.87	60.24	1207.00	2.20	0.5041	0.9766	0.9533	1.0006

EDS Spot 2
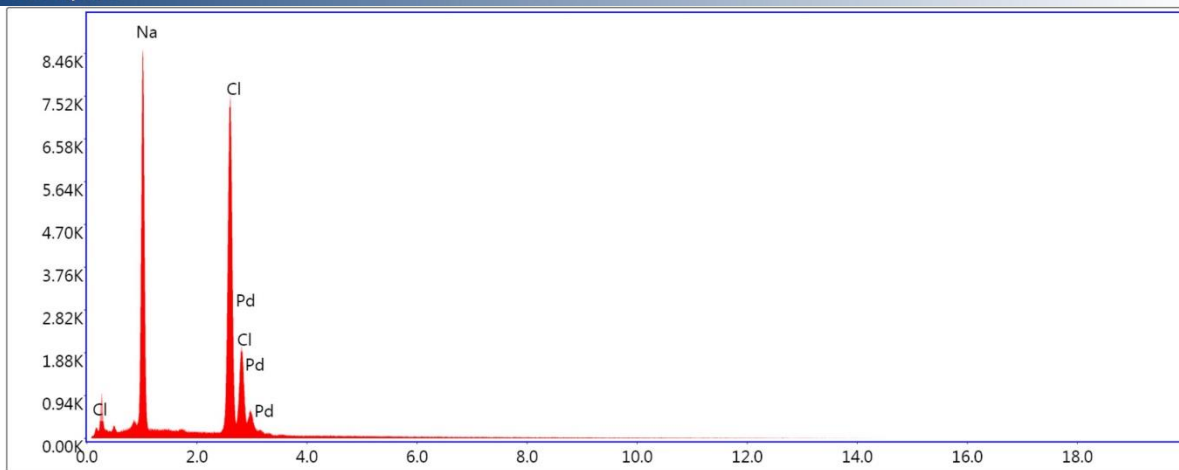
Lsec: 100.0   163 Cnts   1.595 keV   Det: Octane Elite 25

Element	Weight %	Atomic %	Net Int.	Error %	Kratio	Z	A	F
NaK	41.86	52.61	1177.88	4.39	0.2592	1.0434	0.7210	1.0014
ClK	58.14	47.39	1424.99	2.32	0.4345	0.9676	0.9389	1.0009

EDS Spot 3
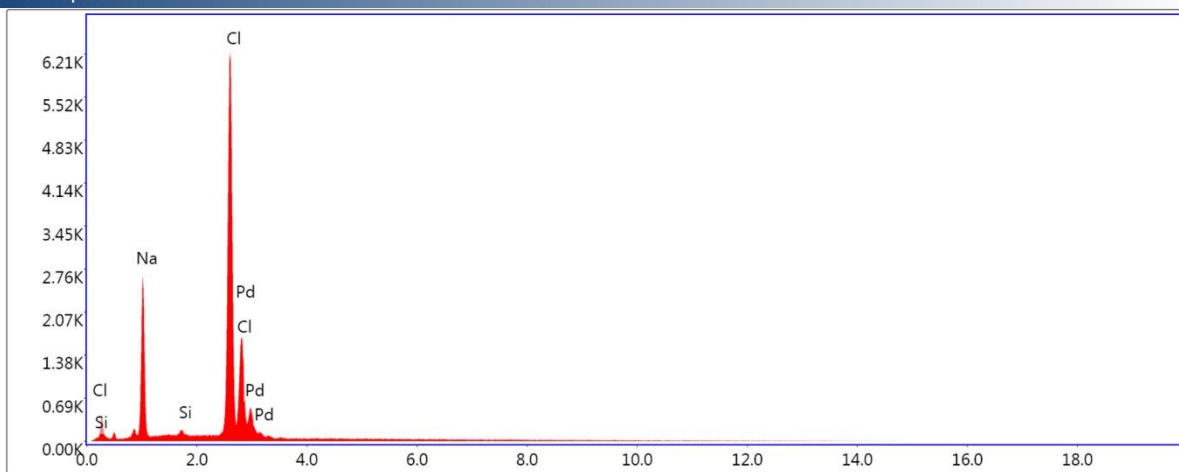
Lsec: 99.9   116 Cnts   1.595 keV   Det: Octane Elite 25

Element	Weight %	Atomic %	Net Int.	Error %	Kratio	Z	A	F
NaK	21.50	29.66	330.42	5.51	0.1157	1.0589	0.6536	1.0019
SiK	0.54	0.61	11.75	18.37	0.0037	1.0573	0.8293	1.0114
ClK	77.96	69.73	1184.71	2.06	0.5748	0.9828	0.9663	1.0004

78
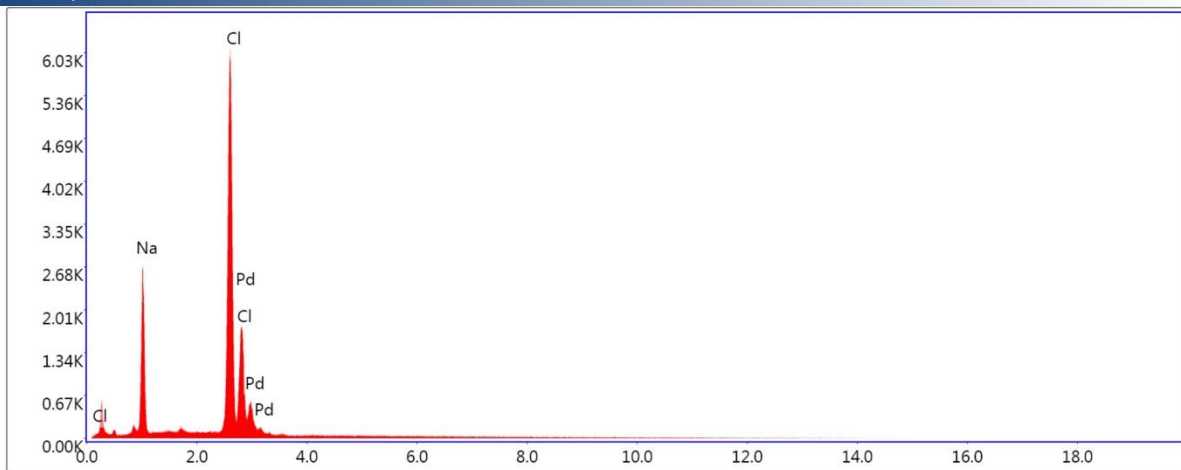
EDS Spot 4

Lsec: 100.0   101 Cnts   1.595 keV   Det: Octane Elite 25

Element	Weight %	Atomic %	Net Int.	Error %	Kratio	Z	A	F
NaK	22.10	30.43	328.47	5.51	0.1156	1.0588	0.6544	1.0018
ClK	77.90	69.57	1144.65	2.08	0.5584	0.9827	0.9672	1.0004

79

EDS Spot 1

Lsec: 100.0   7 Cnts   11.670 keV   Det: Octane Elite 25
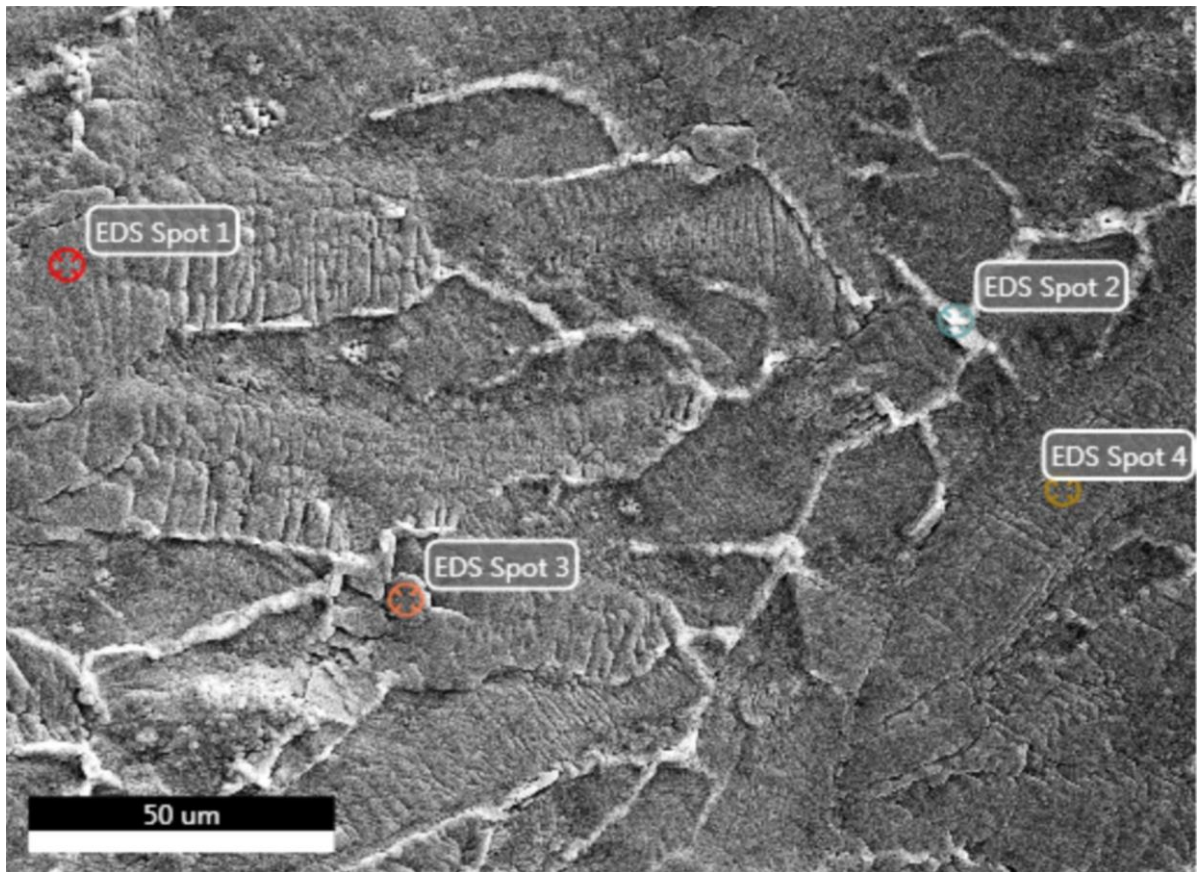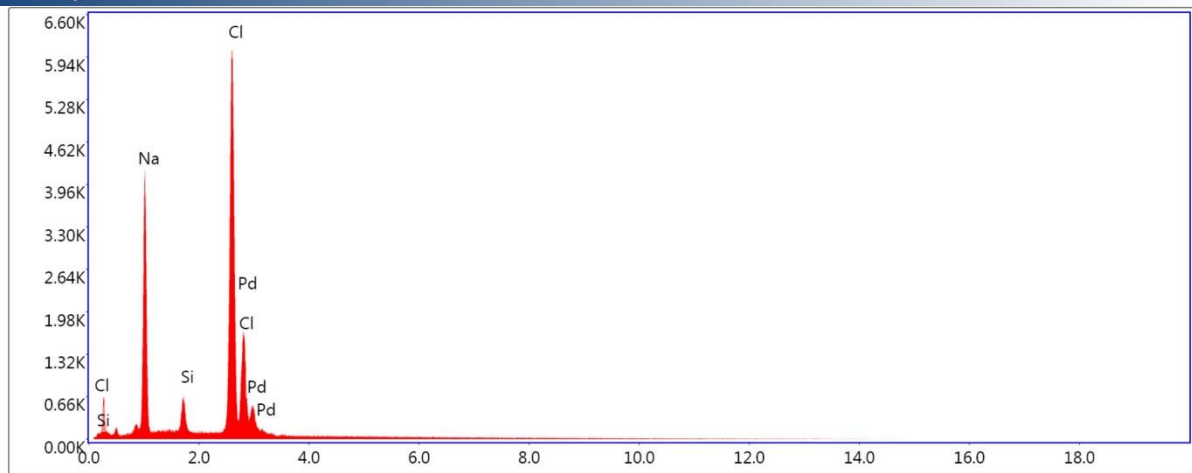
Element	Weight %	Atomic %	Net Int.	Error %	Kratio	Z	A	F
NaK	25.84	40.20	552.32	6.25	0.1594	1.1081	0.5557	1.0016
SiK	2.92	3.72	94.41	5.93	0.0248	1.1085	0.7581	1.0087
ClK	47.78	48.20	1152.11	2.57	0.4605	1.0321	0.9241	1.0104
PdL	23.45	7.88	225.54	4.64	0.1675	0.8075	0.8854	0.9985

EDS Spot 2
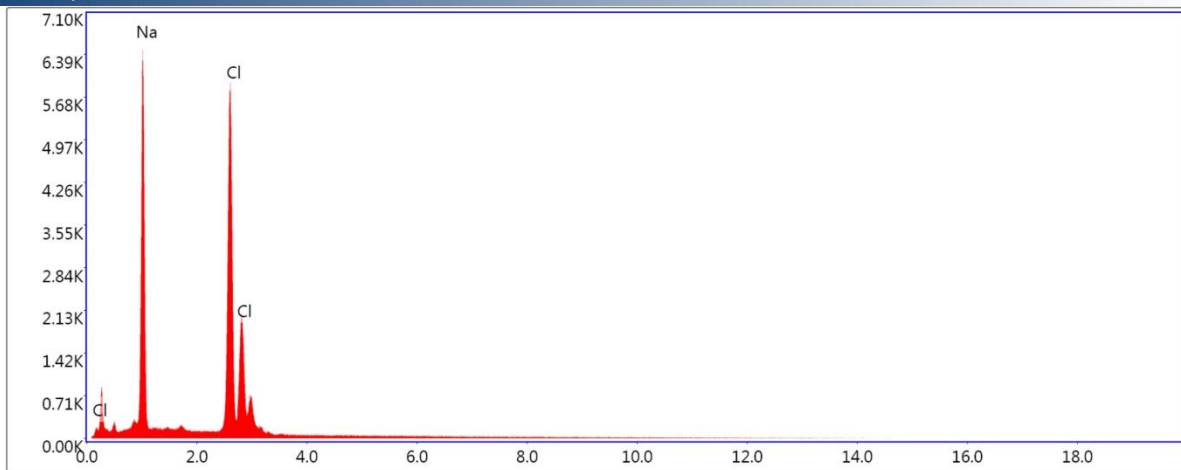
Lsec: 100.0   10 Cnts   11.670 keV   Det: Octane Elite 25

Element	Weight %	Atomic %	Net Int.	Error %	Kratio	Z	A	F
NaK	40.67	51.39	881.21	4.52	0.3046	1.0443	0.7160	1.0014
ClK	59.33	48.61	1129.56	2.30	0.5407	0.9685	0.9403	1.0009

EDS Spot 3
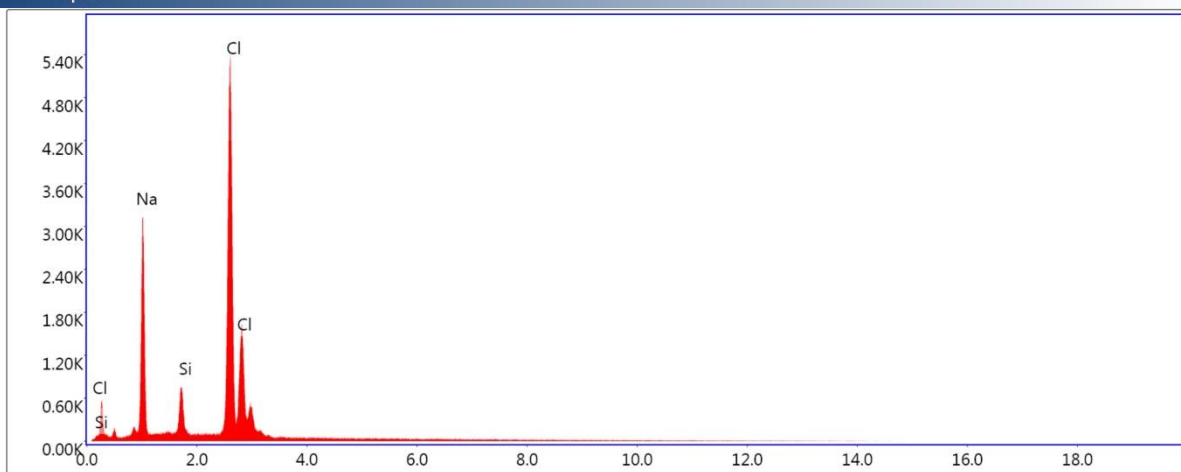
Lsec: 100.0   5 Cnts   11.670 keV   Det: Octane Elite 25

Element	Weight %	Atomic %	Net Int.	Error %	Kratio	Z	A	F
NaK	25.61	34.27	405.39	5.18	0.1822	1.0521	0.6751	1.0018
SiK	5.17	5.66	109.65	5.21	0.0448	1.0504	0.8170	1.0099
ClK	69.22	60.07	1026.23	2.27	0.6389	0.9762	0.9449	1.0006

EDS Spot 4
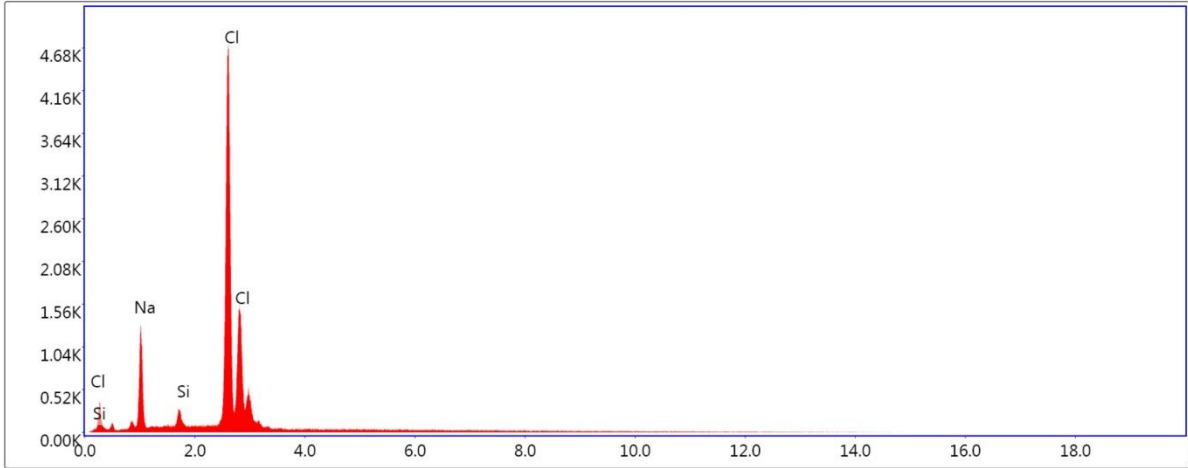
Lsec: 100.0   4 Cnts   11.670 keV   Det: Octane Elite 25

Element	Weight %	Atomic %	Net Int.	Error %	Kratio	Z	A	F
NaK	14.04	20.04	146.02	6.26	0.0946	1.0639	0.6323	1.0021
SiK	1.68	1.96	26.34	8.96	0.0155	1.0625	0.8579	1.0120
ClK	84.28	78.00	902.93	2.00	0.8104	0.9877	0.9732	1.0003

Additional SEM- and EDS results of fragment of flooded 500 mD-core
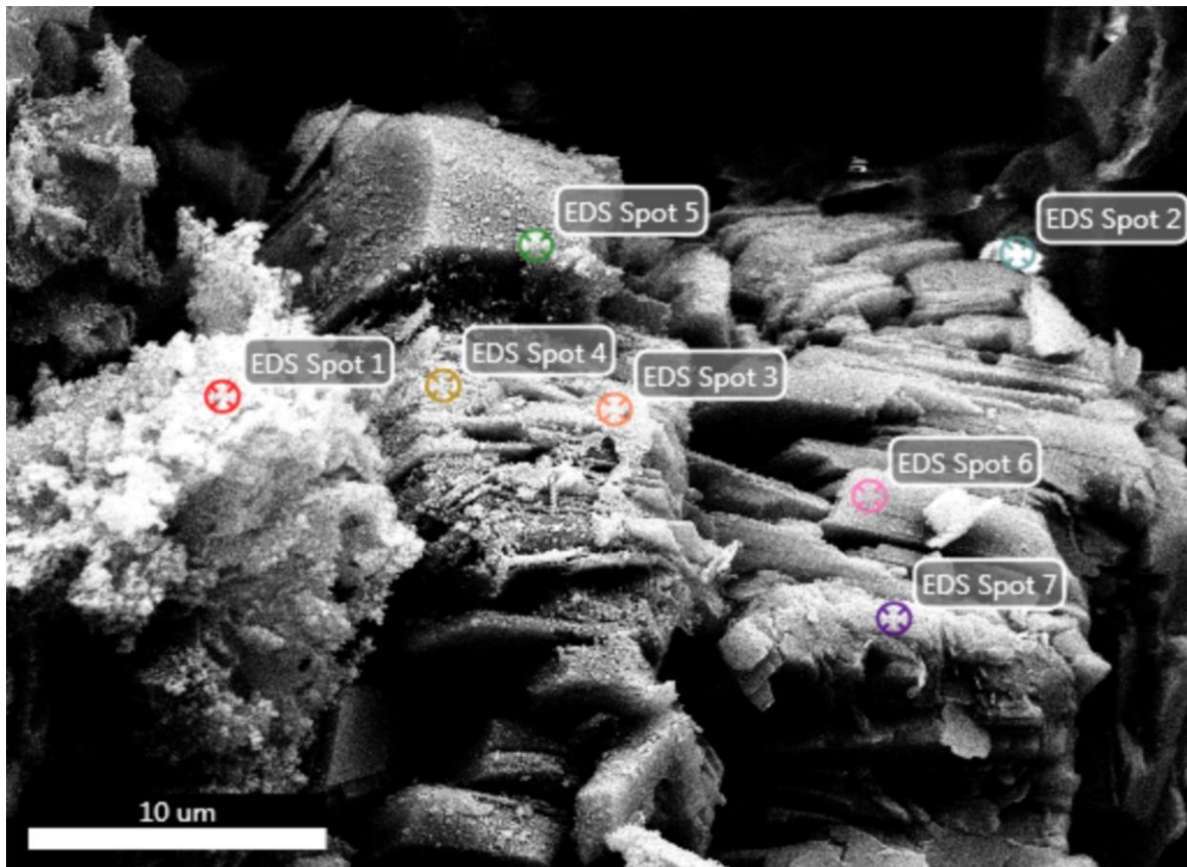
EDS Spot 1
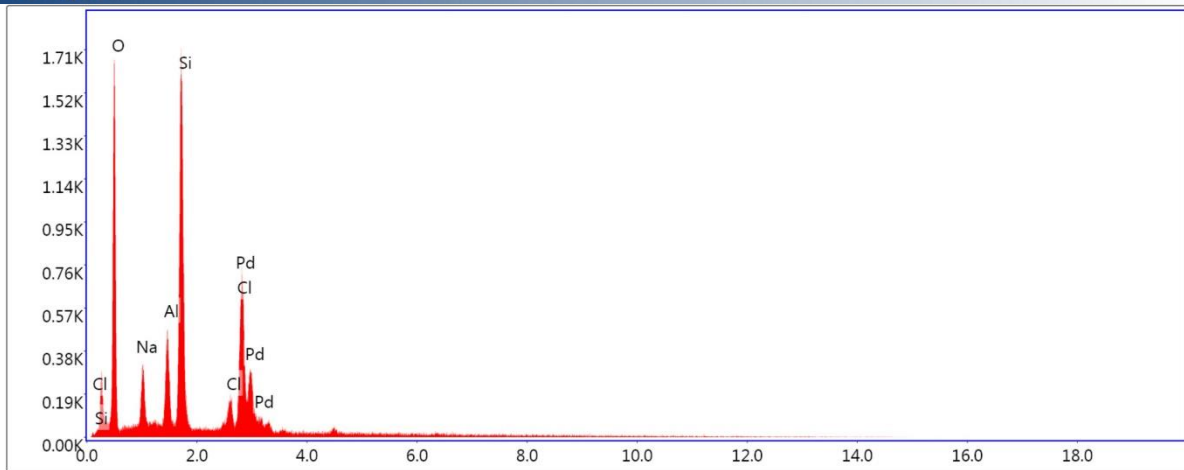
Lsec: 10.0   297 Cnts   1.050 keV   Det: Octane Elite 25

Element	Weight %	Atomic %	Net Int.	Error %	Kratio	Z	A	F
O K	42.97	56.62	1779.66	7.90	0.1193	1.0640	0.4297	1.0000
NaK	7.32	6.71	355.85	8.96	0.0248	0.9616	0.5794	1.0030
AlK	8.55	6.68	642.96	5.83	0.0389	0.9392	0.7913	1.0083
SiK	35.37	26.54	2661.85	4.00	0.1686	0.9586	0.8172	1.0019
ClK	5.80	3.45	276.38	10.77	0.0267	0.8899	0.8476	1.0034

EDS Spot 2
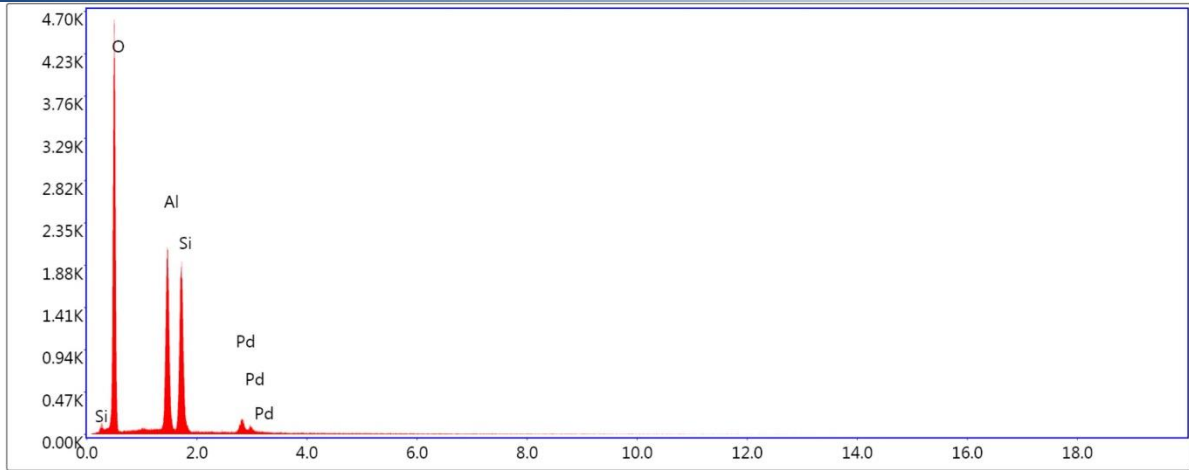
Lsec: 10.0   53 Cnts   1.050 keV   Det: Octane Elite 25

Element	Weight %	Atomic %	Net Int.	Error %	Kratio	Z	A	F
O K	54.56	67.39	5273.95	6.46	0.2797	1.0503	0.5236	1.0000
AlK	22.13	16.21	3289.39	3.87	0.1574	0.9266	0.8188	1.0058
SiK	23.30	16.40	3081.91	4.71	0.1544	0.9456	0.7511	1.0008

EDS Spot 3
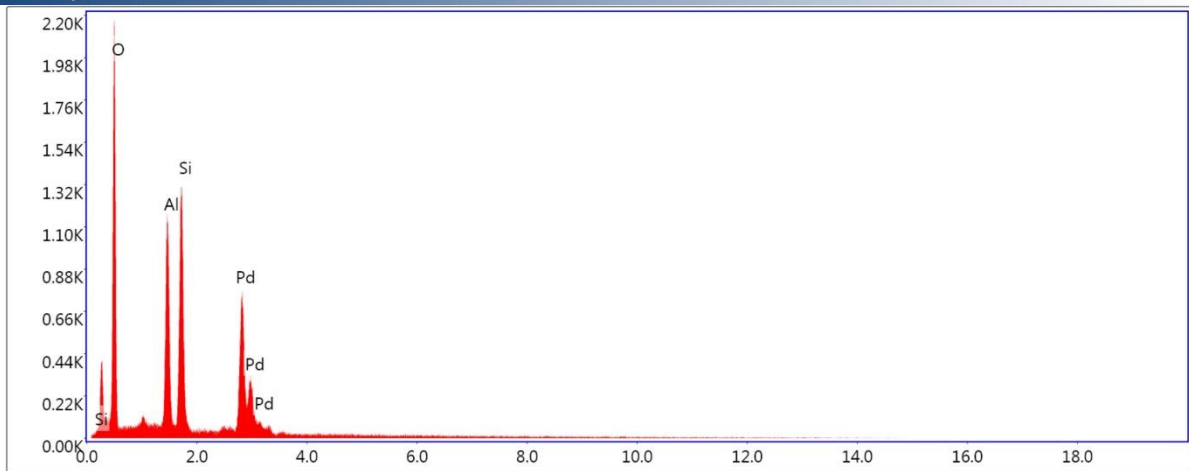
Lsec: 10.0   112 Cnts   1.050 keV   Det: Octane Elite 25

Element	Weight %	Atomic %	Net Int.	Error %	Kratio	Z	A	F
O K	49.33	62.68	2391.56	7.19	0.1550	1.0559	0.4881	1.0000
AlK	21.77	16.40	1771.01	4.16	0.1036	0.9318	0.8320	1.0065
SiK	28.90	20.92	2083.30	4.76	0.1275	0.9510	0.7607	1.0007

EDS Spot 4
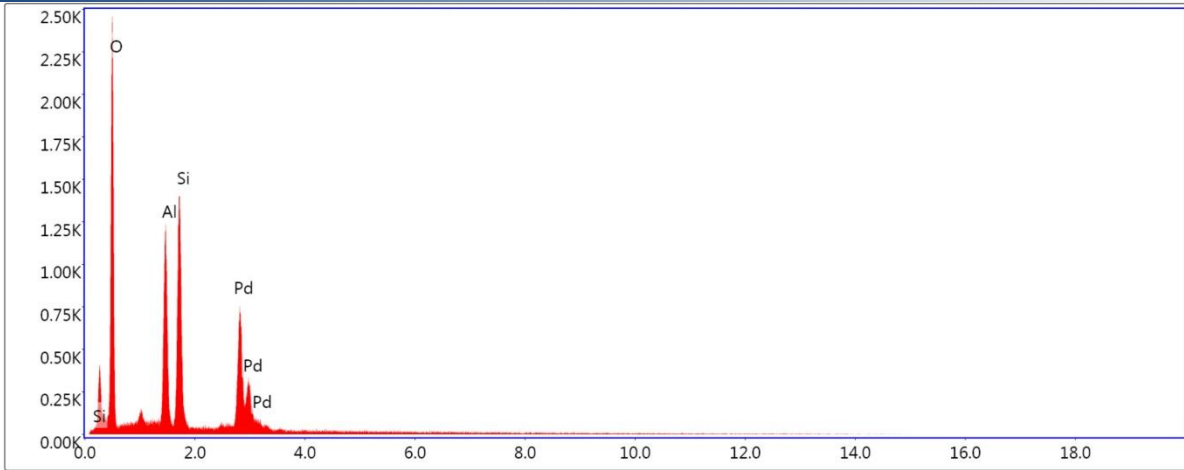
Lsec: 10.0   148 Cnts   1.050 keV   Det: Octane Elite 25

Element	Weight %	Atomic %	Net Int.	Error %	Kratio	Z	A	F
O K	50.81	64.06	2754.78	6.98	0.1684	1.0541	0.4962	1.0000
AlK	20.83	15.58	1855.02	4.16	0.1023	0.9301	0.8280	1.0066
SiK	28.35	20.36	2257.89	4.73	0.1304	0.9493	0.7641	1.0007

EDS Spot 5
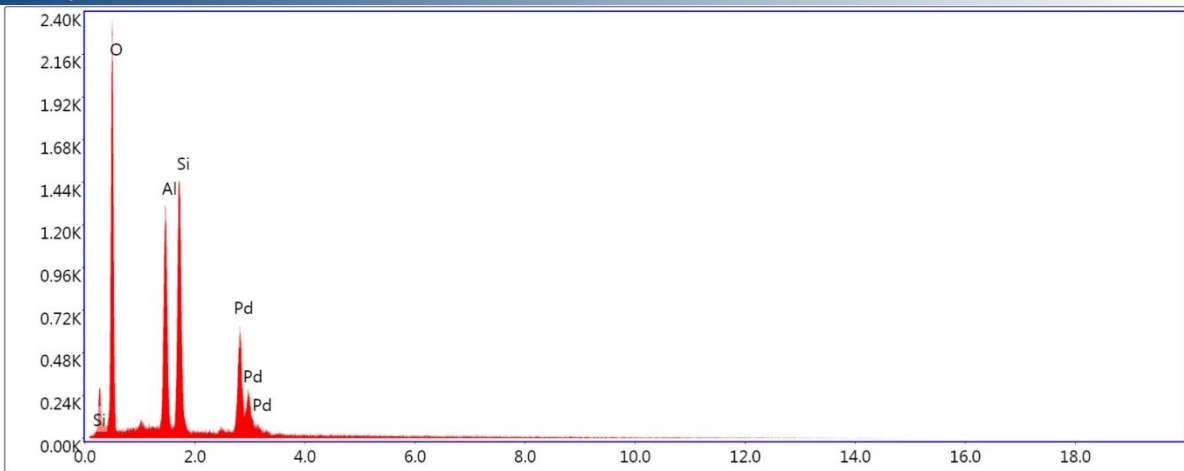
Lsec: 10.0   93 Cnts   1.050 keV   Det: Octane Elite 25

Element	Weight %	Atomic %	Net Int.	Error %	Kratio	Z	A	F
O K	48.65	62.04	2628.35	7.12	0.1702	1.0567	0.4841	1.0000
AlK	21.86	16.53	2002.83	4.06	0.1171	0.9325	0.8338	1.0066
SiK	29.49	21.42	2390.07	4.71	0.1462	0.9517	0.7612	1.0007

EDS Spot 6
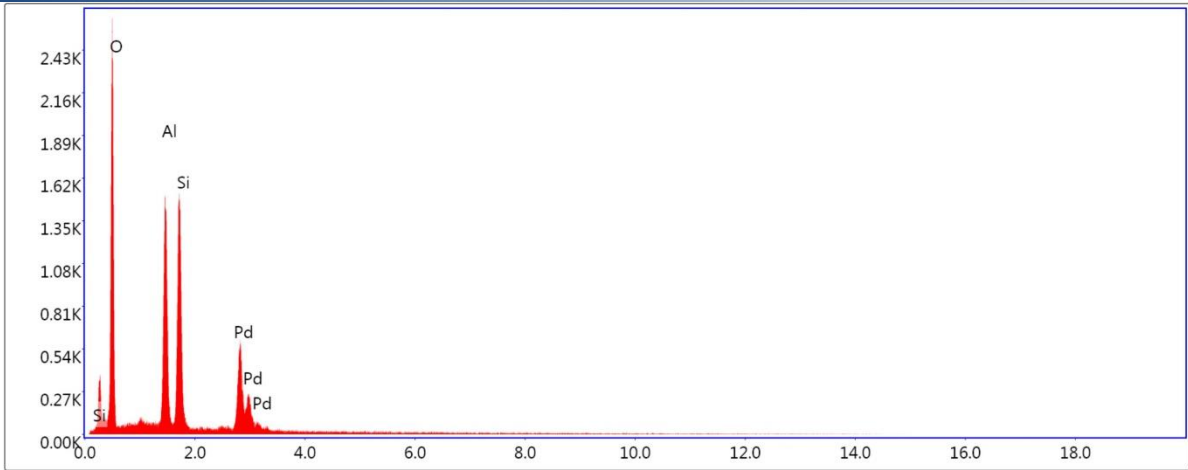
Lsec: 10.0   109 Cnts   1.050 keV   Det: Octane Elite 25

Element	Weight %	Atomic %	Net Int.	Error %	Kratio	Z	A	F
O K	48.47	61.85	2848.05	7.05	0.1767	1.0572	0.4853	1.0000
AlK	23.49	17.77	2335.61	3.89	0.1308	0.9329	0.8346	1.0063
SiK	28.04	20.38	2435.71	4.70	0.1427	0.9521	0.7520	1.0007
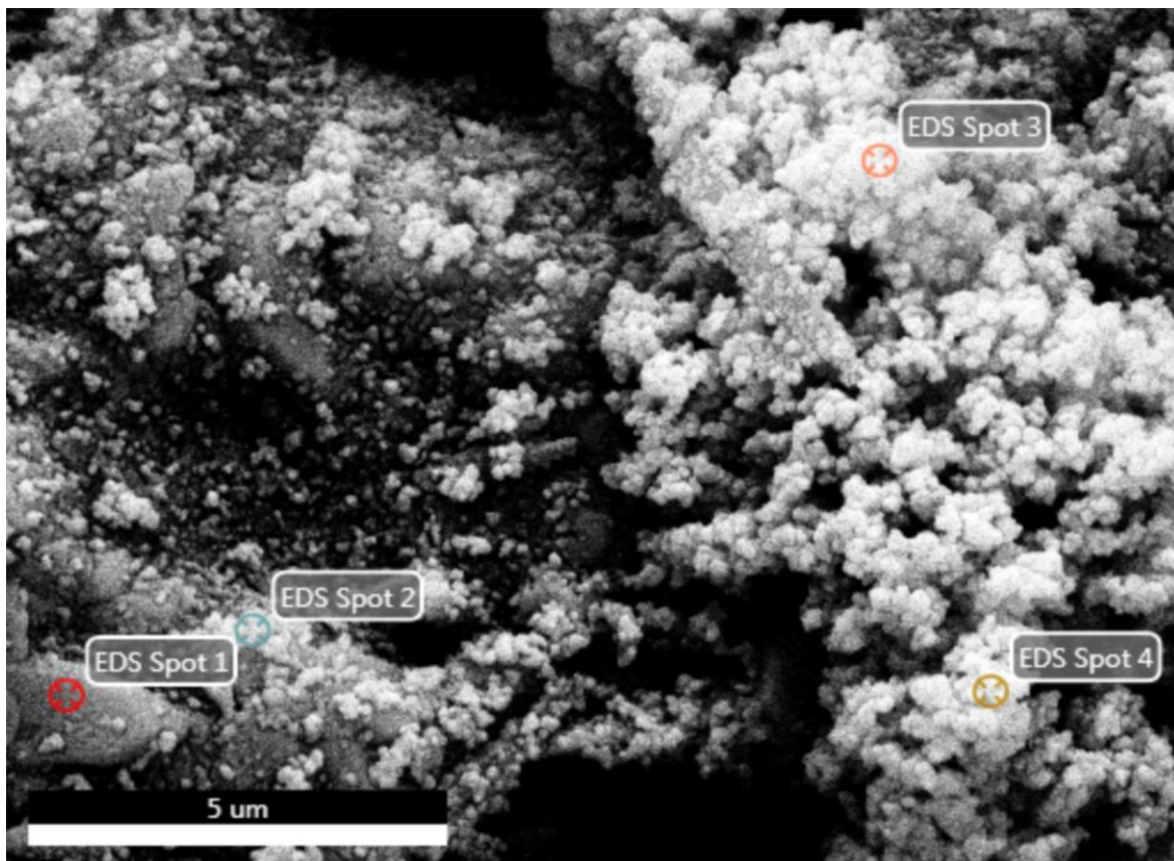
EDS Spot 1
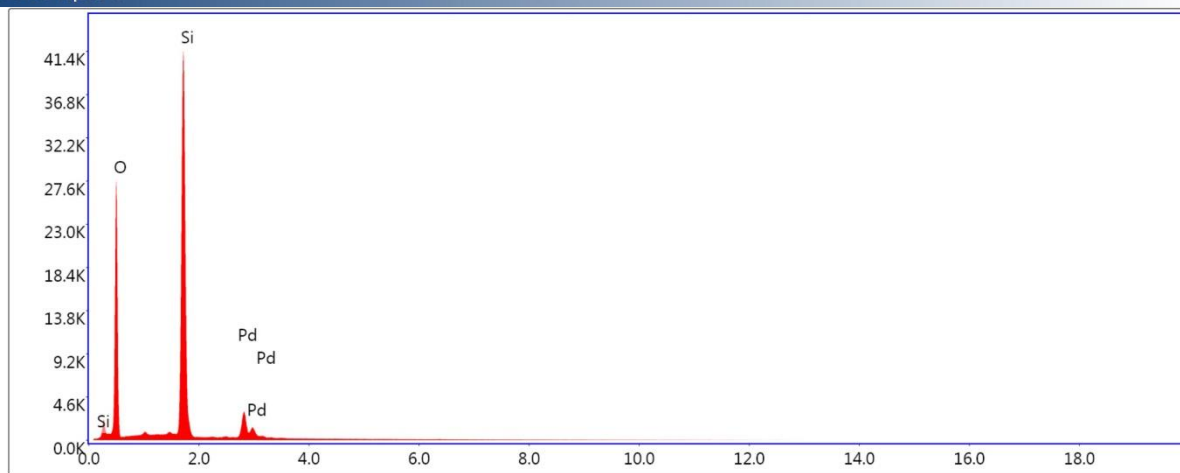
Lsec: 100.0   914 Cnts   1.050 keV   Det: Octane Elite 25

Element	Weight %	Atomic %	Net Int.	Error %	Kratio	Z	A	F
O K	46.63	60.54	2964.45	6.98	0.1875	1.0543	0.4433	1.0000
SiK	53.37	39.46	6645.23	2.36	0.3967	0.9498	0.9091	1.0005

EDS Spot 2
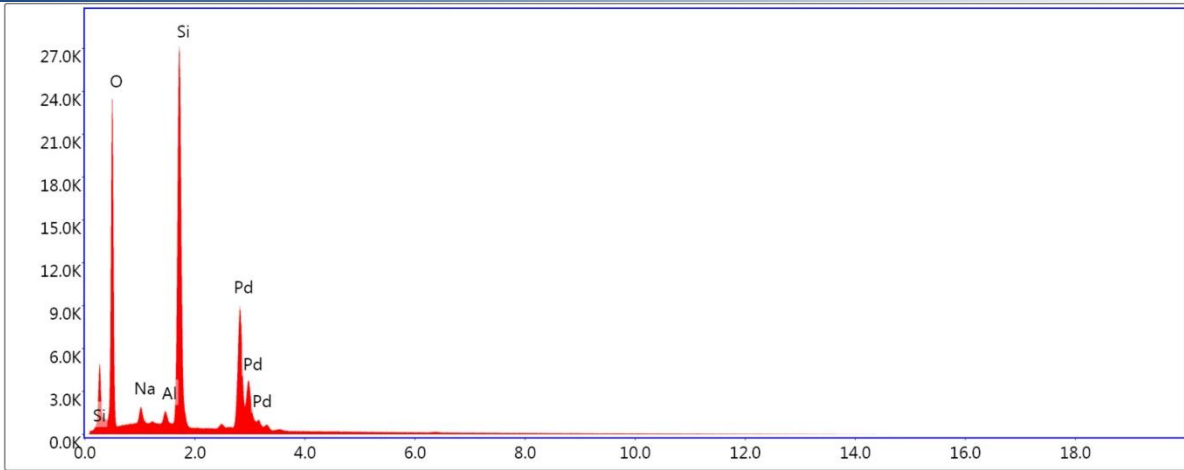
Lsec: 100.0   1.925K Cnts   1.050 keV   Det: Octane Elite 25

Element	Weight %	Atomic %	Net Int.	Error %	Kratio	Z	A	F
O K	47.80	61.21	2572.17	6.76	0.1441	1.0535	0.4680	1.0000
NaK	3.98	3.55	224.93	7.30	0.0131	0.9519	0.5635	1.0033
AlK	2.22	1.69	203.83	5.03	0.0103	0.9297	0.8050	1.0110
SiK	46.00	33.55	4401.03	2.80	0.2327	0.9489	0.8712	1.0006

EDS Spot 3
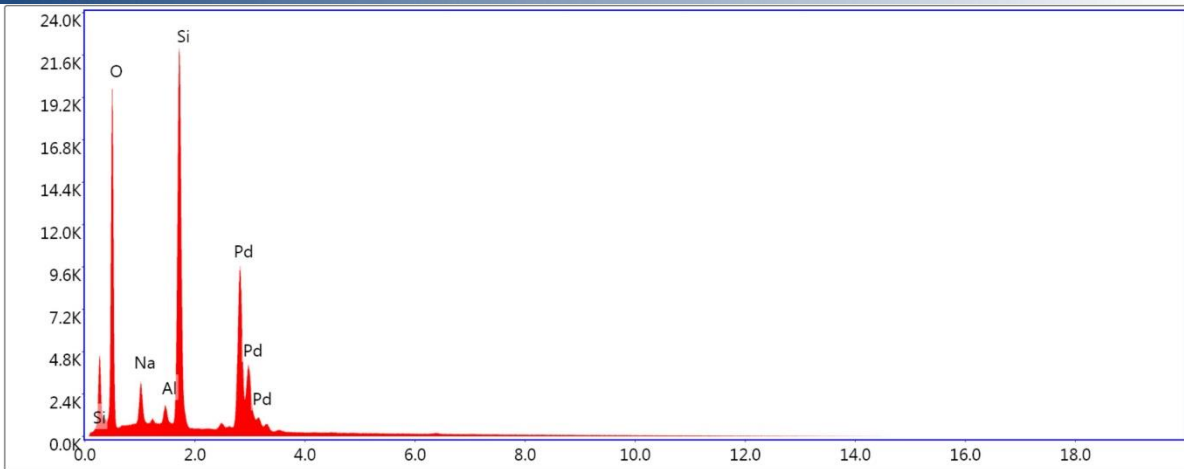
Lsec: 100.0   2.955K Cnts   1.050 keV   Det: Octane Elite 25

Element	Weight %	Atomic %	Net Int.	Error %	Kratio	Z	A	F
O K	45.99	59.15	2148.81	6.74	0.1263	1.0555	0.4719	1.0000
NaK	7.38	6.60	365.19	6.56	0.0223	0.9538	0.5740	1.0031
AlK	2.80	2.13	215.84	5.19	0.0114	0.9315	0.7882	1.0103
SiK	43.84	32.12	3541.20	3.00	0.1964	0.9507	0.8543	1.0006

EDS Spot 4
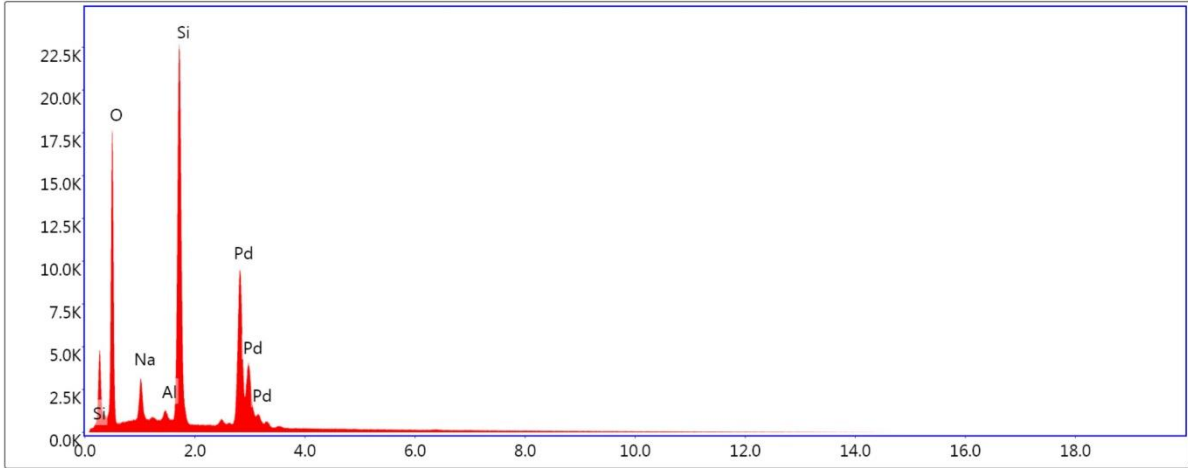
Lsec: 100.0   2.973K Cnts   1.050 keV   Det: Octane Elite 25

Element	Weight %	Atomic %	Net Int.	Error %	Kratio	Z	A	F
O K	43.58	56.79	1887.98	6.94	0.1151	1.0579	0.4579	1.0000
NaK	7.67	6.95	368.91	6.50	0.0234	0.9560	0.5838	1.0031
AlK	1.82	1.40	134.76	6.10	0.0074	0.9338	0.7920	1.0108
SiK	46.94	34.85	3664.76	2.88	0.2108	0.9530	0.8639	1.0006
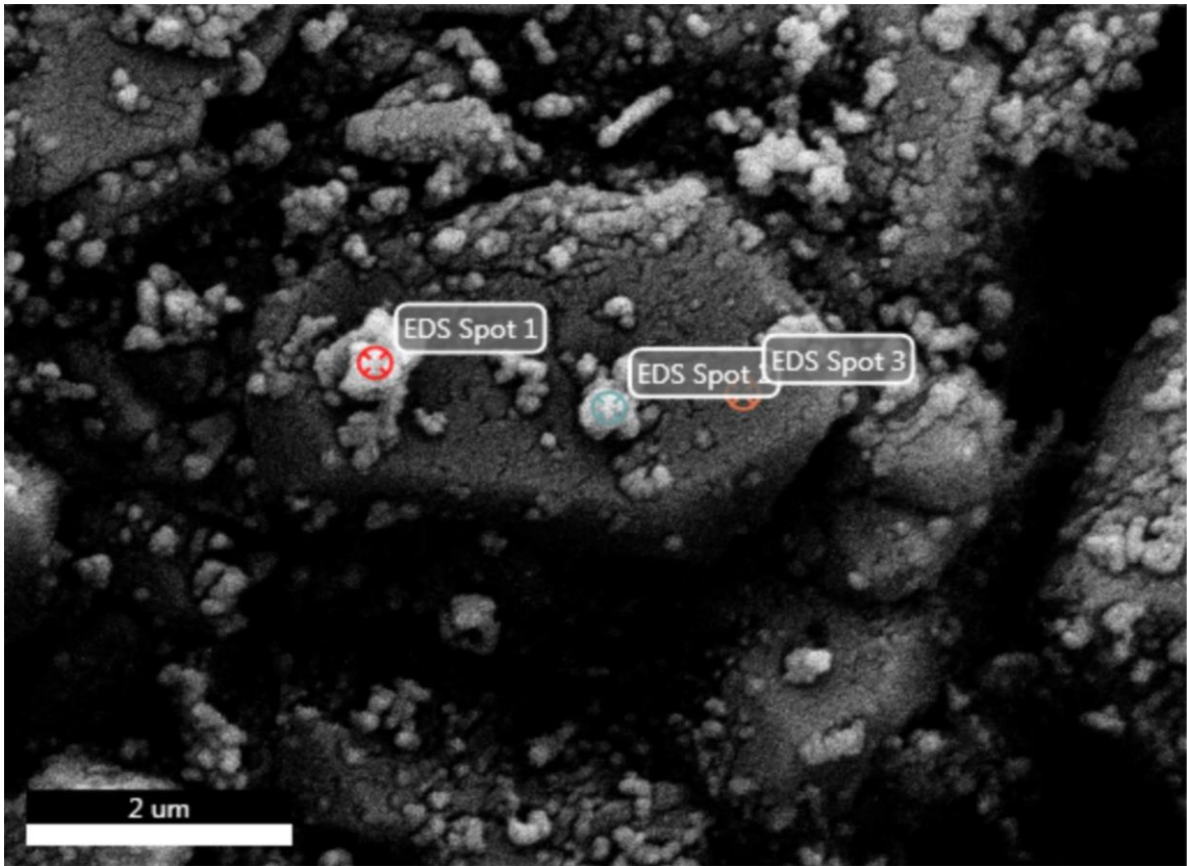
EDS Spot 1
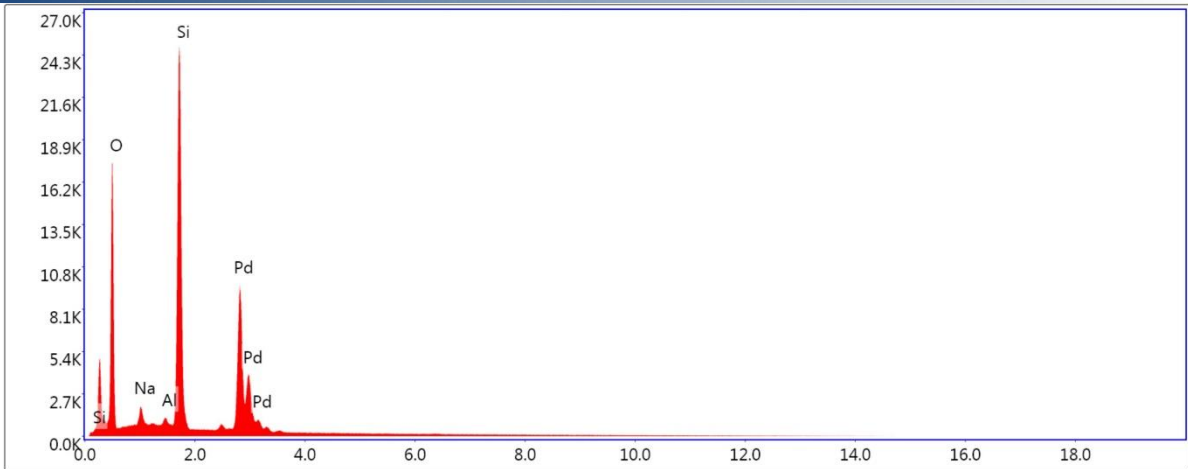
Lsec: 100.0   1.817K Cnts   1.050 keV   Det: Octane Elite 25

Element	Weight %	Atomic %	Net Int.	Error %	Kratio	Z	A	F
O K	44.18	57.72	1864.34	7.04	0.1155	1.0572	0.4475	1.0000
NaK	4.17	3.79	197.83	7.25	0.0128	0.9554	0.5778	1.0034
AlK	1.53	1.18	115.87	6.30	0.0065	0.9332	0.8126	1.0115
SiK	50.13	37.31	3981.25	2.69	0.2329	0.9525	0.8817	1.0005

EDS Spot 2
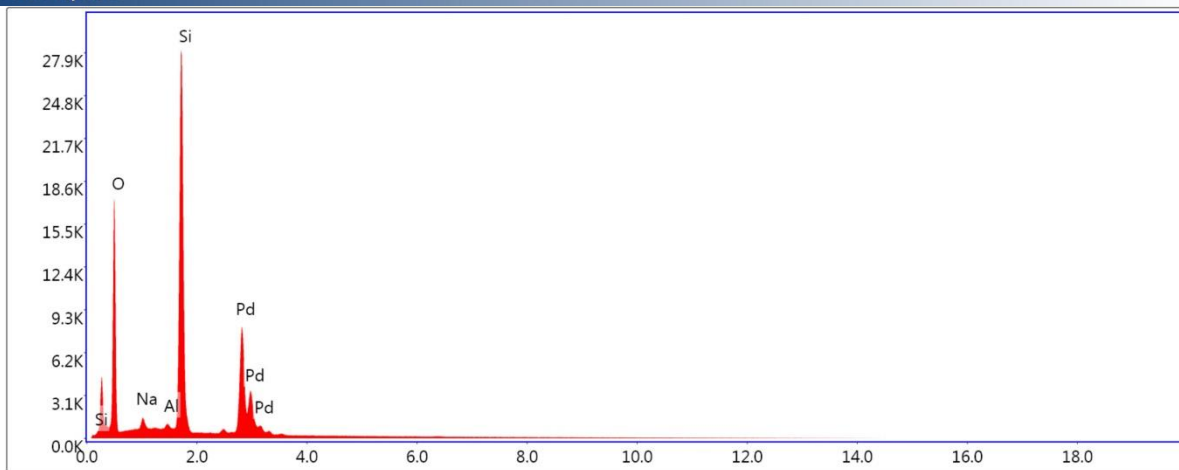
Lsec: 100.0   1.422K Cnts   1.050 keV   Det: Octane Elite 25

Element	Weight %	Atomic %	Net Int.	Error %	Kratio	Z	A	F
O K	42.64	56.33	1838.76	7.13	0.1190	1.0589	0.4339	1.0000
NaK	2.77	2.55	139.89	7.71	0.0094	0.9570	0.5827	1.0035
AlK	1.26	0.99	102.29	6.65	0.0060	0.9347	0.8255	1.0121
SiK	53.34	40.14	4522.53	2.57	0.2761	0.9540	0.8932	1.0005

EDS Spot 3
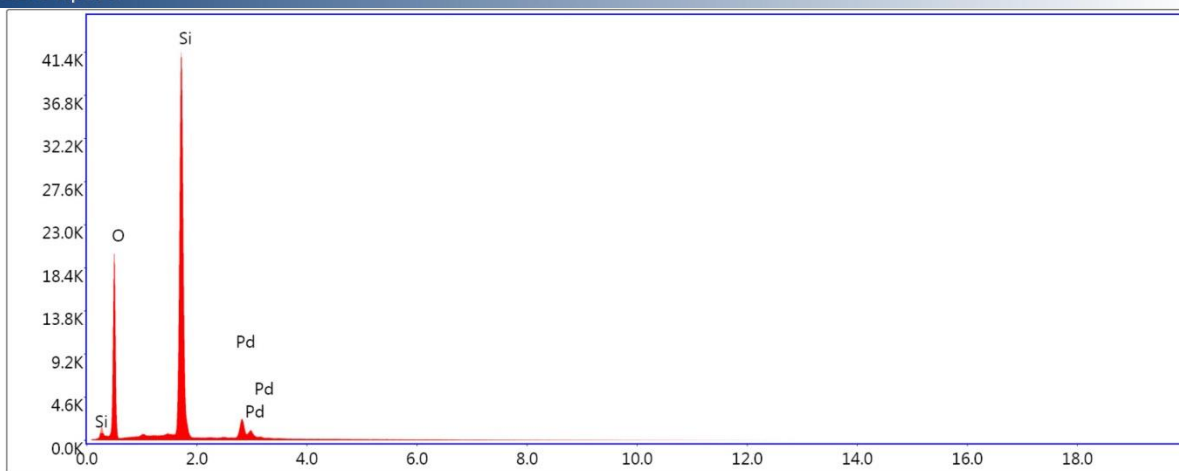
Lsec: 100.0   685 Cnts   1.050 keV   Det: Octane Elite 25

Element	Weight %	Atomic %	Net Int.	Error %	Kratio	Z	A	F
O K	40.40	54.33	2127.87	7.33	0.1558	1.0611	0.4119	1.0000
SiK	59.60	45.67	6704.56	2.24	0.4634	0.9563	0.9207	1.0004

Additional SEM- and EDS results of thin section from the flooded 500 mD core (flooding #1)
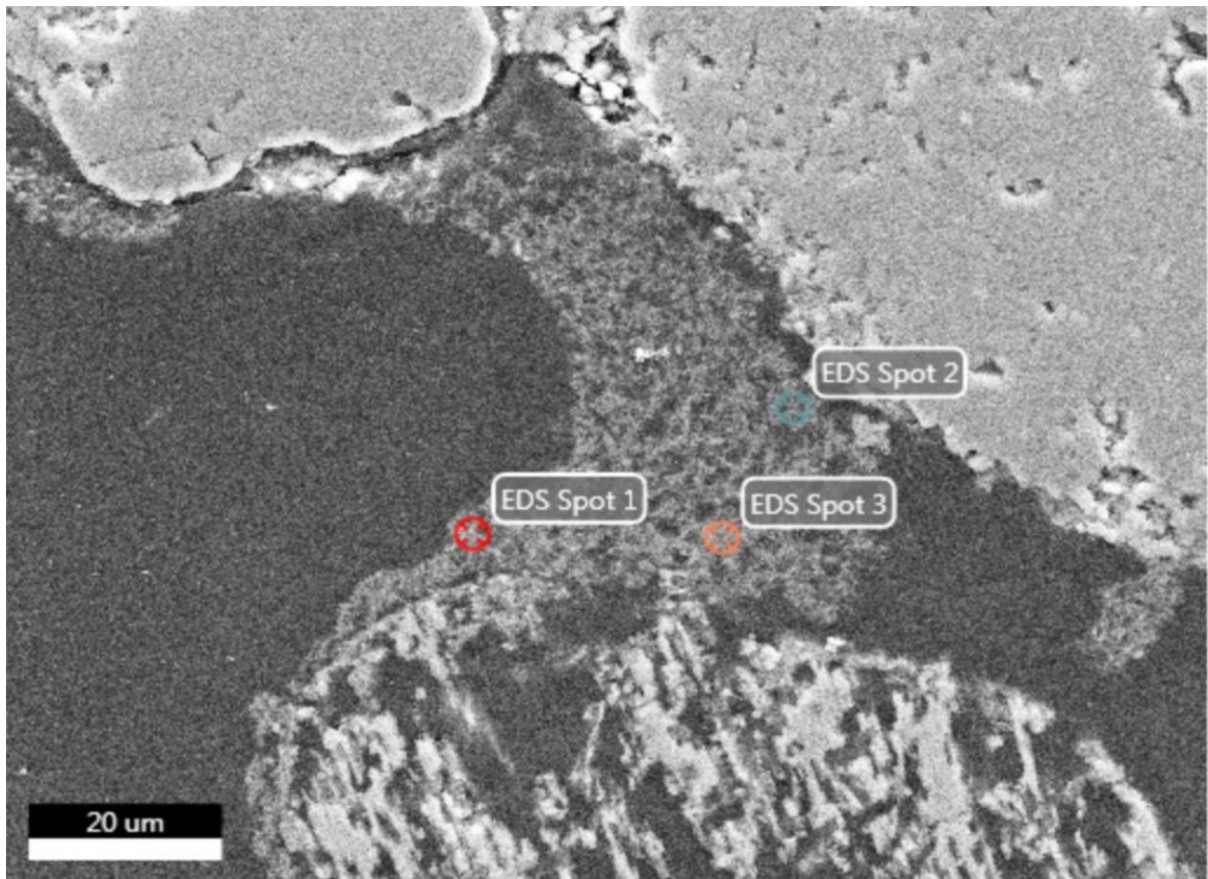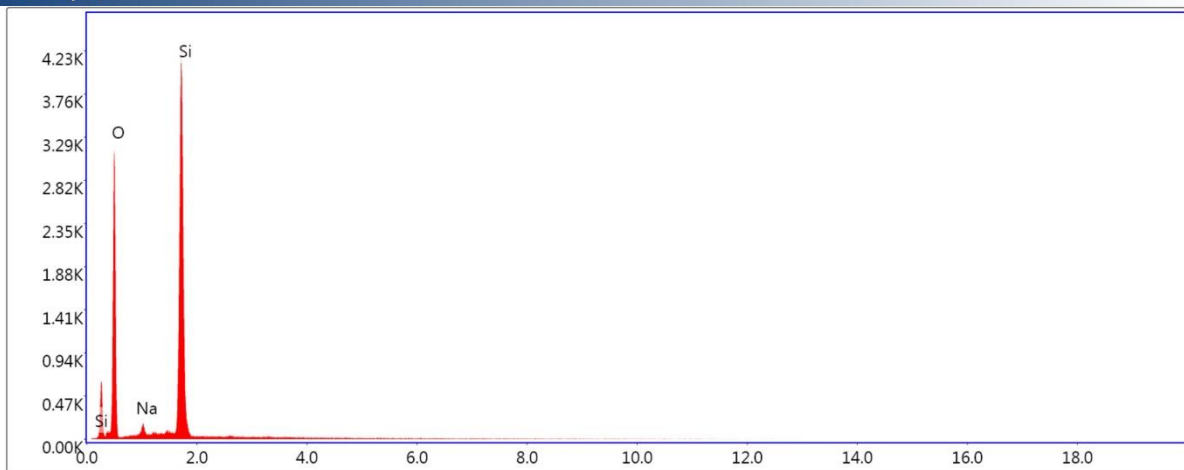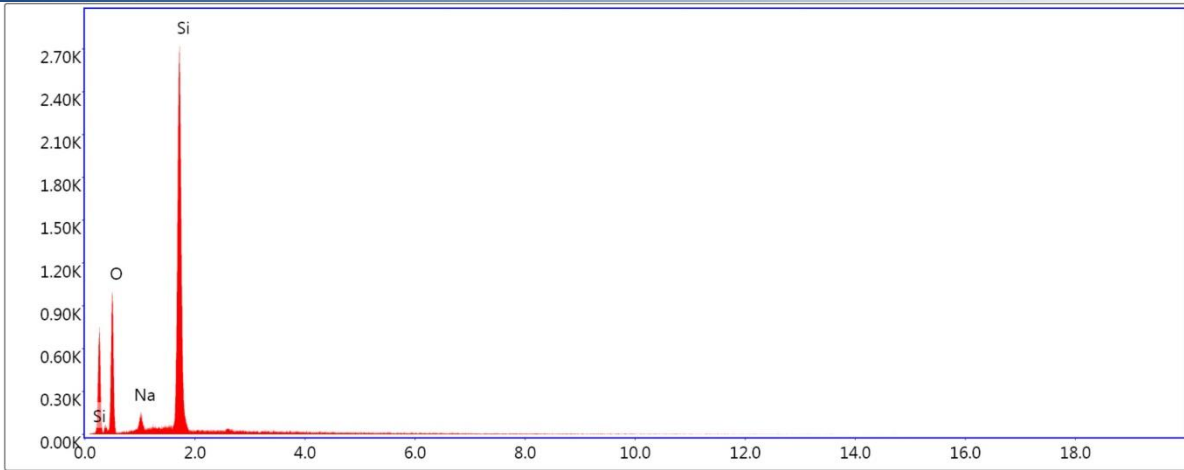

EDS Spot 1

Lsec: 50.0   3 Cnts   10.255 keV   Det: Octane Elite 25

Element	Weight %	Atomic %	Net Int.	Error %	Kratio	Z	A	F
O K	47.86	61.52	677.35	7.28	0.2303	1.0530	0.4569	1.0000
NaK	1.83	1.64	27.77	13.61	0.0098	0.9515	0.5611	1.0034
SiK	50.31	36.84	1335.66	2.79	0.4287	0.9485	0.8978	1.0005

EDS Spot 2

Lsec: 50.0   1 Cnts   10.255 keV   Det: Octane Elite 25

Element	Weight %	Atomic %	Net Int.	Error %	Kratio	Z	A	F
O K	33.28	46.48	195.54	8.86	0.1382	1.0689	0.3884	1.0000
NaK	2.47	2.40	20.24	14.76	0.0149	0.9663	0.6222	1.0038
SiK	64.25	51.12	855.27	2.72	0.5705	0.9636	0.9213	1.0003

EDS Spot 3
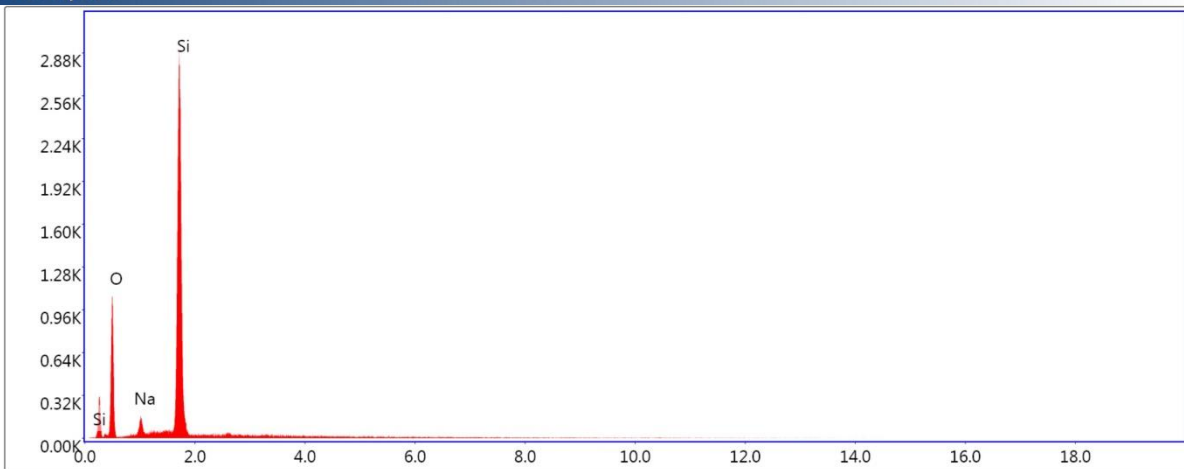
Lsec: 50.0   3 Cnts   10.255 keV   Det: Octane Elite 25

Element	Weight %	Atomic %	Net Int.	Error %	Kratio	Z	A	F
O K	32.96	46.10	208.23	8.79	0.1366	1.0693	0.3876	1.0000
NaK	2.65	2.58	23.49	13.43	0.0160	0.9667	0.6238	1.0038
SiK	64.40	51.32	923.60	2.67	0.5718	0.9639	0.9210	1.0003

93
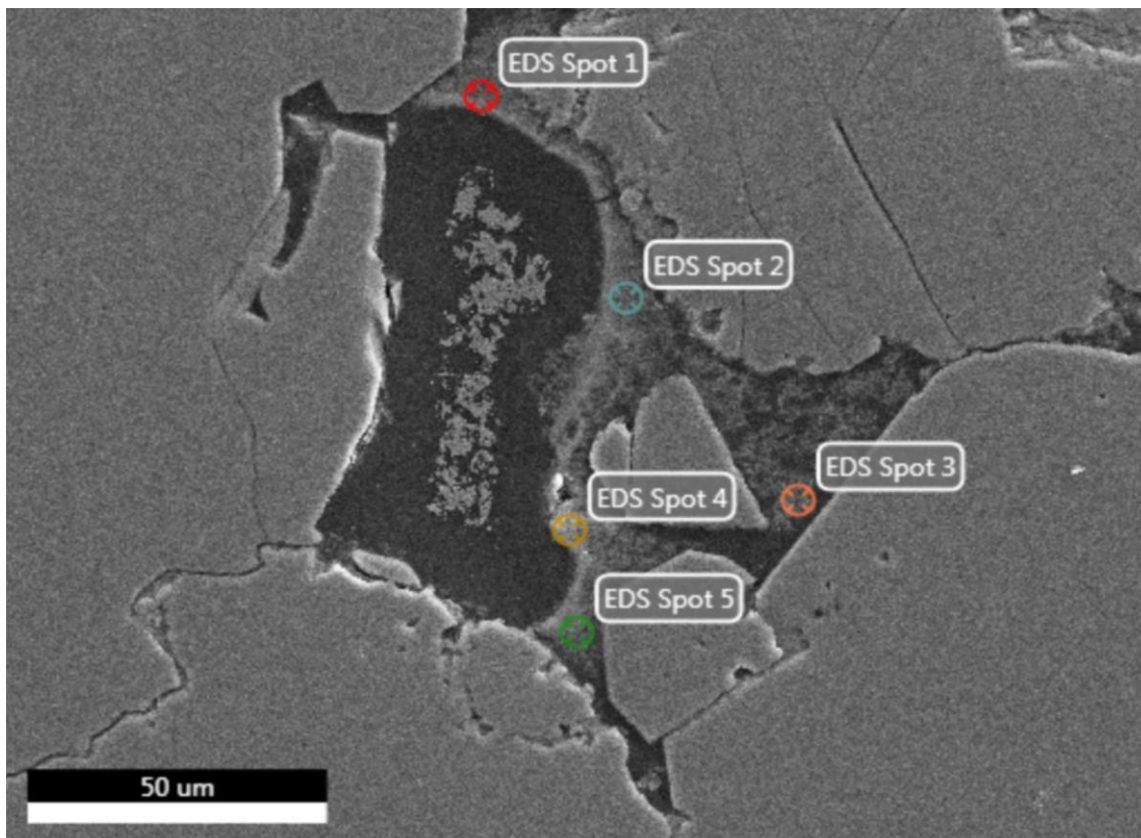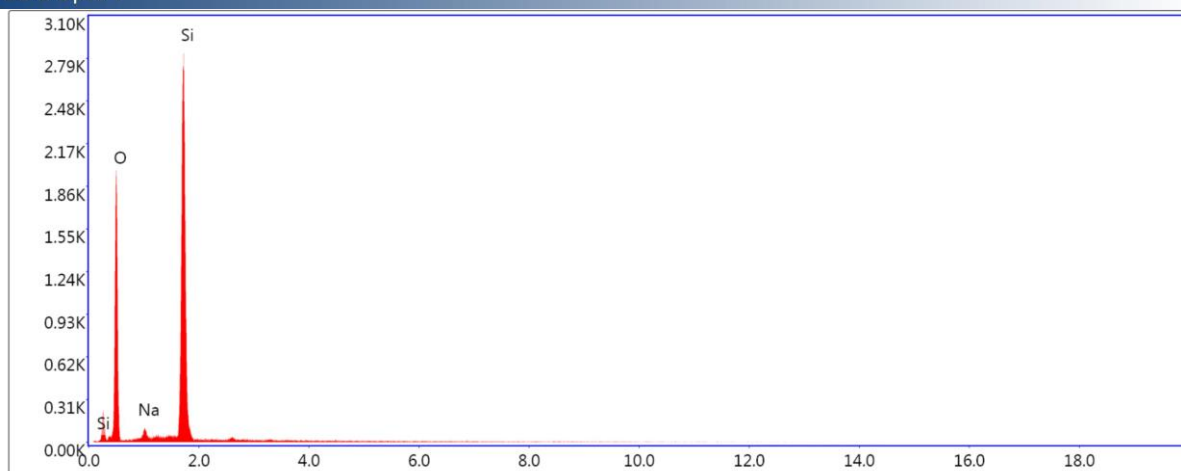
EDS Spot 1

Lsec: 30.0   92 Cnts   1.060 keV   Det: Octane Elite 25

Element	Weight %	Atomic %	Net Int.	Error %	Kratio	Z	A	F
O K	46.56	60.29	717.60	7.50	0.2209	1.0544	0.4498	1.0000
NaK	1.75	1.58	29.65	15.82	0.0095	0.9528	0.5665	1.0034
SiK	51.69	38.13	1521.84	2.87	0.4425	0.9498	0.9007	1.0005
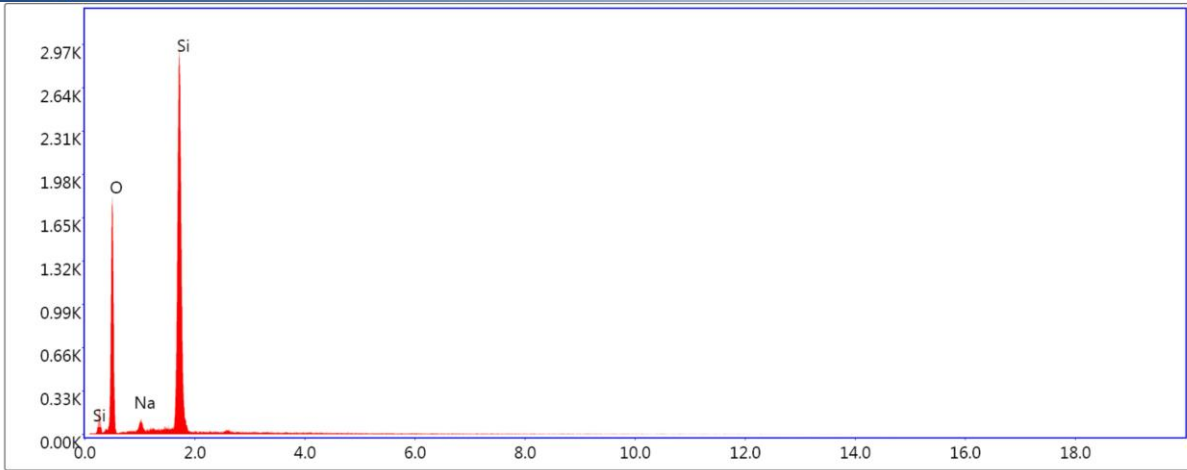
Lsec: 30.0   91 Cnts   1.060 keV   Det: Octane Elite 25

Element	Weight %	Atomic %	Net Int.	Error %	Kratio	Z	A	F
O K	43.97	57.76	639.38	7.76	0.2030	1.0572	0.4366	1.0000
NaK	1.88	1.72	31.46	14.85	0.0104	0.9554	0.5769	1.0035
SiK	54.15	40.52	1557.12	2.81	0.4670	0.9525	0.9048	1.0005
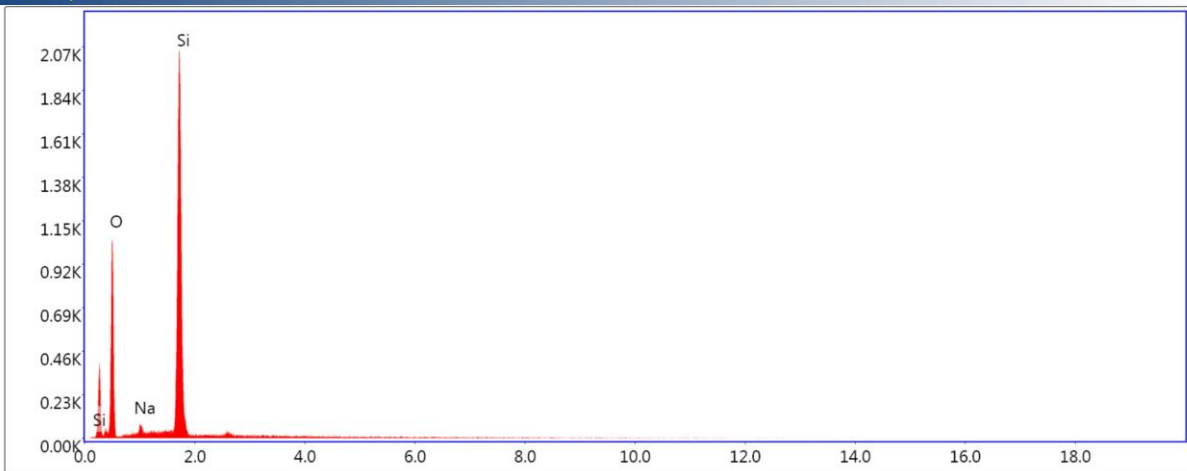
Lsec: 30.0   72 Cnts   1.060 keV   Det: Octane Elite 25

Element	Weight %	Atomic %	Net Int.	Error %	Kratio	Z	A	F
O K	40.61	54.43	366.48	8.23	0.1801	1.0609	0.4179	1.0000
NaK	1.31	1.22	14.50	24.50	0.0074	0.9589	0.5900	1.0037
SiK	58.08	44.35	1093.81	2.86	0.5077	0.9560	0.9138	1.0004

EDS Spot 4
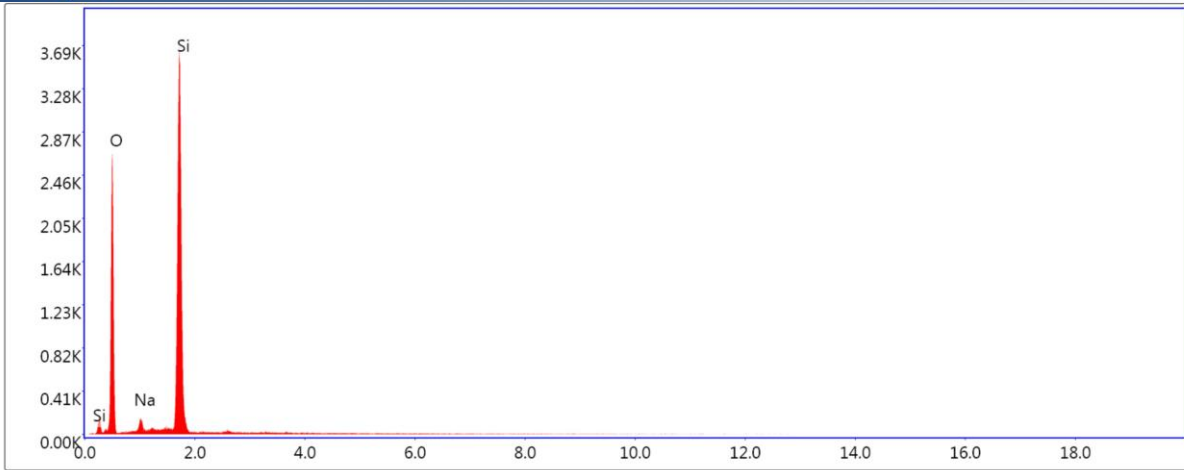
Element	Weight %	Atomic %	Net Int.	Error %	Kratio	Z	A	F
O K	46.52	60.19	950.29	7.37	0.2217	1.0544	0.4520	1.0000
NaK	2.37	2.13	52.90	11.74	0.0128	0.9529	0.5672	1.0034
SiK	51.11	37.67	1978.75	2.81	0.4361	0.9499	0.8977	1.0005

EDS Spot 5

Element	Weight %	Atomic %	Net Int.	Error %	Kratio	Z	A	F
O K	46.93	60.68	784.38	7.45	0.2228	1.0540	0.4503	1.0000
NaK	1.36	1.23	24.91	17.47	0.0074	0.9525	0.5647	1.0035
SiK	51.71	38.09	1651.88	2.81	0.4432	0.9495	0.9020	1.0005
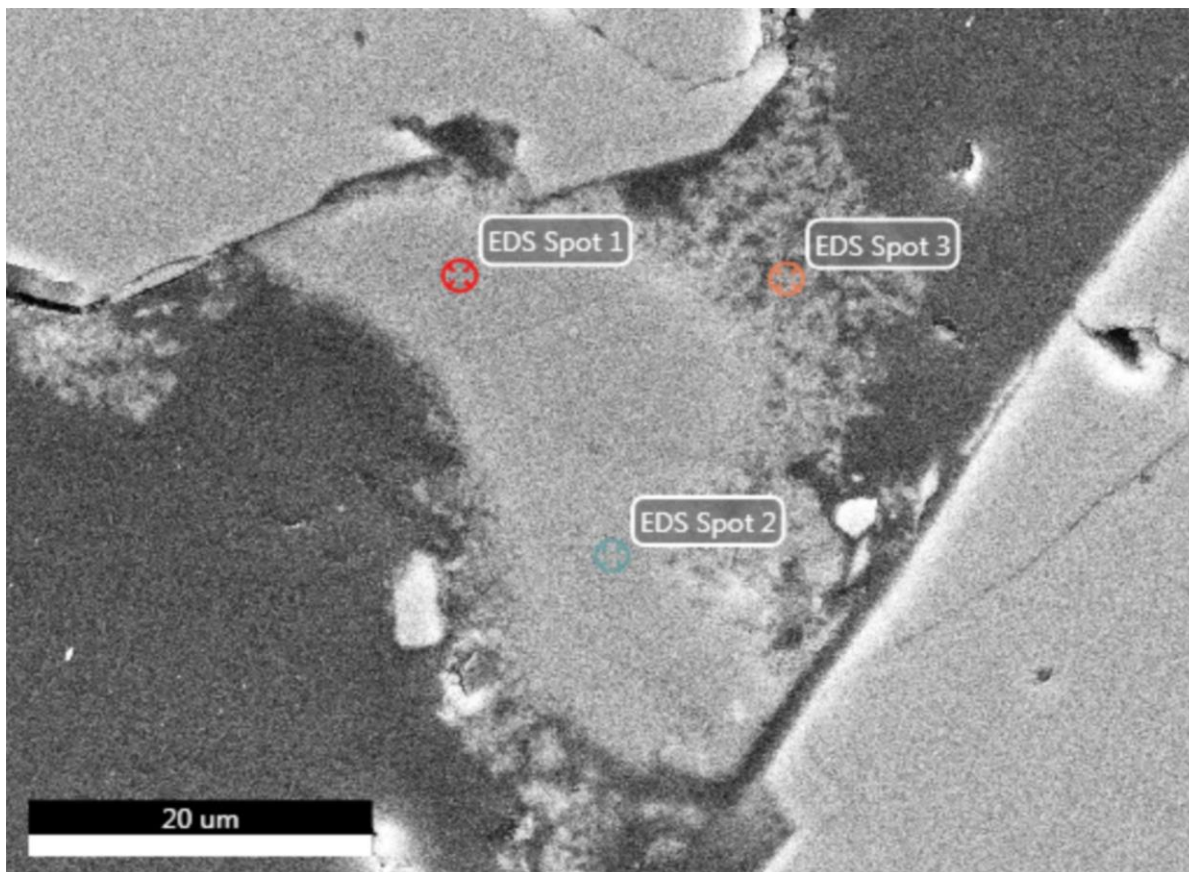
EDS Spot 1
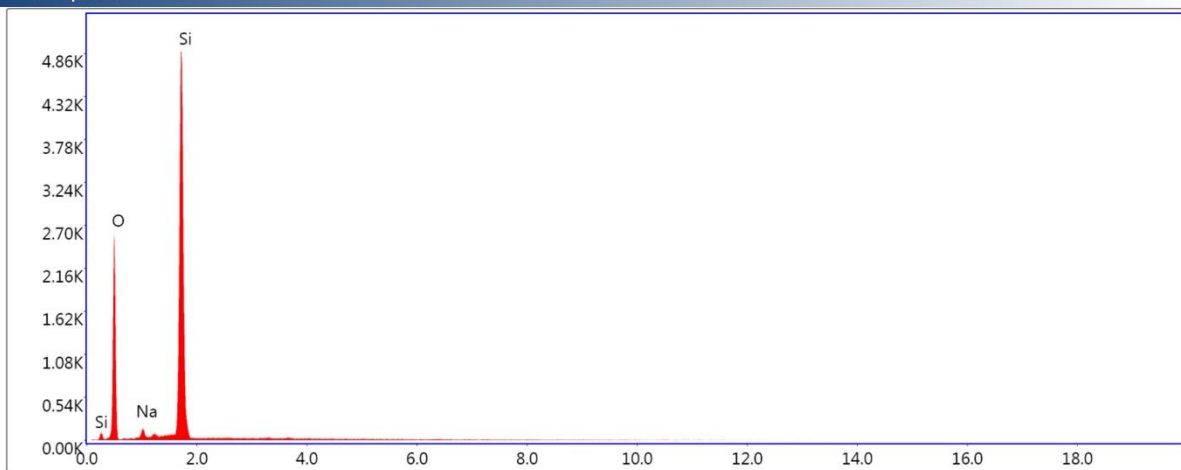
Lsec: 50.0   152 Cnts   1.035 keV   Det: Octane Elite 25

Element	Weight %	Atomic %	Net Int.	Error %	Kratio	Z	A	F
O K	40.80	54.65	535.45	7.73	0.1808	1.0607	0.4178	1.0000
NaK	1.07	0.99	17.19	17.80	0.0060	0.9587	0.5888	1.0037
SiK	58.14	44.36	1595.05	2.57	0.5085	0.9558	0.9146	1.0004

EDS Spot 2
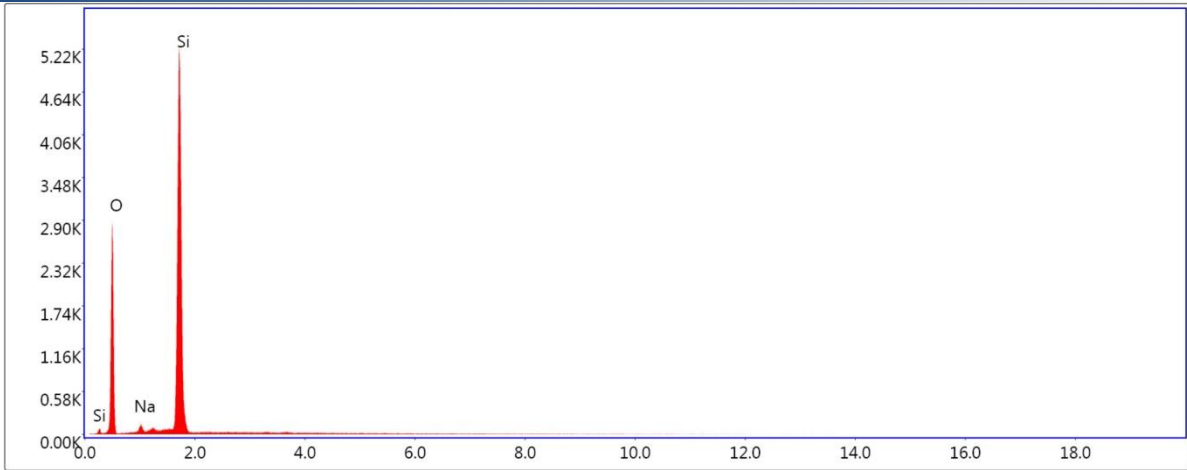
Lsec: 50.0   122 Cnts   1.035 keV   Det: Octane Elite 25

Element	Weight %	Atomic %	Net Int.	Error %	Kratio	Z	A	F
O K	41.80	55.68	596.24	7.65	0.1871	1.0596	0.4224	1.0000
NaK	0.99	0.92	16.98	17.98	0.0055	0.9577	0.5846	1.0036
SiK	57.21	43.41	1684.45	2.57	0.4991	0.9548	0.9132	1.0004

EDS Spot 3
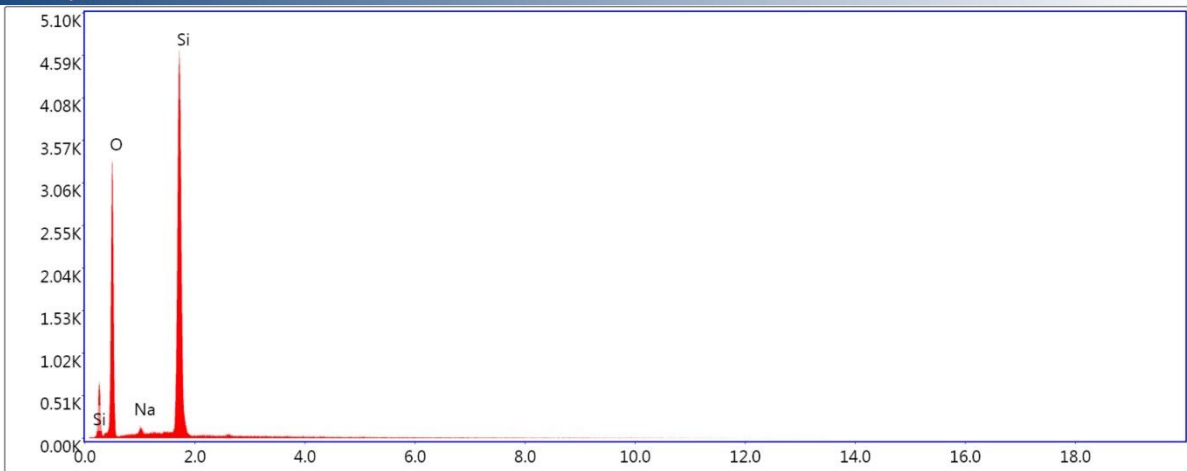
Lsec: 50.0   113 Cnts   1.035 keV   Det: Octane Elite 25

Element	Weight %	Atomic %	Net Int.	Error %	Kratio	Z	A	F
O K	46.95	60.71	718.86	7.33	0.2228	1.0540	0.4502	1.0000
NaK	1.35	1.22	22.65	14.80	0.0073	0.9525	0.5643	1.0035
SiK	51.69	38.07	1513.66	2.73	0.4430	0.9495	0.9019	1.0005

98
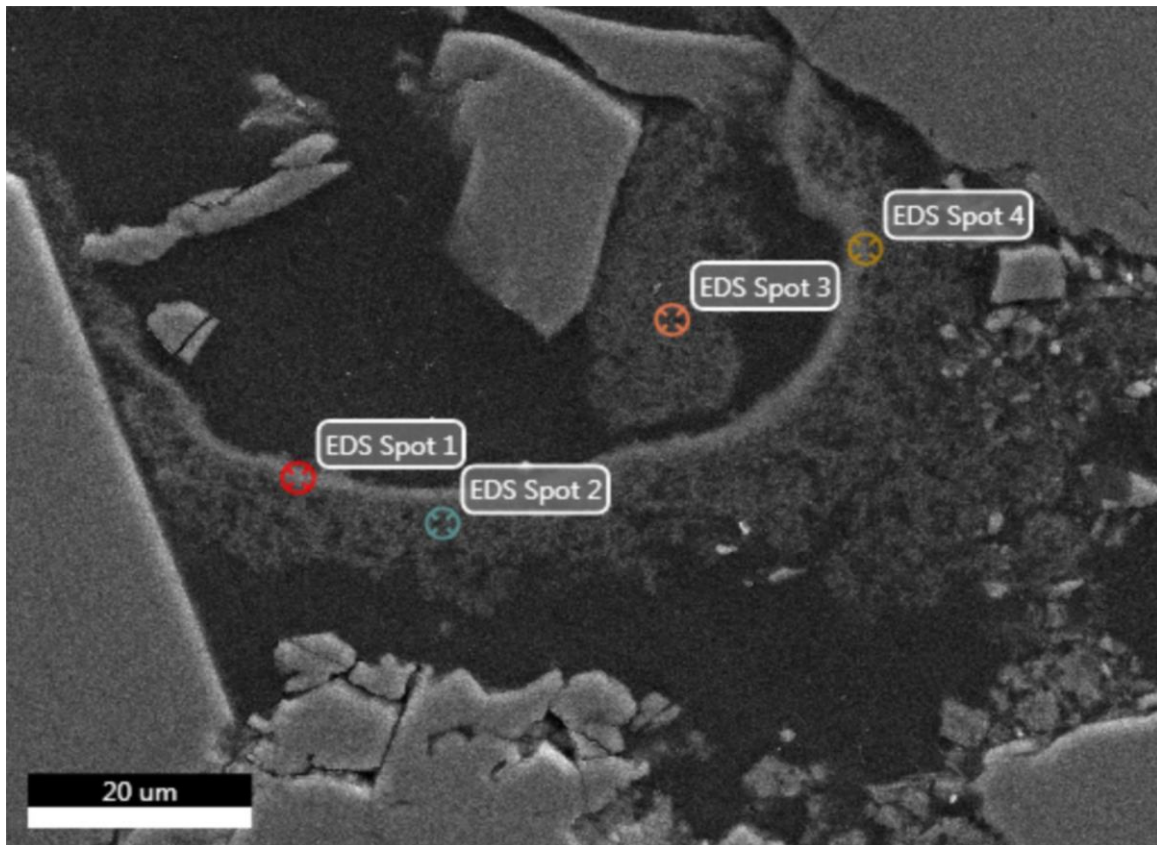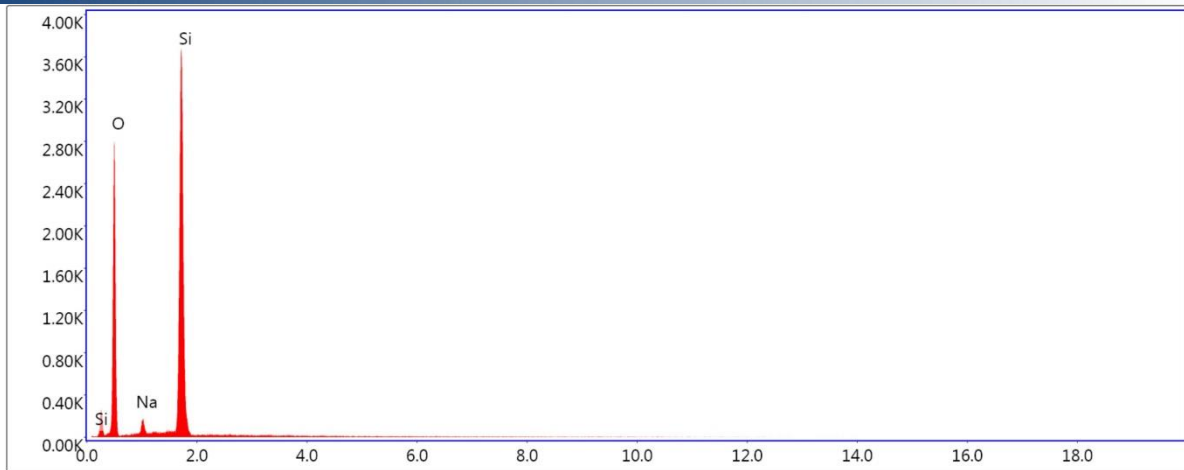
EDS Spot 1

Lsec: 30.0   151 Cnts   1.055 keV   Det: Octane Elite 25

Element	Weight %	Atomic %	Net Int.	Error %	Kratio	Z	A	F
O K	47.33	60.97	989.64	7.31	0.2279	1.0536	0.4569	1.0000
NaK	2.38	2.13	53.52	11.84	0.0128	0.9520	0.5645	1.0034
SiK	50.29	36.90	1967.18	2.83	0.4281	0.9490	0.8964	1.0005

EDS Spot 2
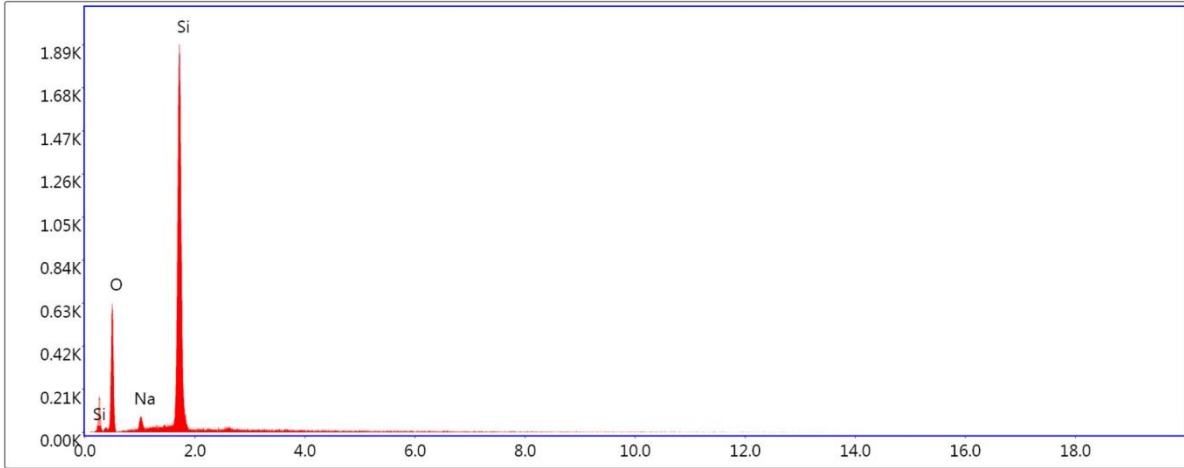
Lsec: 30.0   78 Cnts   1.055 keV   Det: Octane Elite 25

Element	Weight %	Atomic %	Net Int.	Error %	Kratio	Z	A	F
O K	31.86	44.93	211.89	9.13	0.1301	1.0705	0.3816	1.0000
NaK	1.89	1.85	18.02	18.97	0.0115	0.9678	0.6287	1.0039
SiK	66.25	53.22	1021.71	2.73	0.5929	0.9651	0.9272	1.0003

EDS Spot 3
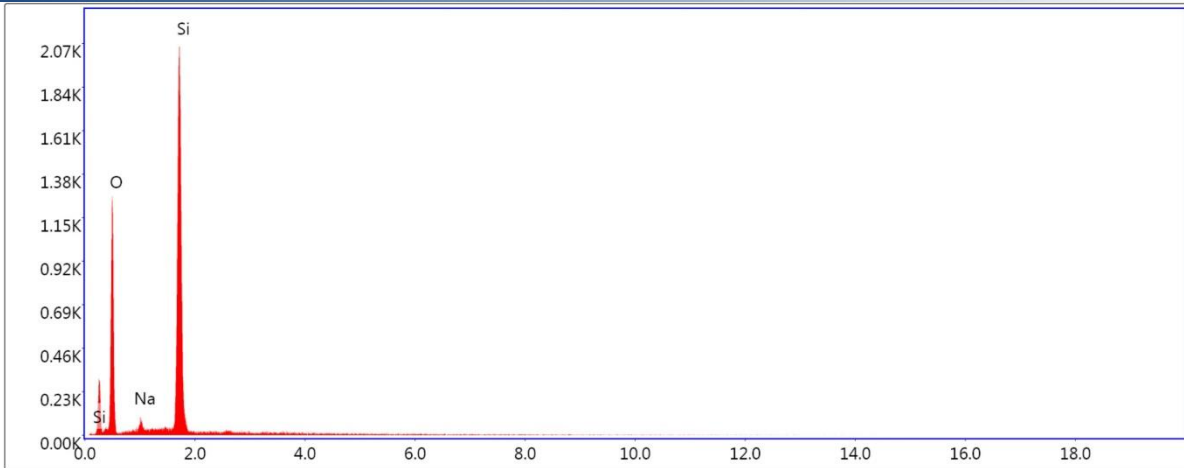
Lsec: 30.0   65 Cnts   1.055 keV   Det: Octane Elite 25

Element	Weight %	Atomic %	Net Int.	Error %	Kratio	Z	A	F
O K	43.99	57.81	453.82	7.95	0.2028	1.0572	0.4360	1.0000
NaK	1.59	1.45	18.85	20.87	0.0088	0.9554	0.5769	1.0035
SiK	54.42	40.74	1113.08	2.94	0.4701	0.9525	0.9064	1.0005

EDS Spot 4
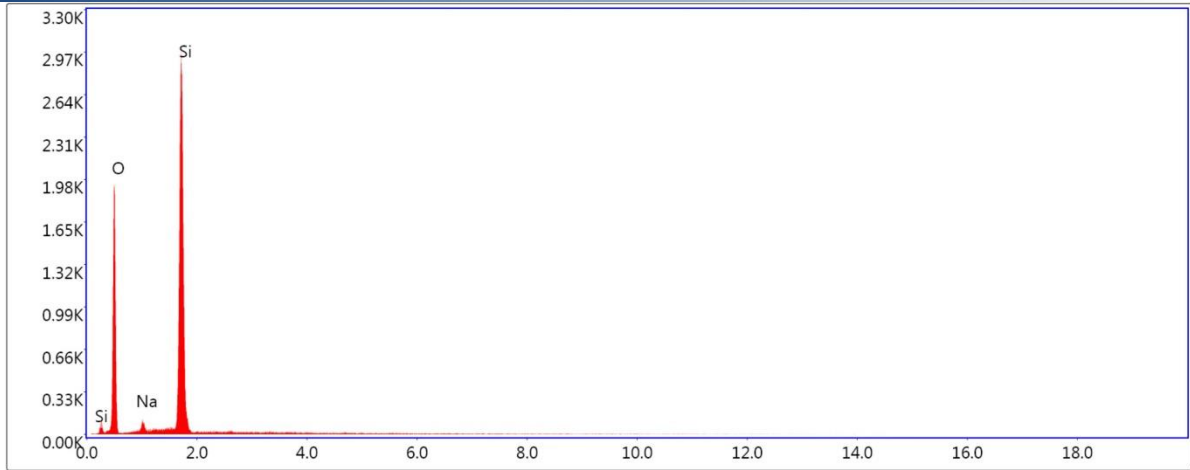
Lsec: 30.0   77 Cnts   1.055 keV   Det: Octane Elite 25

Element	Weight %	Atomic %	Net Int.	Error %	Kratio	Z	A	F
O K	45.09	58.91	692.78	7.60	0.2100	1.0560	0.4410	1.0000
NaK	1.38	1.25	23.95	17.66	0.0076	0.9543	0.5724	1.0035
SiK	53.53	39.84	1610.53	2.81	0.4614	0.9514	0.9054	1.0005

EDS-mapping of a flooded 500 mD core, preformed on a carbon coated thin section made approximately 1,5 cm from the flooding inlet. Sodium is present, however only in limited amounts where the SS is visible in the SEM-image.
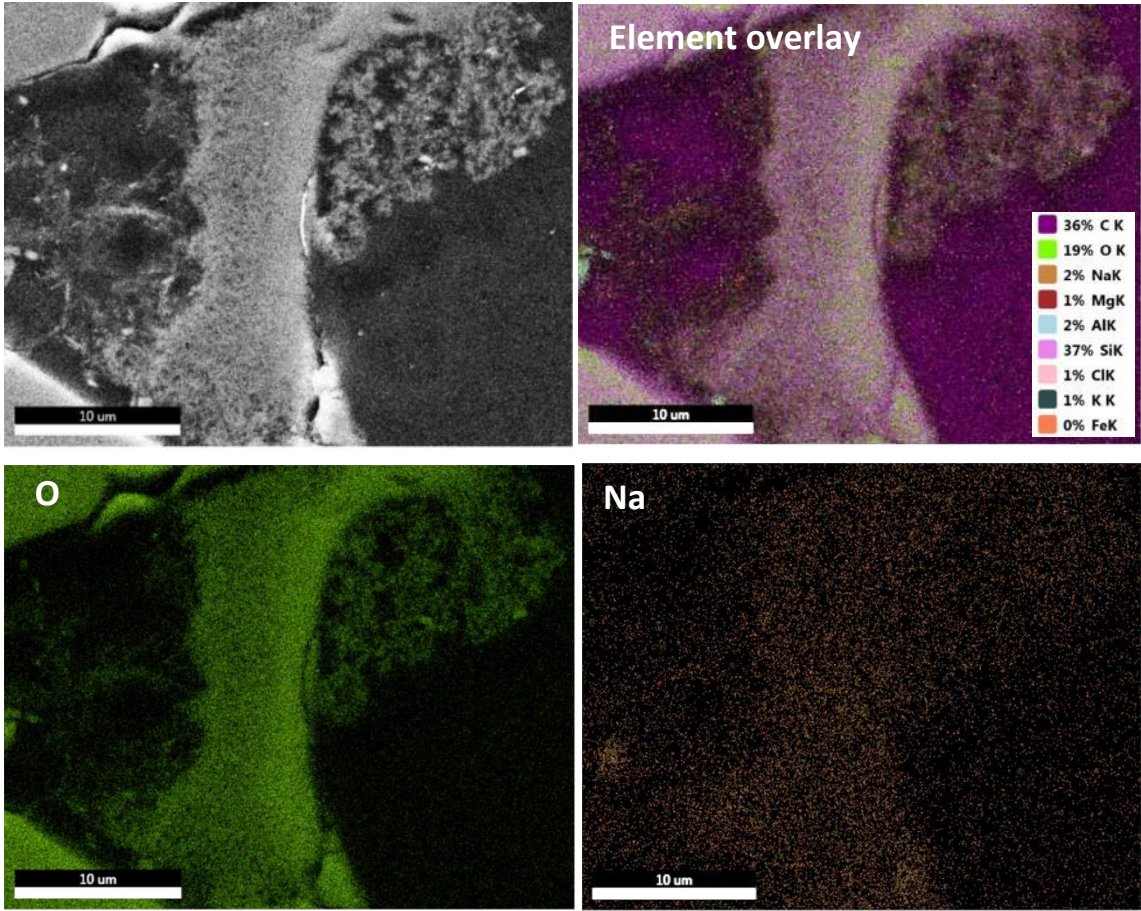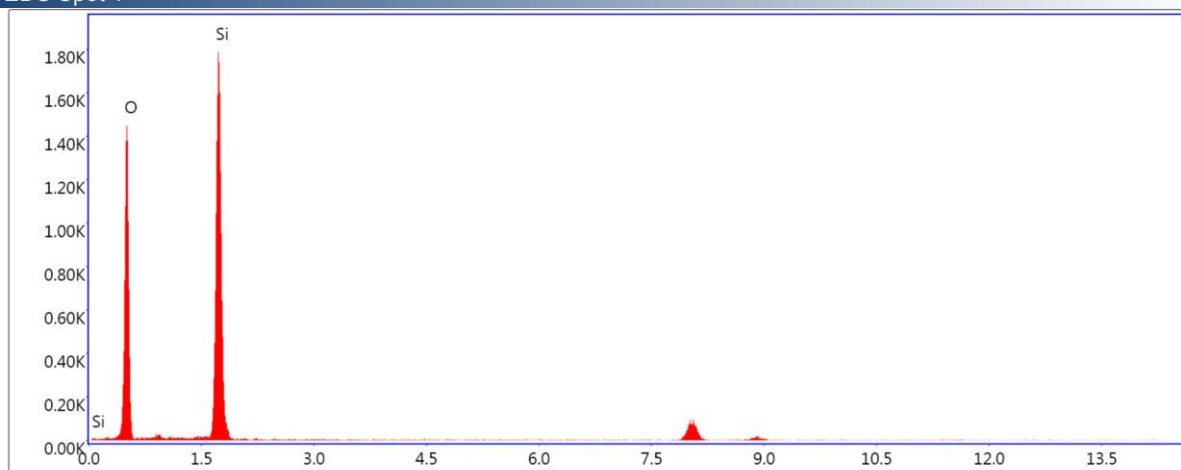
Appendix D

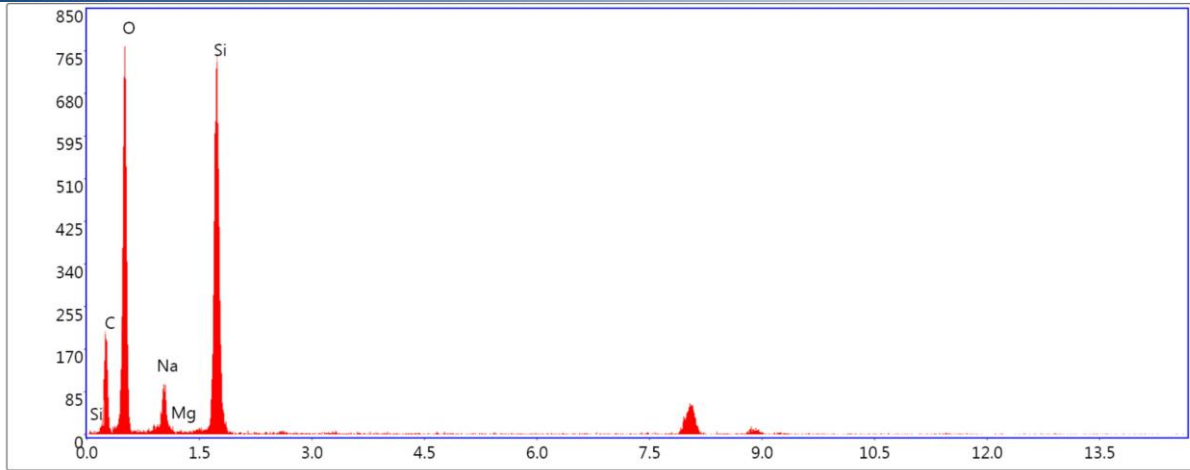Additional TEM- and EDS results of FIB-SEM sample from the flooded 500 mD core (flooding #1)
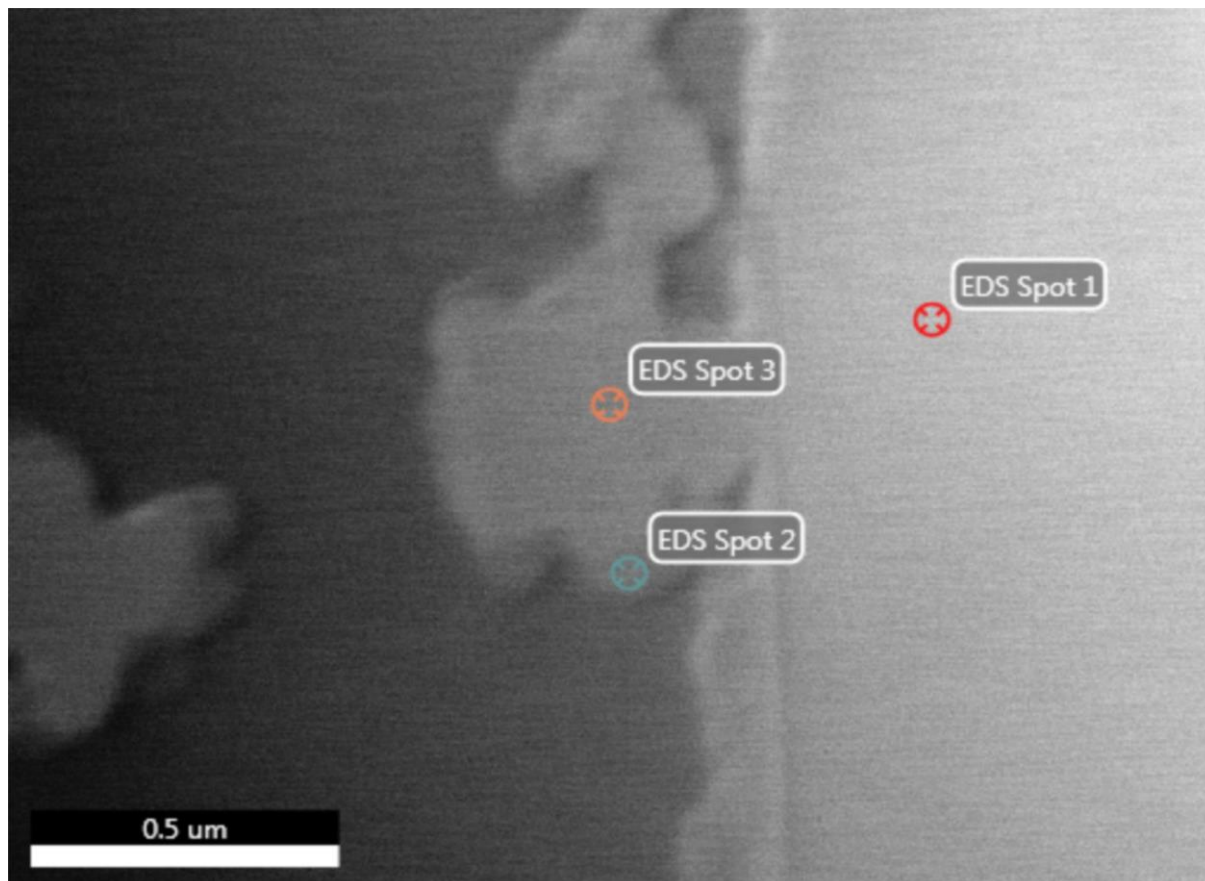
EDS Spot 1

Lsec: 30.0   0 Cnts   10.510 keV   Det: Apollo XLT2 SUTW

Element	Weight %	Atomic %	Net Int.	Error %	Kratio	Z	A	F
O K	74.77	83.88	321.25	7.57	0.3301	1.0212	0.4323	1.0000
SiK	25.23	16.12	488.83	8.21	0.0842	0.9312	0.3581	1.0013

EDS Spot 2

Lsec: 30.0   2 Cnts   10.510 keV   Det: Apollo XLT2 SUTW

Element	Weight %	Atomic %	Net Int.	Error %	Kratio	Z	A	F
C K	28.65	36.74	42.13	10.62	0.0981	1.0430	0.3284	1.0000
O K	56.46	54.35	167.71	9.93	0.1355	0.9990	0.2402	1.0000
NaK	5.86	3.92	29.03	13.38	0.0089	0.9084	0.1680	1.0017
MgK	0.37	0.23	3.43	22.31	0.0007	0.9241	0.1994	1.0032
SiK	8.66	4.75	202.25	8.85	0.0274	0.9098	0.3470	1.0024

EDS Spot 3
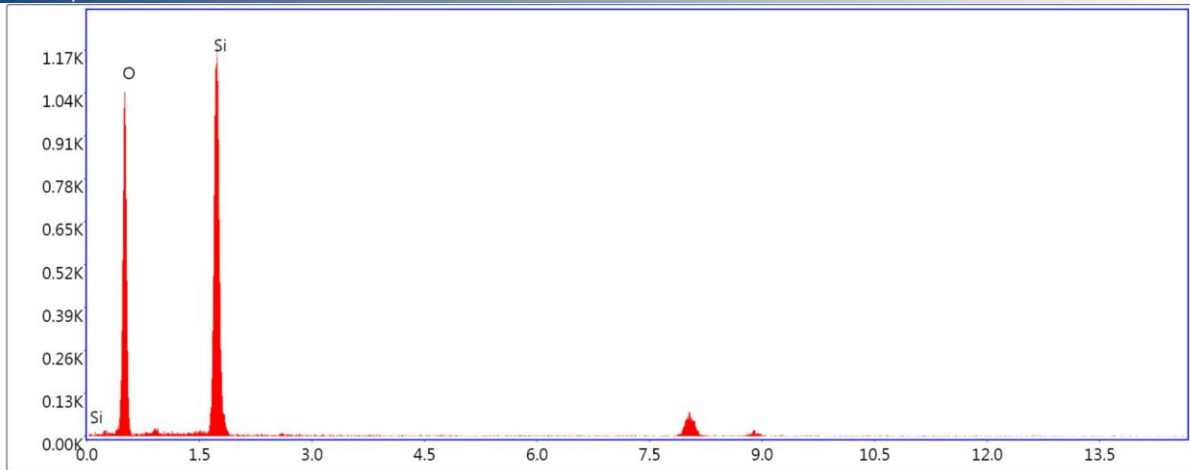
Lsec: 30.0   1 Cnts   10.510 keV   Det: Apollo XLT2 SUTW

Element	Weight %	Atomic %	Net Int.	Error %	Kratio	Z	A	F
O K	75.22	84.20	223.31	7.72	0.3353	1.0208	0.4367	1.0000
SiK	24.78	15.80	327.11	8.39	0.0824	0.9308	0.3567	1.0013
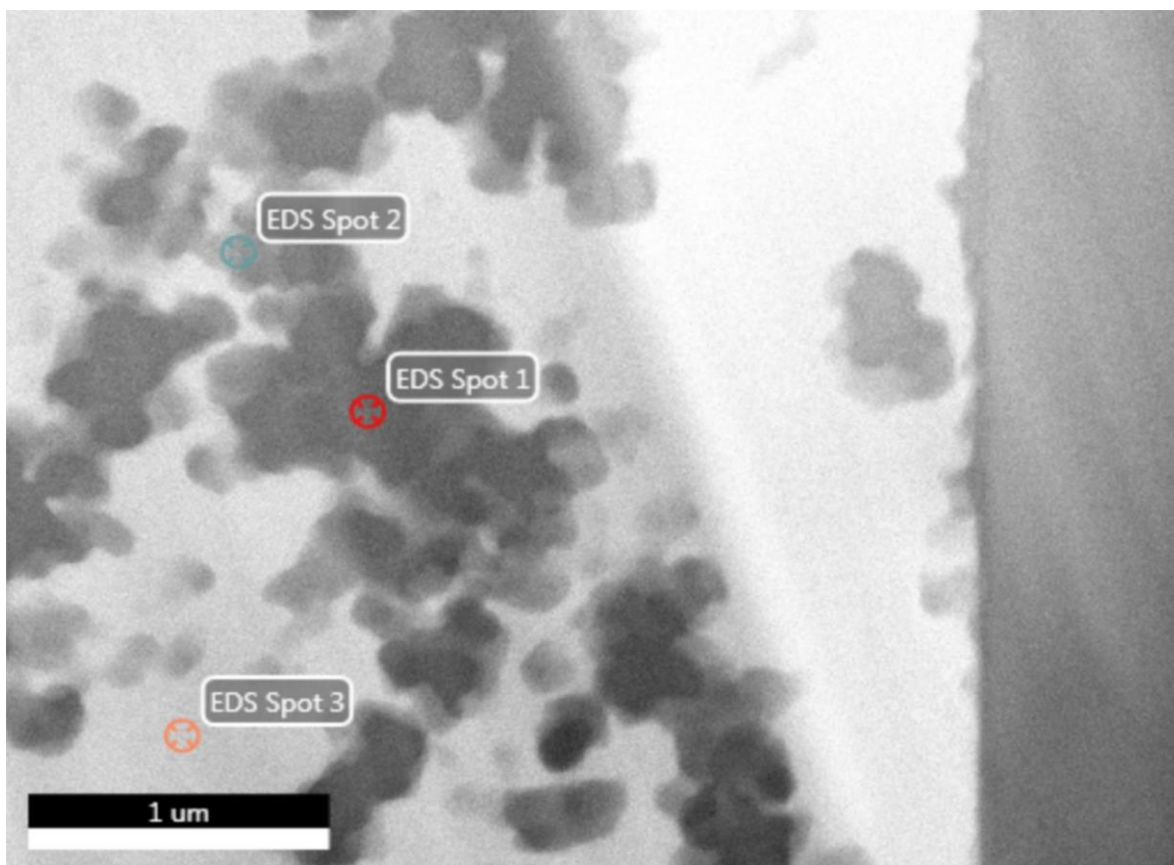
EDS Spot 1
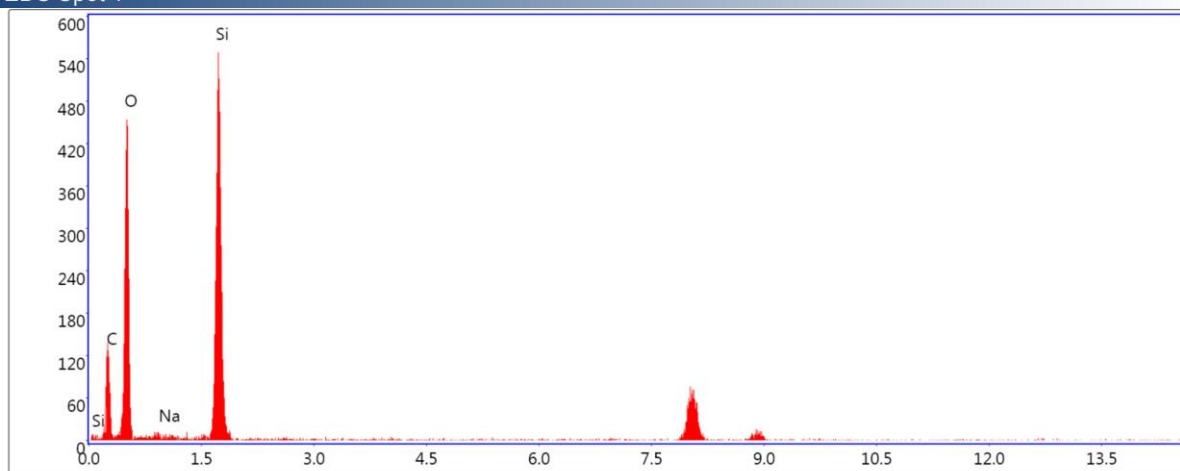
Lsec: 30.0   1 Cnts   10.510 keV   Det: Apollo XLT2 SUTW

Element	Weight %	Atomic %	Net Int.	Error %	Kratio	Z	A	F
C K	31.86	39.97	30.56	10.91	0.1146	1.0378	0.3466	1.0000
O K	57.49	54.13	99.79	10.51	0.1298	0.9939	0.2271	1.0000
NaK	1.59	1.04	4.76	20.79	0.0024	0.9036	0.1637	1.0019
SiK	9.06	4.86	145.17	8.72	0.0317	0.9050	0.3853	1.0025

EDS Spot 2
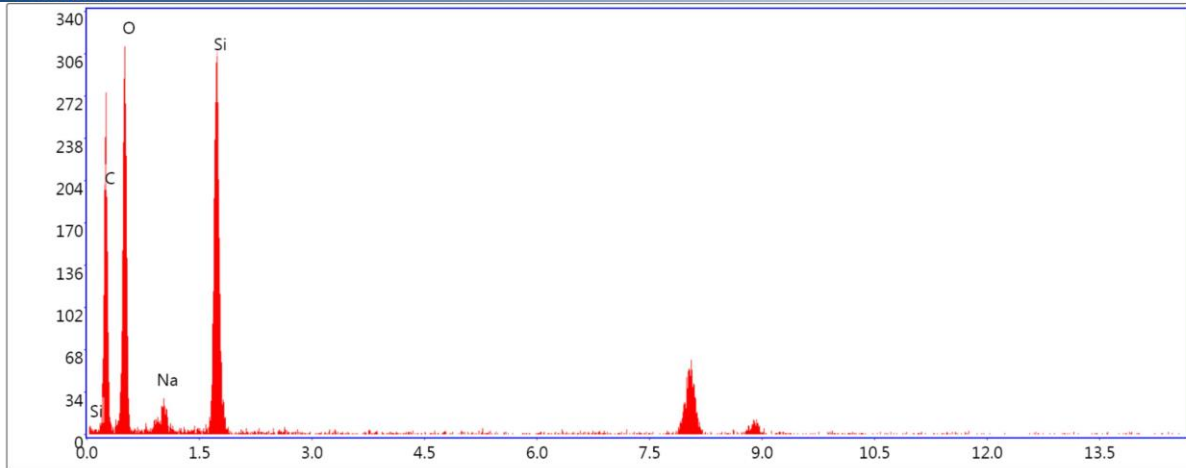
Lsec: 30.0   0 Cnts   10.510 keV   Det: Apollo XLT2 SUTW

Element	Weight %	Atomic %	Net Int.	Error %	Kratio	Z	A	F
C K	43.88	52.48	49.18	9.41	0.1905	1.0307	0.4213	1.0000
O K	47.69	42.82	65.86	11.36	0.0885	0.9868	0.1880	1.0000
NaK	3.43	2.15	10.61	15.32	0.0054	0.8969	0.1762	1.0015
SiK	5.00	2.56	79.24	9.12	0.0179	0.8982	0.3965	1.0031

EDS Spot 3
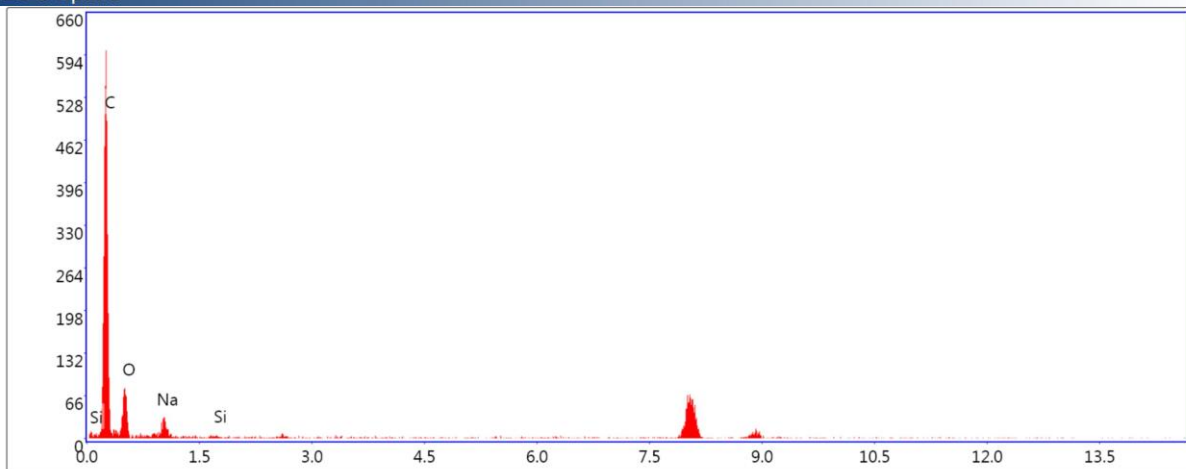
Lsec: 30.0   0 Cnts   10.510 keV   Det: Apollo XLT2 SUTW

Element	Weight %	Atomic %	Net Int.	Error %	Kratio	Z	A	F
C K	73.17	79.05	112.73	5.78	0.5041	1.0139	0.6797	1.0000
O K	23.57	19.12	19.07	13.85	0.0296	0.9701	0.1293	1.0000
NaK	3.17	1.79	10.14	14.64	0.0060	0.8812	0.2144	1.0010
SiK	0.09	0.04	1.45	25.84	0.0004	0.8822	0.4946	1.0052

106

Additional images of the SS in the FIB-SEM sample.